CONTROLLING CONDENSATE OUTLET TEMPERATURE ON AN AIR COOLED CONDENSER IN MATLAB/SIMULINK

by

Kathryn Hyden

Submitted in Partial Fulfillment of the Requirements

for the Degree of

Master of Science in Engineering

in the

Mechanical Engineering

Program

YOUNGSTOWN STATE UNIVERSITY

May, 2014

Controlling Condensate Outlet Temperature on an Air Cooled Condenser in MATLAB/Simulink

Kathryn Hyden

I hereby release this thesis to the public. I understand that thesis will be made available from the OhioLINK ETD Center and the Maag Library Circulation Desk for public access. I also authorize the University or other individuals to make copies of this thesis as needed for scholarly research.

Signature:

Kathryn Hyden, Student Date

Approvals:

Dr. Hazel Marie, Thesis Advisor Date

Dr. William Arnold, Committee Member Date

Dr. Daniel Suchora, Committee Member Date

Ted Thome, Committee Member Date

Dr. Salvatore A. Sanders, Associate Dean of Graduate Studies Date

ABSTRACT

With an ever increasing electrical power demand, the importance of plant simulations remains important for both personnel training and system design. Individual components may be modeled alone to analyze performance of a specific subsystem. One such subsystem of interest is an Air Cooled Condenser (ACC), as it provides an ideal cooling solution to those power plants subjected to strict water usage requirements as well as those lacking a sufficient nearby water source.

An ACC was modeled for simulation in MATLAB/Simulink. The goal of the simulation was to successfully implement a triple cascade control that could maintain the condensate outlet temperature at a designated value. The physical portion of the model consists of three node types: steam/water nodes, metal nodes (pipe wall), and air nodes. The control portion of the model employs a triple cascade control with the use of PID control blocks. There were three variables used to control the temperature; steam extraction percentage, fan speed percentage, and air recirculation percentage. The simulation was then tested under various transient conditions. At present time the physical model is performing exceptionally and the controls sufficiently maintain the desired values under certain conditions, however transient responses require additional tuning. Limitations of the model are addressed and areas for future work are suggested.

ACKNOWLEDGEMENTS

To those who have been involved in my education, you have given me much for which to be thankful. Particularly, I would like to thank Dr. Hazel Marie, my faculty advisor, for her guidance throughout my entire career at YSU. You have provided many wonderful opportunities and prepared me well for my future. I would like to thank Dr. Bill Arnold for proposing this research and assisting me with the model. You have been incredibly supportive to me in class, with my thesis, and in preparation for my professional career. I would like to thank Ted Thome for taking the time, on multiple occasions, to share his expertise on heat transfer, as well as Dan Bolton for imparting some of his valuable control knowledge. To Dr. Suchora: thank you for being the most perfect mentor. I will be forever grateful for your support, encouragement, and advice over the years. I must also thank those who awarded me the Cushwa/Commercial Shearing Fellowship, which provided me financial support.

I want to thank Dave Hull for his flexibility as my internship supervisor and his eagerness to support me through my education in any way possible. Finally, I would like to thank my family and friends for being understanding of my priorities and providing a welcomed occasional distraction from my studies. Specifically, I want to thank my parents for taking an interest in my education and being my unfailing support system. To my siblings: Patrick, your dedication to learning continues to motivate me. Thank you for the healthy competition. Kelly, with your compassion and humor, you have unknowingly brightened many tough days.

TABLE OF CONTENTS

LIST OF TABLES

LIST OF FIGURES

NOMENCLATURE

Symbol	Description
A	Area
b	Cross Sectional Height of a Rectangular Fin
B	Width of a Rectangular Fin
Bo	Boiling Number
C	Integration Constant
Co	Convection Number
Cp	Specific Heat
D	Diameter
f	Friction Factor
F	Force
Fr_L	Froude Number Assuming All Mass Flowing as Liquid
g	Acceleration Due to Gravity
G	Total Mass Flux
h	Heat Transfer Coefficient, Enthalpy
h_{LT}	Heat Transfer Coefficient Assuming All Mass Flowing as Liquid
h_{Nu}	Heat Transfer Coefficient Given by Nusselt Correlation
J_g	Dimensionless Vapor Velocity
k	Thermal Conductivity
L	Length
m	Mass
$\dot{m}$	Mass Flow Rate
n	Dimensionless Correlating Parameter (Shah)
Nu	Nusselt Number
P	Pressure
Pr	Prandtl Number
p_r	Reduced Pressure

p_w	Wetted Perimeter
q	Heat Flux
Q	Heat Energy
$\dot{Q}$	Rate of Heat Transfer
R	Radius, Thermal Resistance
Re_L	Reynold's Number Assuming All Mass Flowing as Liquid
Re_{LS}	Reynold's Number Assuming Liquid Phase Flowing Alone
t	Time
T	Temperature
td	Time Delay
u	Internal Energy
V	Volume
W	Work Energy
x	Vapor Quality
Y	Shah's Dimensionless Correlation Parameter
z	Elevation
Z	Dimensionless Correlation Parameter (Shah)

Greek Letters

μ_l	Dynamic Viscosity of Liquid Phase
Δ	Change In
Ψ	Dimensionless Heat Transfer Coefficient
α	Area Ratio
β	Heat Transfer Coefficient Ratio
ε	Emissivity
η	Efficiency
ρ	Density
σ	Stefan-Boltzmann Constant

Subscripts

ID	Inner Diameter
OD	Outer Diameter
T	Total
f, l	Of Liquid
g	Of Vapor
i	In, Inner
o	Out, Outer

CHAPTER I

INTRODUCTION

1.1 Background

There exists a recent focus on initiatives to find clean, renewable resources for electricity generation. Currently, the majority of electricity generated in the United States is done so using fossil fuels – coal, oil, and natural gas – or nuclear power generation. According to the U.S. Energy Information Administration, only 12% of electricity in the United States comes from renewable sources, such as wind, solar, and hydropower. A breakdown of the sources used for electricity generation, with a projection for future use, is shown in Figure 1.1.

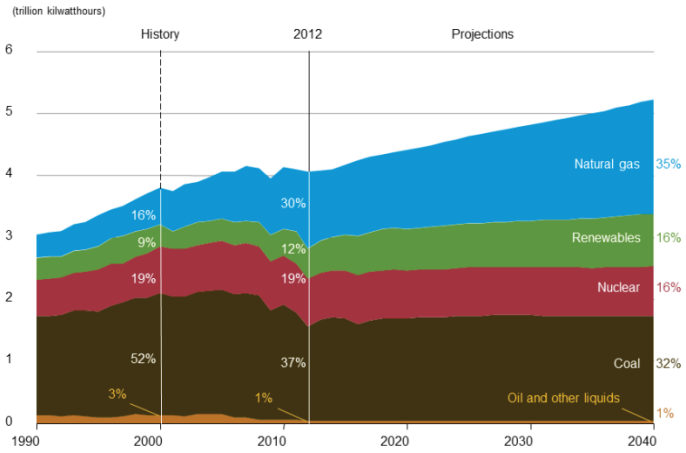

Figure 1.1 Electricity Generation by Fuel Source (EIA, 2013)

With the ever increasing power demand, there is great value in generating electricity in the most efficient way possible. Despite the push for efficient renewable energy sources, the fact remains that a dependable and cost effective method of producing electricity from renewable sources has yet to be discovered; certainly not on a scale large enough to replace nuclear and fossil fuel power generation. Since fossil fuels and nuclear sources continue to be the leading means of power generation in the U.S., it is crucial that resources be concentrated on improving the efficiency of these methods to meet the rising demand.

Whether using coal, natural gas, or nuclear power, electricity is typically generated using steam. The Rankine cycle, in Figure 1.2, illustrates the most basic fundamental processes and components that are required for such power generation. In reality, the system would contain numerous other components in order to achieve optimal operating efficiency.

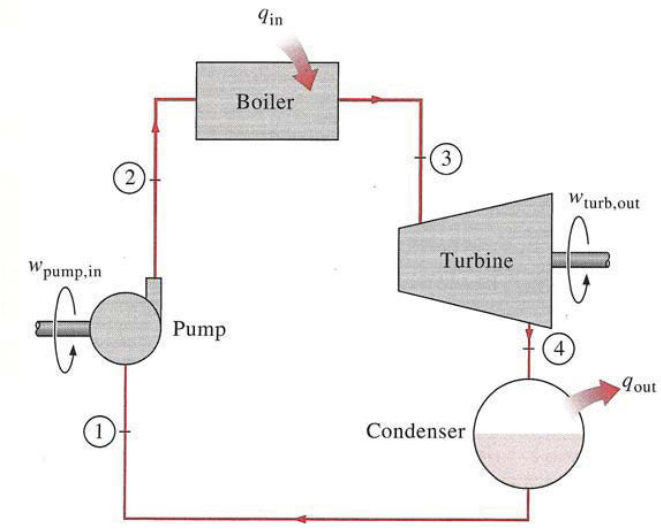

Figure 1.2 The Rankine Cycle (Cengel and Boles, 2008)

The simple Rankine cycle entails four components and four simple processes. The starting point of the cycle is considered to be the pump. The pump serves to compress the water to the required pressure for the boiler as well as to deliver the liquid to the next device. The next process takes place in the boiler. The boiler's function is to allow heat exchange between the combustion gases and the saturated liquid entering the boiler to generate steam. In the case of nuclear generation, the heat of the nuclear reactor supplies the feed water with heat energy in a steam generator. This case will be further discussed later. Steam leaving the boiler is forced through the turbine, causing the blades and shaft to rotate as it cools and expands. In turn, the shaft rotates an electric generator, thus producing electricity. The cycle is completed as the spent steam returns to a liquid state as it passes through a condenser. In the condenser, a substantial amount of heat is rejected from the steam to a heat sink. Depending on the type of condenser, this heat sink could be water or air. Various types of condensers as well as the importance of condensers in this cycle shall be discussed in the following section. In the cycle model, the fluid leaves the condenser as a saturated liquid, enabling the cycle to repeat.

Because power plants do not operate on a simple Rankine cycle, it is worthwhile to mention some of the additional components and processes often present in typical power plant cycles. Such components include steam generators, high and low pressure turbines, moisture separators, reheaters, demineralizers, and feed water heaters. A more detailed and slightly more

realistic diagram of a typical power producing side of a plant is illustrated in Figure 1.3.

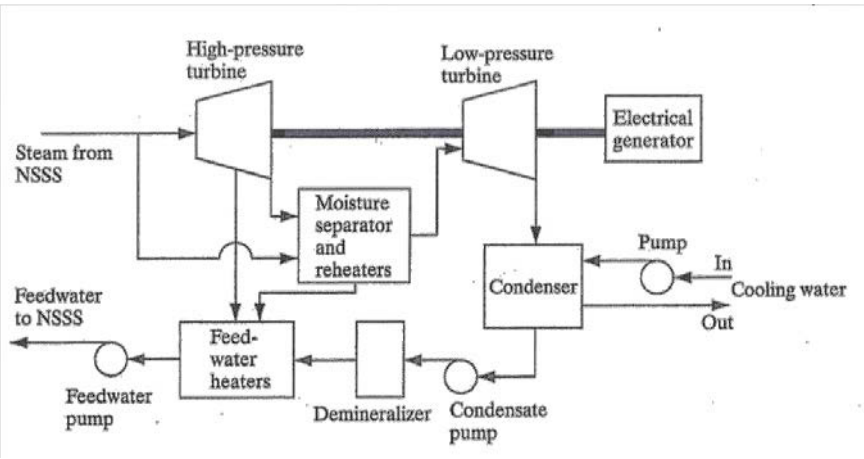

Figure 1.3 Power Producing Side (Lamarsh and Baratta, 2001)

One reason for these additional processes and components is to improve the thermal efficiency of the cycle. When steam passes through a turbine, condensation forms on the turbine blades as the steam's temperature and pressure decrease. This liquid reduces both the turbine lifetime and efficiency. If the steam flowing through the turbines is superheated, this allows for some heat removal from the steam without condensation. By passing superheated steam through the turbines, the water produced is reduced, thus increasing turbine efficiency. A fraction of the dry, superheated steam entering the high pressure turbine is drawn off and passed through a moisture separator. The moisture separator and reheater often exist as a single device, in which liquid water is removed from the turbine and heated as it passes over tubes carrying the supply system steam. The spent steam is then condensed and passed through the

demineralizer as a liquid, where impurities are removed. This eliminates corrosion and helps to increase efficiency by preventing fouling. The water is again heated, this time in the feedwater heaters with steam extracted from the intermediate stage of the turbine. This process is known as regeneration and has been proven to increase the overall efficiency of the cycle. Again, it should be emphasized that neither diagram is an all encompassing depiction of components and systems involved in a power plant, but rather a simplified adaptation of a typical cycle.

1.2 Condenser Function and Types

As previously mentioned, the function of the condenser is to expel a significant amount of heat from the steam to a sink, thus condensing the feedwater back to a liquid state. This process is absolutely essential in order to complete the cycle. In accordance with the second law of thermodynamics, the energy extracted from the steam cannot be converted entirely into work energy in such a cyclic process. Therefore, some of this heat must be exhausted to a sink, which is done in the condenser. As explained in Lamarsh and Baratta (2001), if W is the electrical energy output, and Q_R is the rate of thermal energy output from the reactor or furnace, then the overall efficiency of a plant is defined as $\eta = \frac{W}{Q_R}$. If Q_C is the amount of heat energy rejected to the heat sink in the condenser, it can be approximated that $W \approx Q_R - Q_C$. It follows that overall efficiency can be estimated that $\eta \approx 1 - \frac{Q_C}{Q_R}$. These approximations of course do

not account for energy losses in the various components and piping networks. Lamarsh and Baratta (2001) go on to explain that efficiency is of concern in both fossil and nuclear plants, but for different reasons. In fossil fuel plants, cost of production is established primarily by the cost of fuel. In order to operate at maximum efficiency, fossil plants run the turbines close to the highest permissible temperature dictated by material properties. As efficiency increases, less fuel must be consumed to produce a given amount of heat Q_R. On the contrary, nuclear fuel costs are not of concern as the cost of electricity generated in nuclear power plants is dictated largely by capital costs. Since fuel costs have minimal impact on the cost of electricity generated in nuclear plants, it is possible to operate at relatively low temperatures and efficiencies. This is opportune, as such low temperatures are required to guarantee the integrity of the fuel. In the nuclear industry, concern about efficiency arises due to the large amounts of heat rejection to the environment. This is a major consideration when selecting a type of condenser.

The type of condenser most commonly used in power plants is a shell and tube heat exchanger, consisting of steam passing through a tube on the primary side and cold water flowing across the tubes on the “shell side”, or secondary side. There are various configurations of such heat exchangers, but the simple schematic in Figure 1.4 sufficiently illustrates the general process. The cooling water, or secondary flow, is provided by some large body of water, such as a lake, that is located near the plant. As steam passes through the tubes, heat is

expelled to the cooling water, and the primary fluid condenses to exit the tubes as a saturated liquid. As this heat is rejected to the cooling water, the temperature of this secondary flow rises, and exits as a much warmer liquid. This warm cooling water is then returned to the original source.

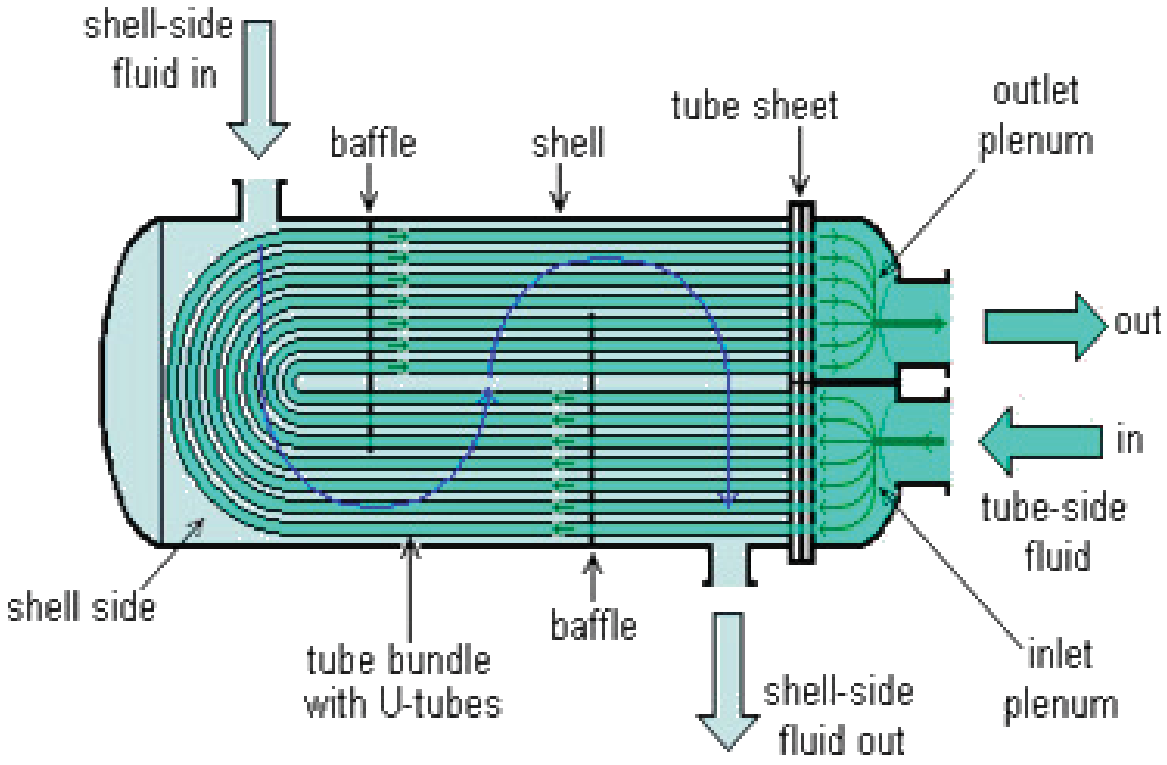

Figure 1.4 Shell & Tube Heat Exchanger (KVA Stainless, 2013)

The shell and tube condenser is a desirable design for various reasons. The high heat transfer rate between the primary and secondary sides allows for a fairly compact size. This in turn, coupled with years of experience using this type of condenser, leads to a lower cost and high reliability. However, as previously mentioned, large amounts of heat rejected back into the environment can cause

permanent damage if done improperly. Such heat rejection which causes lasting harmful effects is termed “thermal pollution”. In order to prevent deterioration of surrounding wildlife, legislation has been passed, prohibiting water from being delivered back to the source unless it meets strict temperature criteria. An additional disadvantage of this design is fouling. Fouling occurs on both shell and tube sides, as water leaves deposits that can only be remedied with a thorough cleaning. This requires shutting down until cleaning is complete.

One way to circumvent stipulations placed on the temperature of discharge water is with cooling towers, often used in combination with shell and tube heat exchangers. In such conjunctures, the cooling tower is placed at the exit of the shell side. The warm liquid, exiting the shell side of the exchanger is sprayed into the cooling tower, which operates on the principal of evaporative cooling. The cooling tower may be either natural draft or induced draft. In the case of an induced draft cooling tower, the warm water is sprayed downward to a pool of cool water. A fan at the exit circulates air upward, picking up moisture from the pool, forcing mixing between the hot wet, and cold wet fluids. Some steam condenses, falling back to the pool at the base, and the remaining warm moist air is exhausted through the flume to the atmosphere. A natural-draft cooling tower operates similarly, but without a fan. This operates like a chimney, with an air inlet towards the bottom. As the air mixes with the warm water being sprayed into the tower, a natural air draft is created, flowing from bottom to top.

Simple schematics of both types of cooling towers, taken from Cengel and Boles (2008) are shown below in Figure 1.5.

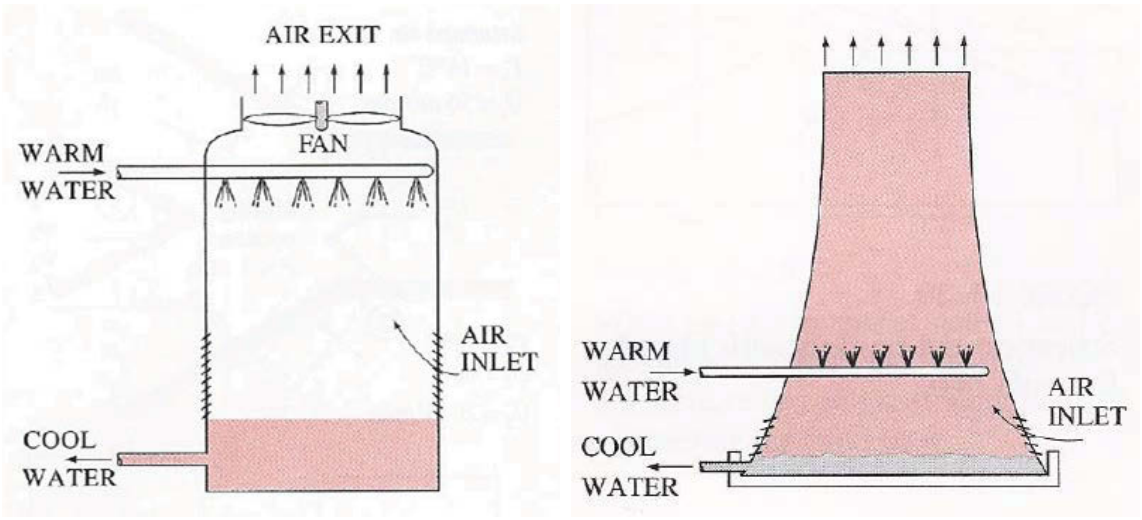

Figure 1.5 Cooling Towers (a) Induced Draft (b) Natural Draft (Cengel and Boles, 2008)

One advantage of cooling towers is that they allow for smaller heat exchangers, resulting in lower pressure drops and higher efficiencies. Although effective in conjunction with heat exchangers, they too present some disadvantages. Again, local legislation limiting discharge into the environment must be adhered to and fouling is an ever present concern. Cooling towers require large amounts of water and therefore are not suited for many areas. Furthermore, construction of cooling towers is rather costly, as they can be over 100 meters in height (Cengel and Boles, 2008).

Another option for steam condensing is the use of air cooled condensers (ACC). This technique is known as dry cooling, as no cooling water is needed. In an ACC, steam exiting the turbine is passed through pipes, or tube bundles, as air is forced across them. Heat from the steam is rejected to the air, thus condensing the steam. Again, there are various configurations of air cooled condensers, some of which will be explained later. Figure 1.6 illustrates a basic A-frame configuration, detailing the major components. Steam exiting the turbine is passed through the inlet manifold, where it enters the condenser. It then flows through pipes know as condensing rows, consisting of multiple finned tubes. The number of tubes and fin pattern depend on the desired capacity of the condenser and overall geometric constraints. As the steam flows through the tube bundles, air flows across, allowing for heat exchange between the hot steam and cool air. The condenser is sized such that when the fluid reaches the ends of the tubes, it has condensed into liquid form. The liquid exits the tubes into the header. The liquid can then be pumped back through the cycle

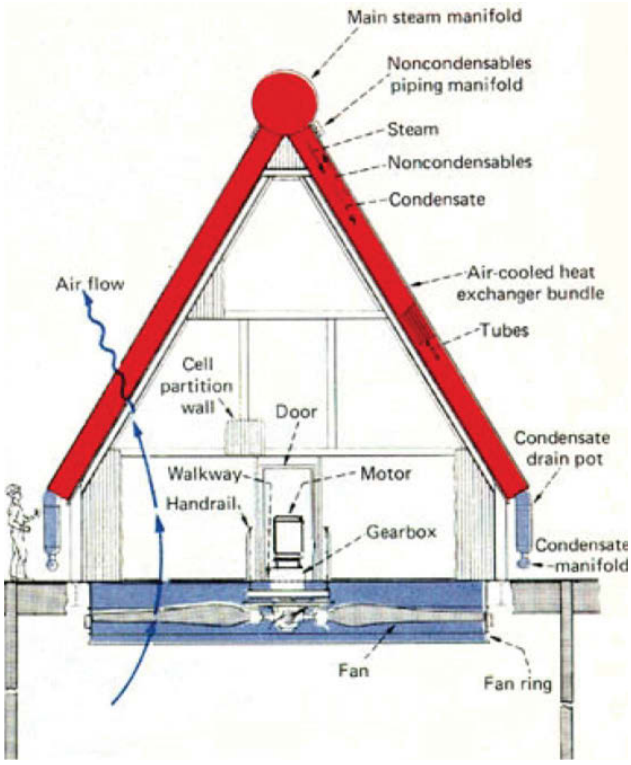

Figure 1.6 A-Frame Air Cooled Condenser (Larinoff, 1978)

As stated, there are various configurations for ACCs. Hudson Products provides information regarding number of passes and fin type through their software ACHE (2013). An additional schematic is shown in Figure 1.7. This depicts a simple three pass air cooler. This was used as a metric for designing the model done in this research.

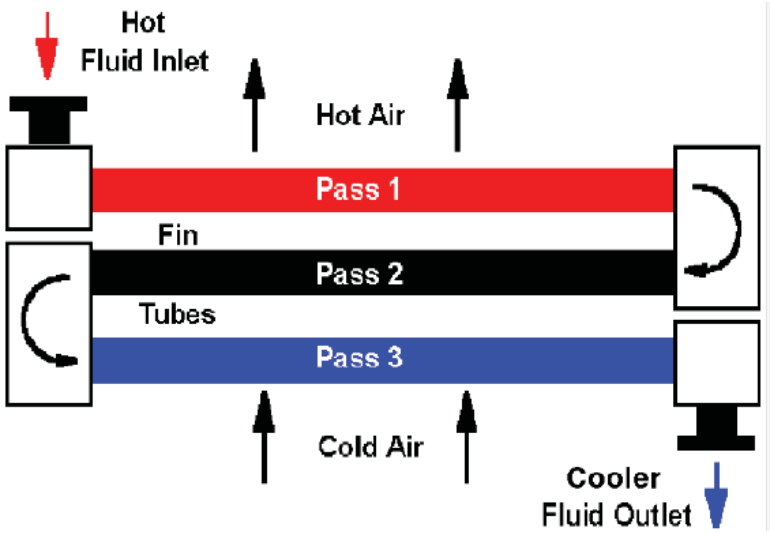

Figure 1.7 3-Pass ACC (ACHE, 2013)

There are also options regarding air flow. The air can be forced across the tubes by use of induced draft or forced draft. The difference between the two is shown in Figure 1.8. In a forced draft condenser configuration, the fans are placed below the tube bundles, pushing the air upward. In this case, cool air is passing through the fan. In an induced draft condenser, the fan is located above the condensing rows and air is pulled upward. This means that the air passing through the fan is much hotter, as it has already acquired heat from the steam in the tube bundles. This results in additional considerations with the materials used in construction of the fan. These materials must be able to withstand much higher temperatures than the materials of a forced draft fan.

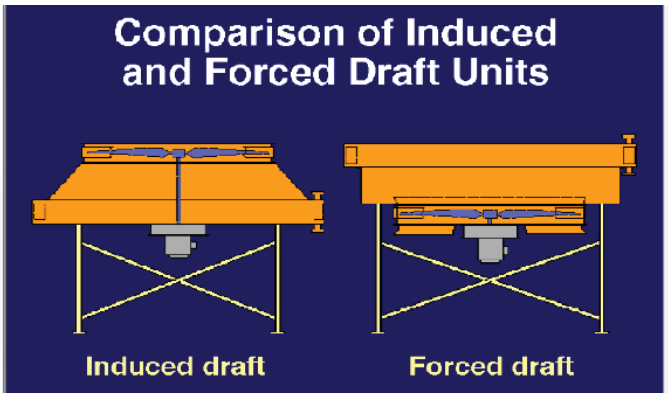

Figure 1.8 Draft Type (ACHE, 2013)

The remainder of this study focuses on forced draft coolers, similar to the one shown below. The diagram shows the louvers, which were previously unmentioned. The louvers control the airflow leaving the unit, and can be used to prevent the water from freezing in extreme temperatures.

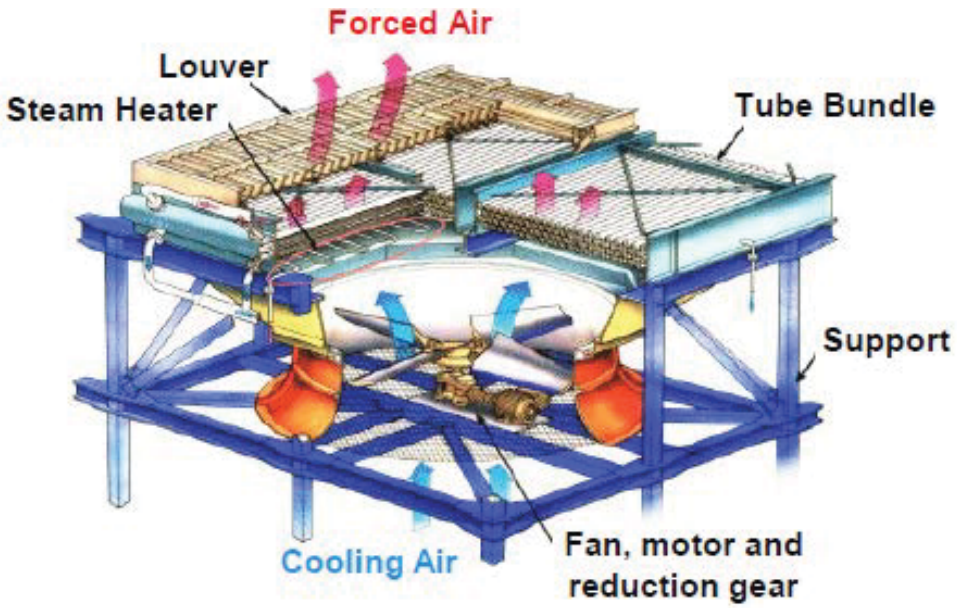

Figure 1.9 Forced Draft Air Cooler (Toshiba Corporation, 2013)

Dry cooling methods provide obvious advantages that are absent with the use of typical water cooled condensers. The most prominent benefit is that no water is required. This allows for large plants to operate in areas with strict water stipulations or those not in close proximity to a large water source. Air cooled condensers do experience fouling due to pollen and dirt carried in the air, but typically allow for easier maintenance. Additionally, they are operable under various weather conditions. This is done through a winterization package, which is offered as an option in the Hudson Products coolers (ACHE, 2013).

It is often desired that the condensate outlet temperature of the cooler be maintained at a certain temperature. Severe fluctuations in the condensate temperature can cause dangerous stressing to downstream components. Although condensers are sized to handle a specified load, using tools like the Hudson calculator, they must operate in extreme conditions. One such instance of ACC use in the nuclear industry is illustrated in Figure 1.10 from Toshiba Corporation (2013). This diagram hints at one circumstance when ACCs might operate under very high pressure, such as the condenser modeled for simulation.

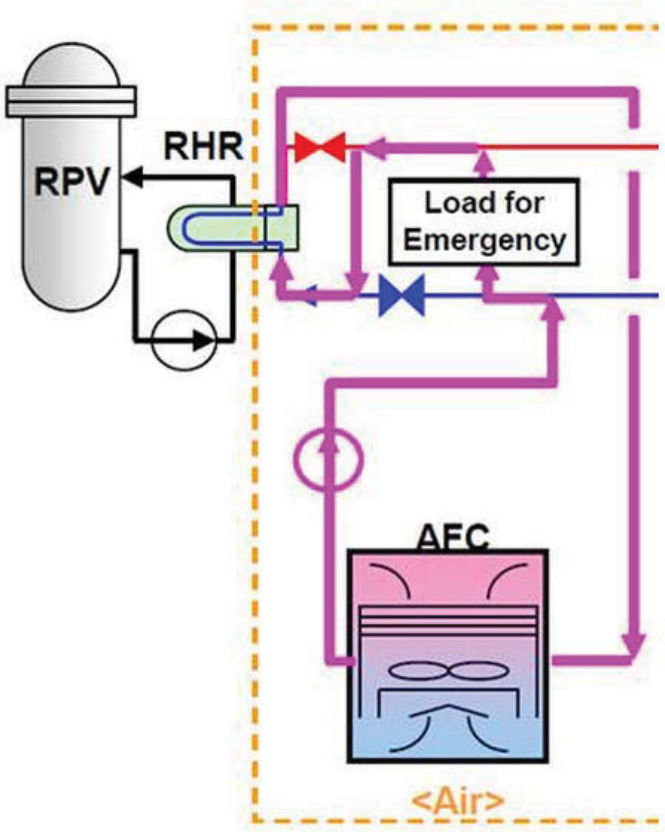

Figure 1.10 ACC Use in the Nuclear Industry (Toshiba Corporation, 2013)

Disturbances can be introduced, which cause fluctuations in the system, thus affecting the outlet condensate temperature. Therefore, it is key to maintain the desired temperature with the use of controls. Methods of controlling the condensate temperature include louver position, fan speed, and recirculation percentage. With the appropriate controls, temperature fluctuations can be minimized, improving operating conditions of the entire system. This is the focus of this research.

1.3 Literature Review

Thermohydraulic modeling has been an area of interest for years. The development of new modeling tools, such as simulation software, has only increased the interest in such modeling. One way to improve the models is through the formulation of heat transfer equations coupled with creation of simpler correlations. These correlations can easily be introduced into a simulation such as the one at hand. One who has made significant contributions in this area is M.M. Shah, who has conducted several studies regarding heat transfer through pipes. In 1976 Shah conducted a study concerning heat transfer during boiling, which was presented in ASHRAE. Although boiling is not of concern for the condenser simulation, Shah developed heat transfer correlations that are based upon the same principles that are required for film condensation heat transfer correlations. The efforts of Shah's 1976 study were later expanded upon in a film condensation paper, and thus are worthy of discussion.

Shah (1976) sought to devise a general heat transfer correlation which could be used for a wider range of flow parameters than at the time was readily available. From this study a CHART correlation was developed. The primary purpose of Shah's CHART was to provide a graphical solution for heat transfer during saturated boiling at subcritical heat fluxes, although it is also applicable at

supercritical heat fluxes under special circumstances. Shah's chart is based on four correlating parameters defined below.

$$\psi = h_{TP}/h_l \tag{1-1}$$

$$Co = (1/x - 1)^{0.8}(\rho_g/\rho_l)^{0.5} \tag{1-2}$$

$$Bo = q/Gh_{fg} \tag{1-3}$$

$$Fr_L = G^2/\rho_l^2 gD \tag{1-4}$$

Shah noted that h_l should be calculated using the well known Dittus-Boelter Equation (1-5).

$$h_l = 0.023{Re_L}^{0.8}{Pr_1}^{0.4}k_1/D \tag{1-5}$$

From comparison of individual studies with these parameters, Shah developed a correlation for ψ, applicable for pressures between 15 and 200 psi, in areas where nucleate effects are dominant (1-6). Shah produced equation (1-7) for low values of Co, at which point all data compared appears to merge into this line of constant slope. Though several iterations, Shah was able to combine these equations into a graphical representation. This was illustrated in his final CHART correlation (Figure 1.11).

$$\psi = 230Bo^{0.5} \tag{1-6}$$

$$\psi = 1.8/Co^{0.8} \tag{1-7}$$

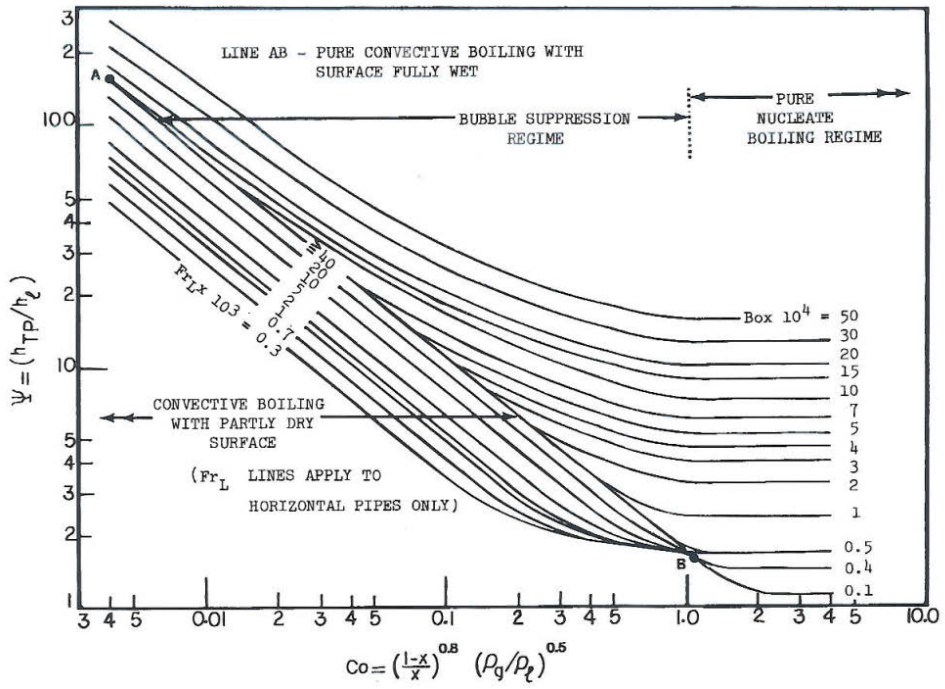

Figure 1.11 Shah's Chart Correlation (1976)

Shah explained that once the dimensionless parameters were obtained through equations (1-2) thru (1-4), the value ψ could be read from the chart. Then from equation (1-1), h_{TP} can be determined. It was concluded that this correlation was in agreement with the wide range of experimental data examined. He identified expression of correlations mathematically rather than graphically, as an area for advancement. He also noted that the CHART correlation may be unreliable at very low pressures and boiling numbers. This is important, as ACC's are often operated at low pressures.

M.M. Shah investigated heat transfer coefficients for film condensation as a successor to his paper regarding heat transfer during boiling in pipes. Shah's findings were presented in "A General Correlation for Heat Transfer during Film

Condensation inside Pipes" which appeared in International Journal of Heat and Mass Transfer (1979). Shah sought to provide a dimensionless formula for approximating heat transfer coefficients for film condensation occurring on the inside of pipes. Shah's study examined various fluids and pipe geometries for a range of parameters.

Motivation for this study came from wide variety of methods attempting to predict heat transfer during film condensation occurring inside channels. At the time of the study, many approaches had been proposed over the past several decades. Shah noted that these techniques ranged from "very arbitrary correlations to highly sophisticated treatments of the mechanics of the flow" (Shah, 1979). Shah sought to develop a simpler correlation, verified with a wide range of experimental data, which could be used as a more general method of predicting heat transfer during film condensation. His research evaluated results from 21 independent studies. Shah (1979) gathered that with a mean deviation of approximately 15%, his correlations could be expected to hold true for all Newtonian nonmetallic fluids over much of the range of practical interest.

Formulation of Shah's film condensation correlation was based upon this earlier research. Shah (1979) found that regardless of flow orientation, the following remained true while the entire pipe remained wetted. These correlations are applicable to both film boiling and condensation.

Shah began by applying equation (1-7), which references dimensionless parameters ψ and Co defined above. Shah calls h_l the superficial heat transfer

coefficient during the liquid phase (equation 1-8). He assigned h_L as the heat transfer coefficient assuming all mass is flowing as liquid. These values were arrived at as shown below. Note that h_L is calculated using the Dittus-Boelter equation, shown earlier in equation (1-5). For initial comparison of the correlation Shah defined another dimensionless parameter, Y (equation 1-9).

$$h_l = h_L(1-x)^{0.8} \tag{1-8}$$

$$Y = h_l/h_g \tag{1-9}$$

After initial analysis of data making comparisons in terms of Shah's Correlation parameter Y, and ψ, Shah (1979) felt there was indication that by replacing $\left(\frac{\rho_g}{\rho_L}\right)$ with reduced pressure p_r the correlation could be improved. This led to the introduction of parameter Z, which is defined below (equation 1-10). He found that equation (1-11) provided the best fit for the data sets he was analyzing. The final form of the correlation can be written in terms of heat transfer coefficients, vapor quality, and reduced pressure (equation 1-12).

$$Z = \left(\frac{1}{x} - 1\right)^{0.8} p_r^{0.4} \tag{1-10}$$

$$\psi = 1 + 3.8/Z^{0.95} \tag{1-11}$$

$$h_{TP} = h_L\left[(1-x)^{0.8} + \frac{3.8x^{0.76}(1-x)^{0.04}}{p_r^{0.38}}\right] \tag{1-12}$$

Determination of the main heat transfer coefficients requires understanding of vapor quality distribution over length. Shah included in his report, a figure which plots vapor quality against dimensionless length. This

figure was developed using results from some experimental studies and is shown below in Figure 1.12.

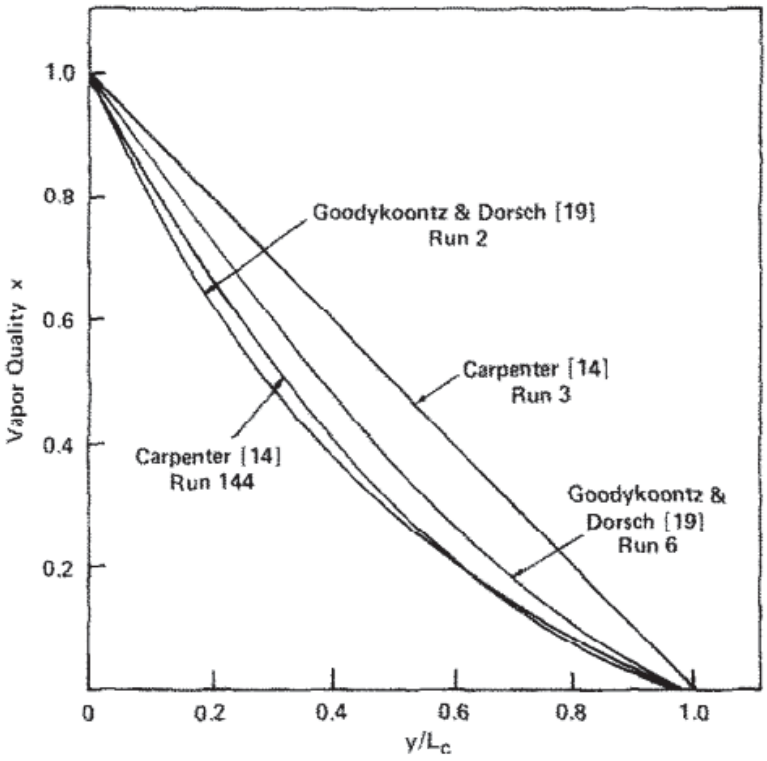

Figure 1.12 Comparison of Studies (Shah ,1979)

Shah (1979) stressed that although linear distribution occurs in relatively few cases, if the change in quality is less than 20 percent, the errors resulting from the linear approximation is insignificant. Even with a 40 percent change in quality, the error associated with this approximation is small. Shah derives an approximation for the mean heat transfer coefficient along the length of the condenser:

$$h_{TPM} = \frac{h_L}{L_2 - L_1} \int_{L_1}^{L_2} \left[(1-x)^{0.8} + \frac{3.8 x^{0.76} (1-x)^{0.04}}{p_r^{0.38}} \right] dL \qquad (1\text{-}13)$$

For cases with non-linear quality variations, the above is usually solved numerically. However, for linear variations in quality over length and vapor qualities from $x = 1$ to $x = 0$, Shah simplified this equation as shown below. Equation (1-14) is used for linear quality variations and equation (1-15) is for $x = 1$ to $x = 0$.

$$h_{TPM} = \frac{h_L}{x_2 - x_1}\left[-\frac{(1-x)^{1.8}}{1.8} + \frac{3.8}{p_r^{0.38}}\left(\frac{x^{1.76}}{1.76} - \frac{0.04x^{2.76}}{2.76}\right)\right]\Bigg|_{x_1}^{x_2} \quad (1\text{-}14)$$

$$h_{TPM} = h_L(0.55 + 2.09/p_r^{0.38}) \quad (1\text{-}15)$$

Shah (1979) evaluated equation (1-12) using $x = 0.5$ and notes that this differs from equation (1-15) by only five percent. According to Shah, when vapor quality variations are smaller, the substitution of arithmetic mean into equation (1-12) yields even closer results. This is true for cases where vapor quality variation is linear and is useful in analyzing mean heat transfer data when assuming linear variation.

For this study, Shah (1979) tested various flow channels and flow directions for a range of temperatures, pressures, and flow patterns. As previously mentioned, data was gathered from 21 individual studies. For thorough examination of the data sets, if any quality distribution was unknown, linear variation was assumed. Shah reiterated that if quality change is less than 40 percent, the error associated with a linear variation approximation is small. Such was the case for the majority of studies analyzed. Shah cited only one

exception; a study in which, “The assumption of linear distribution could be in error here as the quality changes range from 40 to 95%” (Shah, 1979). When quality distribution of a given study was known, Shah’s correlation was calculated using equation (1-13). Otherwise, predictions were made using equation (1-14). One case was examined, in which data was collected concerning flow through an annulus. For analysis of this data, Shah used equation (1-5). He calculated an equivalent diameter, using the equation shown below, where p_w is the wetted perimeter.

$$D_{eq} = \frac{4A}{p_w} \tag{1-16}$$

Deviations were calculated and tabulated for each of the studies. First, individual deviations were calculated.

$$Deviation = \frac{\psi_{PREDICTED} - \psi_{MEASURED}}{\psi_{MEASURED}} \tag{1-17}$$

Then, mean deviation was then calculated as the arithmetic mean of the individual deviations. The mean deviation for all 474 data points was 15 percent when equal weights were given to each set.

The correlation appears to be equally effective for all orientations examined (horizontal, vertical and inclined), diameters ranging from seven millimeters to 49 millimeters, and nominal flow velocities between three meters per second and 300 meters per second. Shah plotted results from his study in the figure shown below.

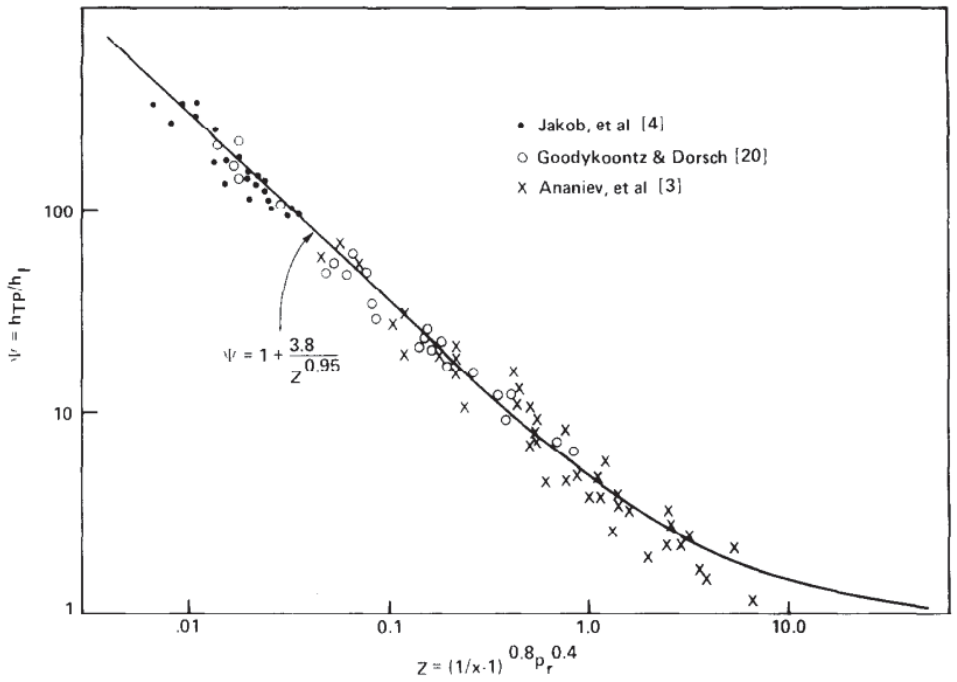

Figure 1.13 Comparison of Water Data with Correlation (Shah, 1979)

Shah (1979) considered some of the limitations of these corrections and discussed possible flaws. The first limitation that he observes is the behavior of vapor qualities between 85 and 100 percent. In this range, Shah found some readings to be substantially higher than the predicted values. Shah attempted to explain this by citing possible causes as entrance effects or shear becoming so high that it causes a breakdown of continuous liquid flow. He too recognized that there may be substantial error in estimation of vapor qualities and heat transfer coefficients at high vapor qualities, as it is difficult to locate the point at which condensation starts.

Shah (1979) also revealed that his correlation should not be used at very low Reynolds numbers. This is simply because there had not been enough data

points analyzed in this low range for the study. Shah recommended using his correlation only for pipe flows characterized by $\mathrm{Re_L} > 350$. Similarly, he suggested that the correlation only be used with annular flows having $\mathrm{Re_L} > 3000$. Shah noted that potential sources of error include impurities in refrigerants, entrance effects, and difficulty in accurately locating the point of condensation completion. Despite these few limitations, Shah concluded that one can feel confident using his proposed correlation in most instances.

For further investigation, Shah (1979) suggested testing at reduced pressures and low Reynolds numbers. He also recommended investigation of a parameter that if introduced, could account for entrainment effects. Lastly, he proposed calculation of heat transfer coefficients using equations for turbulent metallic flows.

Shah later attempted to improve upon these correlations in a study conducted nearly 30 years later. He presented his new findings in a paper titled "An Improved and Extended General Correlation for Heat Transfer During Condensation in Plain Tubes." In the research, an improved version of the previous correlation, covering a wider range of parameters, is suggested. The motivation for this study arose from the limitations he identified with the correlation developed in his previous study. As previously stated, the original correlation displayed some inconsistencies at very low flow rates. At the time, Shah suggested limits for using the equations with accuracy.

In his extension of the original study, Shah (2009) attempted to achieve five specific goals. First, he tried to validate or "modify the lower limit of applicability." The next goal Shah set forth was to make amendments to the previous correlation in order to extend it to the lowest flow rates. At the very lowest flow rates, Nusselt's analytical equations would apply, rendering the correlation unnecessary. Shah's third and fourth goals of the extended research were to conduct testing of the correlation for a wider range of parameters, specifically, testing of new refrigerants and a wider range of reduced pressures. Lastly, Shah expressed his intentions to further modify the correlation if deficiencies are uncovered.

This development of the correlations was based upon 39 individual studies involving 22 different fluids, including water. Shah (2009) arrived at the modified correlation after many trials and introducing a correction factor. He analyzed a wider range of data to establish a suitable correction factor to be used in equation 19a. He suspected that combining the well known Nusselt relation, for predicting heat transfer in vertical tubes (equation 1-19) with equation (1-18-a).

$$h_l = h_{LT}\left(\frac{\mu_f}{14\mu_g}\right)^n \left[(1-x)^{0.8} + \frac{3.8x^{0.76}(1-x)^{0.04}}{P_r^{0.38}}\right] \quad \text{(1-18-a)}$$

$$n = 0.0058 + 0.557p_r \quad \text{(1-18-b)}$$

$$h_{Nu} = 1.32Re_{LS}^{-1/3}\left[\frac{\rho_l(\rho_l-\rho_g)gk_f^3}{\mu_f^2}\right]^{1/3} \quad \text{(1-19)}$$

The combination of the two results in equation (1-20). This equation is suitable for pipe orientations except vertical. For vertical tubes, equation (1-21) should be used.

$$h_{TP} = h_I + h_{Nu} \tag{1-20}$$

$$h_{TP} = h_{Nu} \tag{1-21}$$

These equations were based upon defined flow regimes, depending on pipe orientation. Shah (2009) identified three regimes for heat transfer in vertical and inclined pipes. The boundaries between regimes are dictated by the value of dimensionless vapor velocity, J_g, which is defined as follows:

$$J_g = \frac{xG}{(gD\rho_g(\rho_l - \rho_g))^{0.5}} \tag{1-22}$$

Shah (2009) mapped these boundaries and heat transfer regimes in the figure shown below for flow through vertical and inclined pipes.

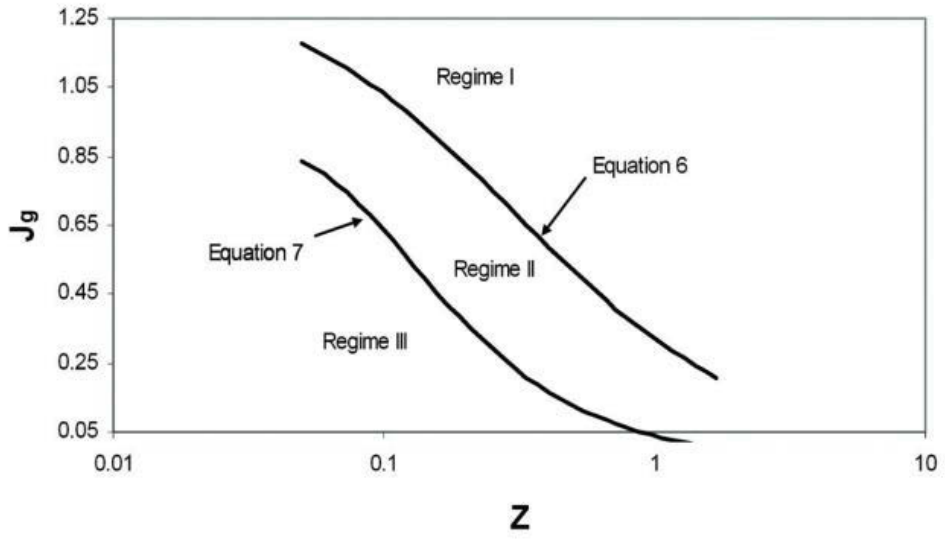

Figure 1.14 Heat Transfer Regimes in Vertical Tubes (Shah, 2009)

Similarly, Shah defined flow regimes for horizontal tubes, but this time only two regimes. He chose to recognize only two regimes in this case because the third would occur only at extremely low flow rates. Recall that this research will make use of horizontal tube rather than vertical tubes.

Shah (2009) stated that for comparison of the correlation with experimental data, only studies with known pressure, flow rates, and vapor quality could be used. Shah again calculated deviations. When using this extended and improved version, Shah's correlation yielded a mean deviation of 14.4% for all 1189 data points. He noted that although the agreement between the correlation and experimental data seem satisfactory for all regimes, the deviation is higher in regime II and near regime boundaries.

Shah (2009) concluded that the results were pleasing for this improved correlation. This time, the correlation was proven to be valid for a much wider range of parameters. The parameters have been expanded such that the new correlation now covers all flows through vertical and horizontal tubes at rates characterized by Reynold's numbers as low as 16,000. Furthermore, the equations can now be used with confidence at reduced pressures as low as 0.0008.

In addition to heat transfer research, there is literature regarding controls which are relevant to the scope of this study. There are many possible control schemes and methods, some more effective than others. One such source is "Techniques of Model-Based Control" by Coleman Brosilow and Babu Joseph.

In one chapter, Brosilow and Joseph (2002) explain the importance of cascade control. Cascade control allows for improved control system performance over single loop control during two circumstances. The first situation in which cascade control permits improved performance is when “disturbances affect a measurable intermediate or secondary process output that directly affects the primary process output that we wish to control”. In this case, implementation of cascade control can minimize effects of disturbances entering a secondary variable of the primary output. The second circumstance under which cascade control typically offers improved performance is when the gain of the secondary process is nonlinear. It was noted that the secondary process in this instance shall include the actuator. Gain variations commonly occur due to setpoint changes or sustained disturbances. According to the authors, enhanced control system performance in this scenario arises because effects of such gain variations are minimized through a cascade control.

Brosilow and Joseph (2002) cited shell and tube heat exchangers as being a prime contender for cascade control. It was illustrated that the primary process output would be the tube side effluent stream. They then identified two potential secondary variables. These secondary variables are steam flow rate and steam pressure, as each effects the other, and in turn, affect the temperature of the effluent. They further explained that choice of secondary control variable depends on the chief disturbance.

Therefore, if the main disturbance in the system is variation in the steam supply pressure, control of the steam flow through the use of a control valve is the optimal solution. It was stated that although this alone will greatly reduce the effect of pressure variations on the effluent temperature, it is still essential to maintain positive control over effluent temperature. This will allow for tracking of setpoint changes and rejection of changes in effluent temperature due to flow variations. The final solution focused the control effort on stem position of the valve, controlled by effluent temperature. This cascade control is illustrated in the diagram below.

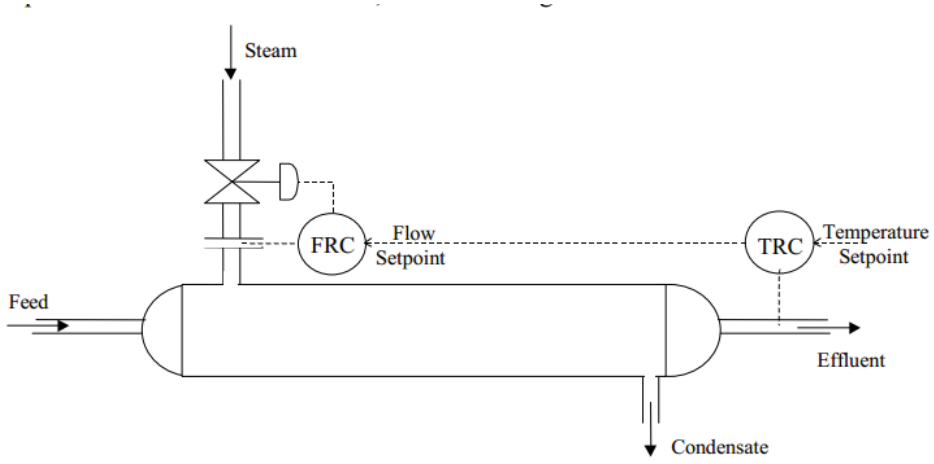

Figure 1.15 Cascade Control of Effluent Temperature via Steam Flow Control (Brosilow and Joseph, 2002)

However, Brosilow and Joseph (2002) explained that if the main disturbance lies in feed flow temperature variations, the ideal secondary variable would be the exchanger pressure. This is illustrated in the Figure 1.16, where the pressure set point, rather than flow rate, is controlled by the effluent temperature.

It was noted that one disadvantage of using this design is that “the inner loop from the steam pressure to the valve stem position may not suppress variations in valve gain as well as with an inner loop that uses the valve to control the steam flow rate.”

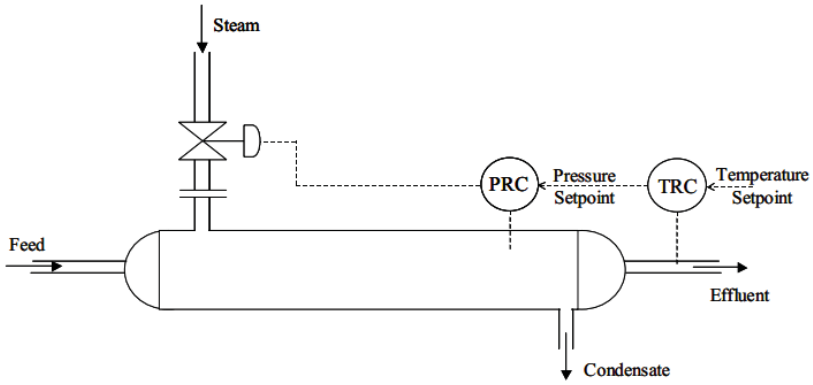

Figure 1.16 Cascade Control of Effluent Temperature via Shell Side Pressure Control (Brosilow and Joseph, 2002)

From this, Brosilow and Joseph (2002) concluded that with the configuration shown in Figure 1.15, cascade control is used to suppress the effect of uncertainty on the control of the primary process variable. They emphasized that cascade control has two objectives. The first is suppression of the disturbance effects on the primary process output and the second is to reduce sensitivity of primary process variable to gain variations of secondary variables. Therefore, it was suggested that “cascade control can be usefully applied to any process where a measurable secondary variable directly

influences the primary controlled variable through some dynamics." Note that this research will extend the described control schemes to three variables.

Another article examined PID controllers rather than cascade controls. As previously mentioned PID controllers, or Three Mode Controllers, refer to Proportional, Integral, and Derivative values to achieve control for a particular process. PID controllers are often used for temperature control, such as in temperature control of condensate temperature. PID temperature controllers require precise tuning of the PID coefficients. In some cases, a controller contains an autotune algorithm, making this tuning process fairly simple for the user. Unfortunately, many times controllers do not come equipped with such autotuning software, or the algorithms available do not sufficiently control the process to the desired output. Such is the case with the control blocks that were implemented in this research. Therefore, it is commonly necessary to implement trial and error tuning strategies. OMEGA Engineering, Inc., a global leader in process measurement and control, published an article recommending a specific tuning strategy (OMEGA, 2014). They noted that the suggested procedure is not the only method available, but all other methods make use of a similar trial and error technique.

Prior to disclosing the tuning strategy, the author defined some key terms used in his instructions. One such term was "cycle time." Cycle time, sometimes referred to as "duty time," is defined as the total time for the controller to complete one on/off cycle. The cycle time is comprised of both on time and off

time while the controller cycles within the proportional band. For example, OMEGA explained that if there is a control having a 20 second cycle time, with on and off times of ten seconds each, there would be a 50 percent power output. The author defined “proportional band” as a temperature range expressed in percentage of full scale that the controller’s proportioning action occurs. It was noted that a wider proportional band (PB) will result in the proportional action taking place in a greater region around the setpoint. This is also known as “gain”, and is the reciprocal of the proportional band. The term “rate”, also known as “derivative,” senses the rate of change of the system temperature and automatically adjusts the proportional band to correct any overshoot or undershoot. The “integral,” or “reset,” term also adjusts the proportional band, but to compensate for droop rather than over and undershoot of the response. Additional terminology will be addressed as it arises.

The author recommended starting by turning off power and disabling any control outputs where possible. Then, the cycle time should be set. An appropriate cycle varies by system, but OMEGA (2014) recommends beginning with a cycle time of five seconds. Systems with faster response times will require smaller cycle times. After selecting the cycle time, the Proportional Band 1 function should be tuned. The author recommended setting this proportional band function at 5% while turning off both reset and rate functions.

The author then offered various procedures for control scenarios including heating and cooling, as well as some simplified versions. The procedure varies

slightly, based on the desire control, but the author notes that procedures may be similar. Primary and secondary tuning parameters (for dual three mode outputs) should be set and tuned independently. The first tuning procedure explained was for a heating control, but is nearly identical to the procedure that should be used for cooling control. The author instructed the user to enable outputs and start the process, running it at a setpoint which would require heat input in order to achieve temperature stabilization. For a cooling control, a setpoint should be chosen that would require cooling before stabilizing. This is the only deviation from the technique, and the rest of the procedure should be followed for both cooling and heating controls. With rate and reset functions turned off, the system should respond with a steady state temperature deviation between setpoint and actual temperatures. This is known as “droop.” It was advised to note any regular oscillations in the temperature display and suggested that a recorder be used for ease of monitoring the process.

If the initial response exhibits oscillations, a different tuning strategy is applied. If the oscillations do not appear to be regular, the PB should be divided by two. This should be repeated as many times as is necessary to obtain regularity in oscillations. If regular oscillations appear during the initial response, the PB should be multiplied by two. This should be repeated until oscillations no longer occur. Figure 1.17 illustrates an ideal response along with two typical initial responses.

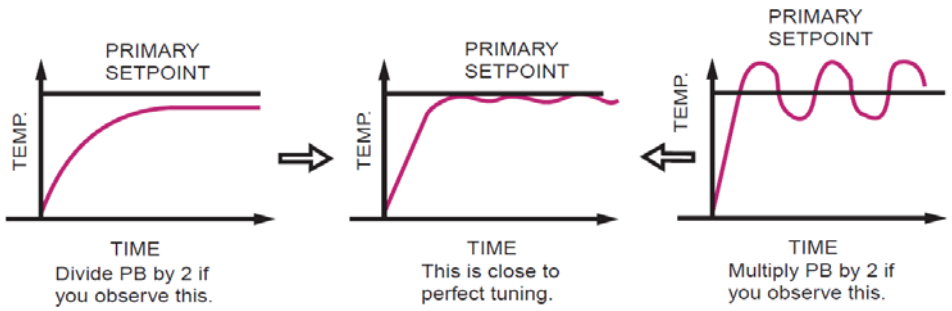

Figure 1.17 Temperature Oscillations (OMEGA, 2014)

The author explained that once the PB has been adjusted as described above, it should be very near to its critical setting. At this point, minor adjustments should be made in order to produce a response with oscillations just occurring in temperature measurements. If at this point no oscillations occur, even with a minimal PB setting, the controls should be tuned using the approach for responses with no oscillations. The presentation of this process will follow. After a critical PB is achieved, temperature and time measurements must be taken to calculate a final temperature deviation. The author illustrated this in Figure 1.18. The PB should then be increased until the droop has increased by 65 percent. Calculations can then be made with new measurements, as shown in Figure 1.19. This is done by multiplying the initial temperature deviation by the temperature deviation with the increased PB. For convenience, a nomogram is also provided in Figure 1.20 to easily calculate the final temperature deviation.

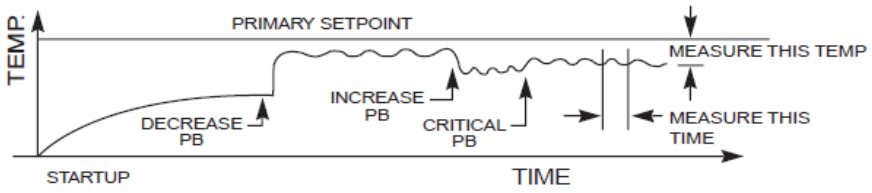

Figure 1.18 Oscillation Time (OMEGA, 2014)

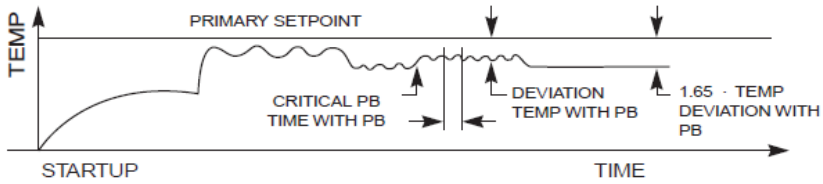

Figure 1.19 Calculating Final Temperature Deviation (OMEGA, 2014)

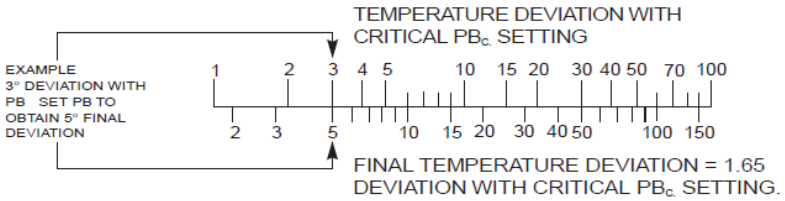

Figure 1.20 Nomogram I (OMEGA, 2014)

Lastly, rate and reset functions need to be set to finalize optimal tuning. Using the following equation or nomogram in Figure 1.21, the RESET value, or repeats per minute, can be calculated, where $T_0 = \text{oscillation time}$ from Figure 1.18.

$$RESET = \frac{8}{5} \times \frac{1}{T_0} \tag{1-23}$$

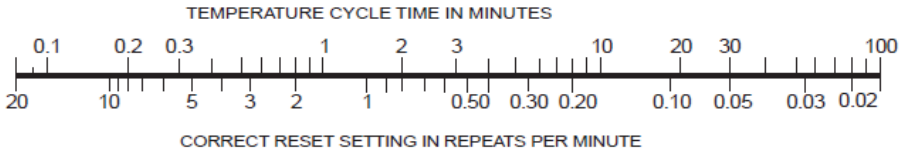

Figure 1.21 Nomogram II (OMEGA, 2014)

Similarly, the RATE value should be set in minutes based on the equation shown below or the nomogram provided by the author.

$$RATE = \frac{T_0}{10} \tag{1-24}$$

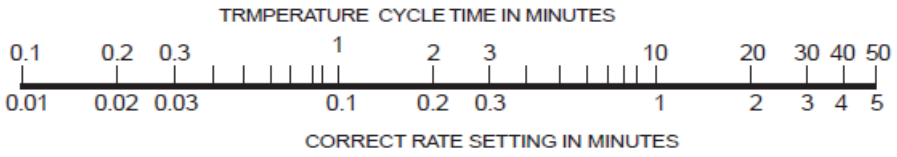

Figure 1.22 Nomogram III (OMEGA, 2014)

In the case that overshoot should occur, the author recommended decreasing the reset value (OMEGA, 2014). The rate then too must be changed according to the following equation.

$$RATE = \frac{1}{6 \times RESET} \tag{1-25}$$

This may need several adjustments to achieve balance between response time and settling time. The author warned that a fast response time is traditionally associated with larger overshoot and shorter settle time than a slow response time.

If no oscillations are observed during the initial response, the droop should be measured with the minimum PB setting of one percent. The PB should then be increased until the temperature deviation has increased by 65 percent. Again, the same nomogram provided in Figure 1.20 can be used as a means of conveniently determining an acceptable final temperature deviation.

The reset function should then be set to a high value and rate should be set to a corresponding value. The author recommends values of 10 resets/min and 0.02 min. This reset action should result in temperature stabilization at the setpoint. Since no critical oscillation time has been identified, the optimal reset and rate settings must be determined through trial and error. The author suggests starting by increasing the set point by ten degrees and observing the overshoot. The setpoint should then be returned to its original value. The overshoots associated with each setpoint should be compared. Excessive overshoot hints at reset and rate values that are too high, while overdamping of the response implies that the rate and reset values are too low. Illustrations are provided in Figure 1.23. Corrections should be made by making incremental changes in parameters until a satisfactory result is obtained.

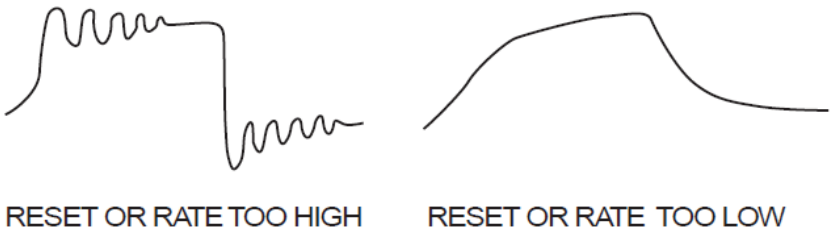

Figure 1.23 Setting RESET and/or RATE (OMEGA, 2014)

The OMEGA publication then addressed a more simplified tuning procedure for PID controllers. This process applies a graphical technique for analyzing a response to a step input and it is again suggested that a recorder be used to read the process variable. Following this method, the process should be started from ambient and run at full power with no control loop. After a slight

delay, heat should reach the sensor and the process variable will rise. Over some time, the process variable will reach a constant, maximum slope. Both the slope of this line, and the time that the maximum slope was reached should be recorded. Then the system power should be turned off. The author then introduces the lumped system time delay, denoted Td, and explains that this value can be obtained by extending the maximum slope line and the ambient temperature. The Td is then the elapsed time between this intersection and the starting time. This time can be found using either the graphical method, as shown in Figure 1.24, or the equation below. Then, parameter setting can be obtained using equations (1-26) thru (1-29).

$$Td = time\ to\ max\ slope - (PV\ @max.slop - ambient)/\ max\ slope \quad (1\text{-}26)$$

$$PB = Td \times max\ slope\ \times \frac{100}{span} \quad (1\text{-}27)$$

$$RESET = \frac{0.4}{td} \quad (1\text{-}28)$$

$$RATE = 0.4 \times td \quad (1\text{-}29)$$

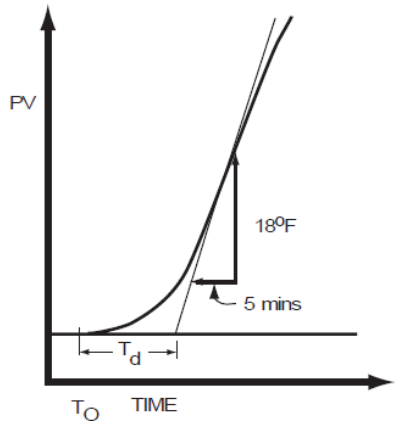

Figure 1.24 System Time Delay (OMEGA, 2014)

The author (OMEGA, 2014) advised the user to restart the system once the above adjustments have been made, this time bringing the process to setpoint with the controller in the loop. Upon observing the response, if excessive overshoot or oscillation occurs, minor adjustments should be made to the parameters. Parameters should be changed only slightly and one at a time in order to observe the effect it has on the system. The author suggested widening the proportional band, lowering the RESET value, and increasing the RATE setting.

Though no studies have been found regarding Matlab/SIMULINK condenser simulation and control, Scott Anderson (2008), in conjunction with The Babcock and Wilcox Company, has developed a Matlab simulation for a boiler system, typically seen in a power plant. Many principles and methodology techniques that were used in this study can be applied to the condenser simulation at hand. Anderson first examined two types of boiler systems: A once-through steam generator and a common drum boiler. He ultimately decided to model the drum boiler, in which the drum acts as a volumetric medium for steam separation. The drum boiler (Figure 1.25) allows sub cooled water to flow through a tube where it is heated to above boiling point. The water and steam mixture is then separated upon reaching the drum.

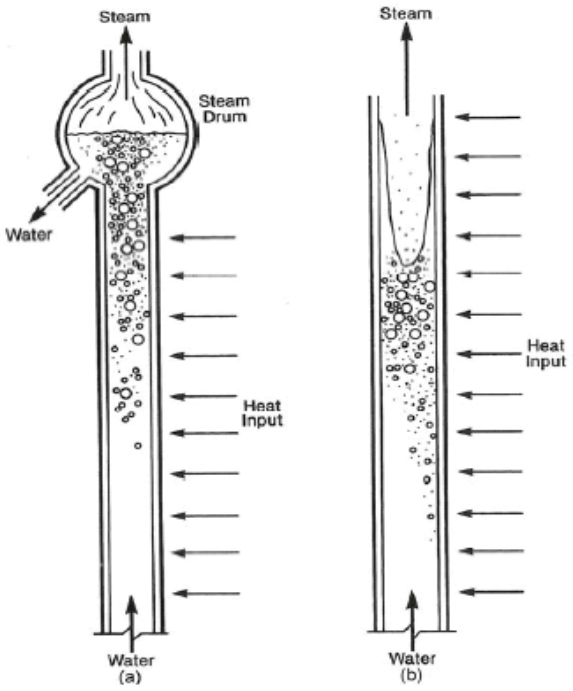

Figure 1.25 Boiler Systems: (a) Steam Drum (b) Once-Through (Anderson, 2008)

For simulation, Anderson (2008) broke the boiler system into seven individual components, and three fluid circuits. This simplified approach is illustrated in Figure 1.26. Feed water runs through the economizer where exhaust gases from the furnace are used to pre-heat the water. This water then travels through pipes to the steam drum where liquid and vapor are separated. The liquid then flows through the downcomer to the base of the furnace. Supply tubes then transport liquid water to individual furnace panels where waterwall tubes circulated the water around the furnace, thus generating steam. Again, the mix is fed back to the drum where liquid and vapor are separated. Liquid water remains in this circuit (DEFD) while steam is removed and delivered to the

superheater. Here, additional heat is added, increasing enthalpy and work potential of the turbine. The superheated steam is then sent to the turbine valve.

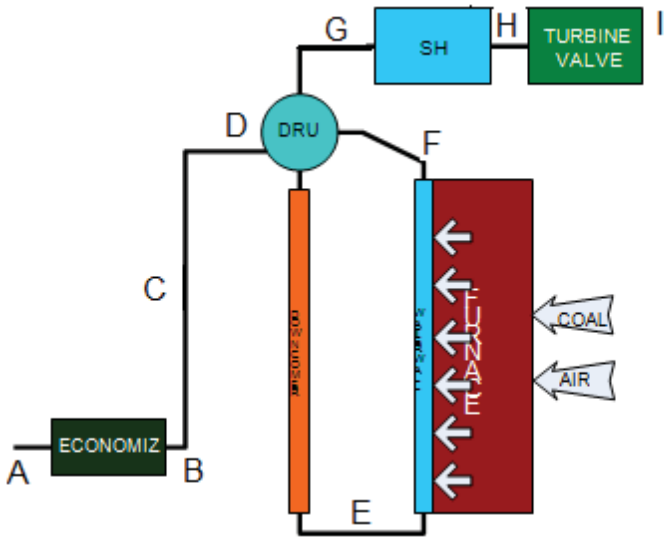

Figure 1.26 Simplified Approach to Boiler System (Anderson, 2008)

Additionally, a pressure flow solver was developed to adjust the mass flow rate such that the drum could remain at a constant pressure.

Anderson (2008) identified some governing equations used for computations in the individual components. Both downcomer and waterwall components were modeled applying conservation of mass, energy, and momentum with the following simplifications. Anderson began these derivations by assuming a homogeneous fluid. Taking the time derivative for a control volume, he arrived the conservation of mass equation (equation 1-30).

$$\frac{d\rho}{dt} = \frac{(\dot{m}_{in} - \dot{m}_{out})}{V} \tag{1-30}$$

Using conservation of momentum and newton's second law to determine acceleration, the pressure drop could be found. Assuming constant density and velocity at control volume interfaces resulted in equation (1-31).

$$\Delta P = \frac{fL\dot{m}_{ave}^2}{2DA^2\rho_{ave}} \pm \rho_{ave} gL + \frac{L}{A}\left(\frac{d(\dot{m}_{ave})}{dt}\right) + \left(\frac{\dot{m}_{in}^2}{\rho_{in}A^2} - \frac{\dot{m}_{out}^2}{\rho_{out}A^2}\right) \quad (1\text{-}31)$$

When applying the first Law of Thermodynamics (Conservation of Energy), Anderson assumed constant volume for a homogeneous fluid and neglects gravitational and kinematic terms, yielding equation (1-32).

$$\dot{m}_{in}\dot{h}_{in} - \dot{m}_{out}\dot{h}_{out} + \dot{Q} = V\frac{d(\rho_{ave}u_{ave})}{dt} \quad (1\text{-}32)$$

From these equations, exit enthalpy, pressure, and mass flow rates were be computed from the inlet conditions. Relationships for enthalpy, pressure, and time are developed for the drum by again applying conservation of mass, momentum, and energy. Since there were two inlet and two outlet flow streams, the conservation of mass equation became equation (1-33). Assuming a homogeneous constant volume solution, while neglecting gravitational and kinematic terms and utilizing the relationship $u = h - \frac{P}{\rho}$, results in more extensive momentum (1-34) and energy (1-35) equations.

$$\frac{d\rho}{dt} = \frac{(\dot{m}_{eo}+\dot{m}_{wo}-\dot{m}_{st}-\dot{m}_{di})}{V} \quad (1\text{-}33)$$

$$\frac{dP}{dt} = \frac{\left(h+\frac{\rho}{d\rho/dh}\right)(\dot{m}_{eo}+\dot{m}_{wo}-\dot{m}_{st}-\dot{m}_{di})-(\dot{Q}+\dot{m}_{eo}\dot{h}_{eo}+\dot{m}_{wo}\dot{h}_{wo}-\dot{m}_{st}\dot{h}_{st}-\dot{m}_{di}\dot{h}_{di})}{V\left(\rho\left(\frac{d\rho/_{dP}}{d\rho/_{dh}}\right)+1\right)} \quad (1\text{-}34)$$

$$\frac{dh}{dt} = \frac{(\dot{Q}+\dot{m}_{eo}\dot{h}_{eo}+\dot{m}_{wo}\dot{h}_{wo}-\dot{m}_{st}\dot{h}_{st}-\dot{m}_{di}\dot{h}_{di})+\left(\frac{1}{d\rho/_{dP}}-h\right)(\dot{m}_{eo}+\dot{m}_{wo}-\dot{m}_{st}-\dot{m}_{di})}{V\left(\rho+\left(\frac{d\rho/_{dh}}{d\rho/_{dP}}\right)\right)} \quad (1\text{-}35)$$

The furnace component utilized common heat transfer equations to transfer gas side properties to the waterwall. This heat transfer was considered to be purely radiative and is given by equation (1-36)

$$Q = \varepsilon\sigma A_{surface}(T_2^4 - T_1^4) \quad (1\text{-}36)$$

Anderson (2008) explained that the pressure solver is proprietary but discloses that it functions based on a relay signal to the drum, containing instructions for how much liquid must exit the drum in order for drum pressure to be maintained. At the time of the study, the remaining components were not fully developed but would be based upon the same conservation principles, applying appropriate assumptions for each component to make simplifications.

Anderson's study also addressed numerical diffusion, a phenomenon occurring in most simulation software packages in which energy is conserved but the enthalpy profile becomes distorted prior to exiting the component. He explained that this was caused by using a lumped mass approach in which outlet properties are computed from average properties over the element. The effect of any enthalpy spikes became increasingly worse with slowed rates. Anderson developed a highly proprietary algorithm to confront such diffusion, by tracking inlet enthalpy and delaying transport across elements. Although such an algorithm will not be included in the scope of the study at hand, this could be a future consideration for continuation of the current condenser simulation.

Anderson (2008) incorporated a flow stream compressor into this model. Because all properties must be transferred from component to component, individual connections can cause the system model to become quite cluttered. Anderson developed a compressor which enabled simple transfer of properties between components. This compressor converted all properties into a single array, allowing for a single connection between components. Once the properties were transferred, they were again expanded for computations within the next block. For material properties, the m-file XSteam was used, and for air properties an m-file was created. XSteam will be used for the condenser model.

1.4 Scope of Work

The objective of this research was to model an air cooled condenser in MATLAB/Simulink that would handle a specified condensing load while controlling the outlet condensate temperature to a specified value, thus minimizing stressing of downstream components. A secondary goal was to minimize fan use, and thus electric use. This was done using a triple cascade control, measuring temperature, fan speed, and steam extraction percentage. Condenser parameters were assigned based on a generic condenser for desired output. Reasonable values were determined using software made available through Hudson Products ACHE software (2013). This calculator supplies typical design information such as fan speed and number of tubes based on desired output temperatures. Construction of the Simulink model consisted of fluid flow

through pipe segments and airflow across the pipes through a number of pathways. There was two pass steam flow through the tube bundles and three airflow pathways. The values obtained through the Hudson Products Calculator served as experimental data which was used for comparison purposes only. This study did not model Hudson ACC products directly, but future studies could address specific products. Recommendations were made for further development of this simulation.

CHAPTER II

GOVERNING EQUATIONS

2.1 Steam Side Nodes

The steam side nodes implement equations derived from standard conservation of mass, momentum, and energy equations. With some customary assumptions, these equations can be simplified for ease of use. The final equations were implemented in the simulation to calculate exit properties of the element and transport these properties to the adjacent elements. The water side nodes can be considered simple pipe segments, as shown below.

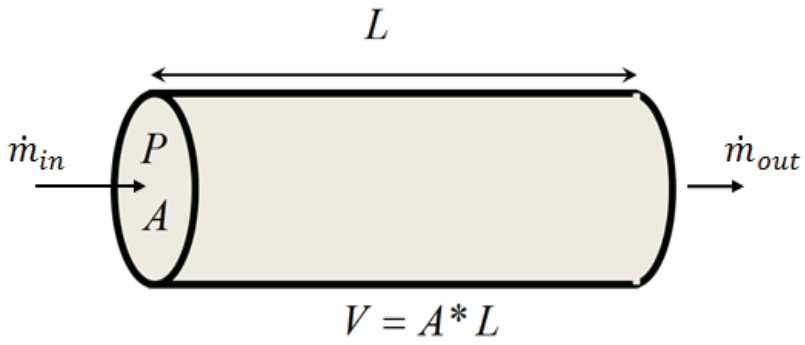

Figure 2.1 Pipe Segment

2.1.1 Conservation of Mass - Pipe Segments

The first equations which were considered are those for conservation of mass. Density for a homogenous fluid is given by:

$$\rho = \frac{m}{V} \tag{2-1}$$

The mass entering the control volume over a time period must equal the total of the mass leaving the control volume plus the change within the control volume. Symbolically, this is stated:

$$\left(\frac{\Delta m}{\Delta t}\right)_{in} \Delta t = \left(\frac{\Delta m}{\Delta t}\right)_{out} \Delta t + \Delta m \tag{2-2}$$

Where Δm can be defined as:

$$\Delta m = \left(\rho_f\right)V - (\rho_i)V = (\Delta\rho)V \tag{2-3}$$

Substitution of the above into equation (2-2) gives:

$$\left(\frac{\Delta m}{\Delta t}\right)_{in} \Delta t = \left(\frac{\Delta m}{\Delta t}\right)_{out} \Delta t + (\Delta\rho)V \tag{2-4}$$

Dividing through by Δt and rearranging results in equation (2-5).

$$\left(\frac{\Delta m}{\Delta t}\right)_{in} - \left(\frac{\Delta m}{\Delta t}\right)_{out} = \left(\frac{\Delta\rho}{\Delta t}\right)V \tag{2-5}$$

This can be written in derivative form as equation (2-6). The final form appears in equation (2-7).

$$\left(\frac{dm}{dt}\right)_{in} - \left(\frac{dm}{dt}\right)_{out} = \left(\frac{d\rho}{dt}\right)V \tag{2-6}$$

$$\dot{m}_{in} - \dot{m}_{out} = V\frac{\partial\bar{\rho}}{\partial t} \tag{2-7}$$

2.1.2 Conservation of Momentum – Pipe Segments

The conservation of momentum equations first require defining pressure drops associated with frictional, hydrostatic, inertial, and acceleration effects. These pressure drops are defined in equations (2-8) through (2-11).

Frictional pressure drop results from loss of energy to friction between the fluid and pipe walls. The final form of the pressure term is shown below.

$$\Delta p_f = \frac{fL\dot{m}_{ave}^2}{2DA^2\overline{\rho}} \tag{2-8-a}$$

Where f is the friction factor. This can be read from Moody's Diagram or determined from equation (2-8-b). This can be arranged in terms of pressure drop (2-8-c).

$$f \equiv \frac{-(dp/dx)D}{\rho(u)^2/2} \tag{2-8-b}$$

$$\Delta p_f = f\frac{\overline{\rho}(\overline{u})^2 L}{2D} \tag{2-8-c}$$

Substitution of $\dot{m}_{ave} = \bar{\rho}A\bar{u}$ produces the final form of the equation which was shown in equation (2-8-a).

The hydrostatic pressure term accounts for the pressure change due to a change in height. This is shown in equation (2-9) for a vertical pipe. Note that in cases of horizontal pipes, this pressure change is negligible.

$$\Delta p_g = \overline{\rho}gL \tag{2-9}$$

Both inertial (equation 2-10-b) and acceleration (equation 2-11-c) pressure terms arise from momentum changes, within the control volume, and at the control volume faces, respectively. This uses the relationship $F = \frac{d(mv)}{dt}$ and the equation shown below.

$$(\Delta p_i)A = F = \left(\frac{d(mv)}{dt}\right) \tag{2-10}$$

Within the control volume, this is written as equation (2-10-a) and can be rearranged as equation (2-10-b) for the inertial pressure drop.

$$(\Delta p_i)A = \left(\frac{d(\rho V v)}{dt}\right) = V\left(\frac{d(\dot{m}/A)}{dt}\right) \tag{2-10-a}$$

$$\Delta p_i = \frac{L}{A}\frac{\partial \dot{m}_{ave}}{\partial t} \tag{2-10-b}$$

At the faces of the control volume the equation can be approximated as shown in equation (2-11-a). Simplification results in the final equation (2-11-b).

$$(\Delta p_a)A = F \cong \left(\frac{(\rho_{out}V_{out})v_{out} - (\rho_{in}V_{in})v_{in}}{\Delta t}\right) \tag{2-11-a}$$

$$\Delta p_a = \left(\frac{\dot{m}_{out}^2}{A^2\rho_{out}} - \frac{\dot{m}_{in}^2}{A^2\rho_{in}}\right) \tag{2-11-b}$$

For this study, it was decided that a pressure solver would not be used, as it can create instability in the model. Instead, a flow boundary condition was used at the steam inlet and a constant pressure drop was imposed across each segment. The full momentum equation can be implemented later when a steam generation process (nuclear, fossil, etc.) is selected and a pressure-flow solver implemented.

2.1.3 Conservation of Energy – Pipe Segments

Derivation of the energy equations for the steam segments stems from the First Law of Thermodynamics (equation 2-12). Some reasonable assumptions can be made in order to simplify the full equation.

$$\frac{dE}{dt} = \dot{Q} - \dot{W} + \sum_{in} \dot{m}_{in}\left(u + \frac{P}{\rho} + \frac{V^2}{2} + gz\right)_{in} - \sum_{out} \dot{m}_{out}\left(u + \frac{P}{\rho} + \frac{V^2}{2} + gz\right)_{out} \quad (2\text{-}12)$$

Mechanical and potential energy can be neglected in most cases. Furthermore, there is no shaft work in simple pipe flow, so the $\dot{W}$ term drops out. Recognizing that $h = u + \frac{P}{\rho}$, allows the equation to be further simplified to equation (2-13).

$$\frac{dE}{dt} = \dot{Q} + \sum_{in} \dot{m}_{in} h_{in} - \sum_{out} \dot{m}_{out} h_{out} \quad (2\text{-}13)$$

Since pipe flow is an open system with a fixed volume, the energy term can be written as:

$$E = mu = \rho V u \quad (2\text{-}14)$$

In general form, conservation of energy through a control volume (such as a pipe segment), is given as equation (2-15). Note that this equation does not account for any heat generation. The energy storage term is defined in equation (2-16).

$$(\dot{m}_{in} h_{in})\Delta t = (\dot{m}_{out} h_{out})\Delta t + Energy\_Storage \quad (2\text{-}15)$$

$$\Delta(mu) = \left((\rho u)_f\right)V - \left((\rho u)_i\right)V = \left(\Delta(\rho u)\right)V \quad (2\text{-}16)$$

After substitution and dividing through by Δt, equation (2-16) can be written in derivative form:

$$\left(\dot{m}_{in} h_{in}\right) = \left(\dot{m}_{out} h_{out}\right) + V\frac{d(\rho u)}{dt} \quad (2\text{-}17)$$

If a heat source is generated within or flows into the control volume, another term, $\dot{Q}$, needs to be added. This heat source could come from electrical heating, chemical reactions, or standard heat transfer. In the case of the ACC, this term

arises from heat transfer between the steam and metal, and the metal and air. Upon adding this term, a simplified but complete conservation of energy equation is arrived at, which is applicable for pipe flow in the condenser model. The final form is shown in equation (2-18).

$$\left(\dot{m}_{in}h_{in}\right)+\dot{Q}=\left(\dot{m}_{out}h_{out}\right)+V\frac{d(\rho u)}{dt} \tag{2-18}$$

2.2 Air Flow

Air nodes will make use of similar equations, with further simplifications. For simulation purposes, air will flow through designated pathways, thus creating the same result as if the air were flowing past the tubes. These equations are somewhat simplified as ideal gas laws can be reasonably applied. The additional equation shown below can be used to easily calculate enthalpy values for the air.

$$h = C_p(T - T_0) \tag{2-19}$$

When applying the final form of the conservation of mass equation derived above (equation 2-6), the right hand side becomes zero in this scenario. This is based on the assumption of no swell. As the air passes quickly through each element, there is no chance for accumulation of volume, thus causing the term on the right side to be zero. Therefore, the mass conservation equation for the air flow becomes:

$$\dot{m}_{in} = \dot{m}_{out} = \dot{m} \tag{2-20}$$

To account for heat transfer through the air nodes, the conservation of energy equation from above (equation 2-18) is manipulated and the above relationship is

substituted to obtain average enthalpy (equation 2-21) for the air nodes. Average enthalpy can then be used to determine outlet temperatures using equation (2-19).

$$h_{ave}\rho = \left[\dot{m}(h_{in} - h_{out}) + \dot{Q}\right]\frac{\Delta t}{V} + \rho h_{out} \quad (2\text{-}21)$$

2.3 Heat Transfer Calculations

The metal nodes are where the heat transfer calculations take place. The heat transfer rate calculated in the metal nodes is then linked to the water and air sides. This calculation involves only one governing equation (equation 2-22).

$$\dot{Q} = hA(T_2 - T_1) \quad (2\text{-}22)$$

The equation above was used for simplicity, however derivations and simplifications of the complete heat transfer equations used to arrive at equation (2-22) are shown below. Pipes often use log mean temperature, but the model breaks the pipe into small sections, justifying use of ΔT, and avoiding all numerical problems. For heat transfer in a cylinder of length, L , three resistances are developed for radial heat transfer across two boundaries, as shown in Figure 2.2.

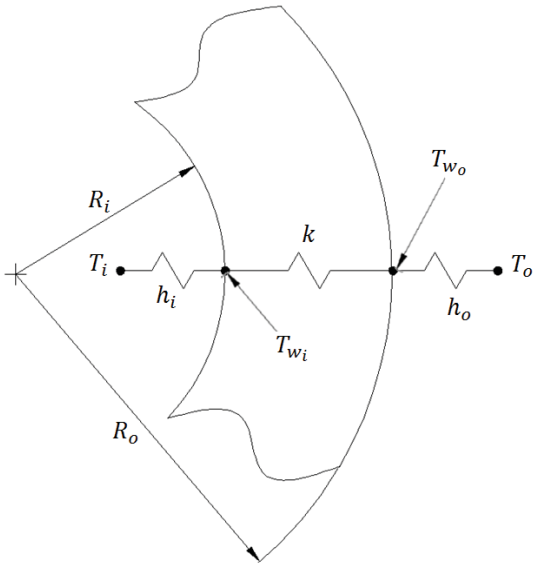

Figure 2.2 Heat Transfer Through Cylinder

For steady state heat transfer balance, heat transfer through the inside wall (Q_i), must be equal to heat transferred across the thickness of the wall (Q_m). Similarly, the heat transferred across the thickness of the wall must be equal to that transferred through the outer boundary (Q_o). Note from equations (2-23) through (2-26), that the heat transfer through the metal is due to conduction and the heat transfer between metal and fluid sides is convection.

$$Q_i = h_i \pi 2 R_i L (T_i - T_{w_i}) \tag{2-23}$$

$$Q_m = 2\pi L \frac{k}{ln\left[{R_o}/{R_i}\right]} (T_{w_i} - T_{w_o}) \tag{2-24}$$

$$Q_o = h_o 2\pi R_o L (T_{w_o} - T_o) \tag{2-25}$$

$$Q_i = Q_m = Q_o = Q \tag{2-26}$$

Solving each heat equation for temperature change, ΔT:

$$T_i - T_{w_i} = \frac{Q}{2\pi R_i L h_i} \tag{2-27}$$

$$T_{w_i} - T_{w_o} = \frac{Q ln\left[{R_o}/{R_i}\right]}{2\pi L k} \tag{2-28}$$

$$T_{w_o} - T_o = \frac{Q}{2\pi R_o L h_o} \tag{2-29}$$

Adding equations (2-27) through (2-29), a new heat transfer equation (2-30) is developed in terms of fluid temperatures only. Note that the bracketed term contains the resistance terms for each heat transfer equation. This can be rearranged into equation (2-31).

$$T_i - T_o = \frac{Q}{2\pi R_o L}\left[\frac{R_o}{R_i h_i} + R_o \frac{ln\left[{R_o}/{R_i}\right]}{k} + \frac{1}{h_o}\right] \tag{2-30}$$

$$Q = 2\pi R_o L \left[\frac{R_o}{R_i h_i} + R_o \frac{ln\left[{R_o}/{R_i}\right]}{k} + \frac{1}{h_o}\right]^{-1} (T_i - T_o) \tag{2-31}$$

This equation is in the form $hA(T_i - T_o)$, from equation (2-22), where the bracketed term is the overall heat transfer coefficient. Note that this coefficient is a function of both inside and outside tube diameters, but that during parameterization of the model, it was assumed that this value was based on the tube outer diameter only. It should be emphasized that for the model, a lumped approach was used.

The heat transfer rate is calculated for both air and water sides of the pipe wall. The net heat transfer rate of the metal is calculated and used to solve for the new temperature of the metal after each time step. Further equations must be used to calculate an overall heat transfer rate. For this calculation, the equations developed by Shah (1979) and parameters generated through the Hudson

Products calculator was used. Determination of this value will be further explained in the parameters section. The governing equations used for heat transfer modeling are derived below.

Using thermal resistance equivalencies, heat transfer coefficients for the water and air sides can be determined. This will allow for heat transfer coefficients to be employed in the simulation such that the manufacturer's overall heat transfer coefficient will be maintained. When applying these correlations, it is crucial to know what terms are accounted for in an overall heat transfer coefficient, such as the ones provided by the ACHE (2013) calculator. Typically the area that is used for overall heat transfer resistance, or total area (A_T) is the "bare tube" surface area, A_{OD}. We can begin by defining the relationship between thermal resistances (equation 2-23).

$$R_T = \frac{1}{h_T A_T} = \frac{1}{h_T A_{OD}} = R_{ID} + R_{OD} = \frac{1}{h_{ID} A_{ID}} + \frac{1}{h_{OD} A_{OD}} \tag{2-23}$$

Therefore, the overall heat transfer coefficient, h_T, can be defined as a function of inside and outside heat transfer coefficients and areas.

$$\frac{1}{h_T A_{OD}} = \frac{1}{h_{ID} A_{ID}} + \frac{1}{h_{OD} A_{OD}} \tag{2-24}$$

With the addition of two new dimensionless parameters, the equation can further be simplified. Let $\beta = h_{ID}/h_{OD}$ and $\alpha = A_{OD}/A_{ID}$. Rearrangement of equation (2-24) yields an equation for the inside heat transfer coefficient shown below. This can further be simplified into the final form in equation (2-25).

$$h_{ID} = h_T\left(\frac{A_{OD}}{A_{ID}} + \frac{h_{ID}}{h_{OD}}\right) \tag{2-24}$$

$$h_{ID} = h_T(\alpha + \beta) \tag{2-25}$$

It is important to note that both α and β are greater than one, and that β can be obtained through condensation heat transfer correlations (Shah, 1979). If the inside heat transfer coefficient is β times greater than the outside heat transfer coefficient, the outside heat transfer coefficient can be written in a similar manner:

$$h_{OD} = h_T\left(\frac{h_{OD}A_{OD}}{h_{ID}A_{OD}} + 1\right) = h_T\left(\frac{\alpha}{\beta} + 1\right) \tag{2-26}$$

Or simply:

$$h_{OD} = \frac{h_{ID}}{\beta} \tag{2-27}$$

With known physical geometry, an overall heat transfer coefficient, and the use of published condensation equations, internal and external convective heat transfer coefficients can easily be determined. The proof below is provided to demonstrate that the proposed method of heat transfer correlation will conserve the overall heat transfer coefficient.

By definintion:

$$R_T = \frac{1}{h_{ID}A_{ID}} + \frac{1}{h_{OD}A_{OD}} = \frac{1}{h_T(\alpha+\beta)A_{ID}} + \frac{1}{h_T\left(\frac{\alpha}{\beta}+1\right)A_{OD}}$$

Multiplying through by $h_T A_{OD}$ and rearranging:

$$R_T = \frac{1}{h_T A_{OD}}\left[\frac{A_{OD}}{(\alpha+\beta)A_{ID}} + \frac{A_{OD}}{h_T\left(\frac{\alpha}{\beta}+1\right)A_{OD}}\right] = \frac{1}{h_T A_{OD}}\left[\frac{\alpha}{(\alpha+\beta)} + \frac{1}{\left(\frac{\alpha}{\beta}+1\right)}\right]$$

Using a common denominator and simplifying:

$$R_T = \frac{1}{h_T A_{OD}}\left[\frac{\frac{\alpha}{\beta}}{\left(\frac{\alpha}{\beta}+1\right)} + \frac{1}{\left(\frac{\alpha}{\beta}+1\right)}\right] = \frac{1}{h_T A_{OD}}\left[\frac{\frac{\alpha}{\beta}+1}{\left(\frac{\alpha}{\beta}+1\right)}\right] = \frac{1}{h_T A_{OD}}$$

Finally, it is shown that the definition of total thermal resistance is maintained:

$$R_T = \frac{1}{h_T A_{OD}}$$

It should be noted that the overall heat transfer coefficient is dominated by the term with the largest resistance, or smallest h value. For cases of air flow over a tube h_o can be very small.

2.4 Fin Theory

In order to improve heat transfer across the tube, fins can be added in order to increase the surface area, as is the case with ACCs. Some correlations have been derived for heat transfer through annular fins and fin efficiency. Because the current condenser simulation is intended to be only a generic model, the following derivations are not used during simulation. However, it is important that the fin theory be addressed for future improvements.

For this derivation, begin by considering a rectangular fin, such as the one shown in Figure 2.3. Heat transfer across section Δx will be evaluated. The heat balance across this section is shown in equation (2-38).

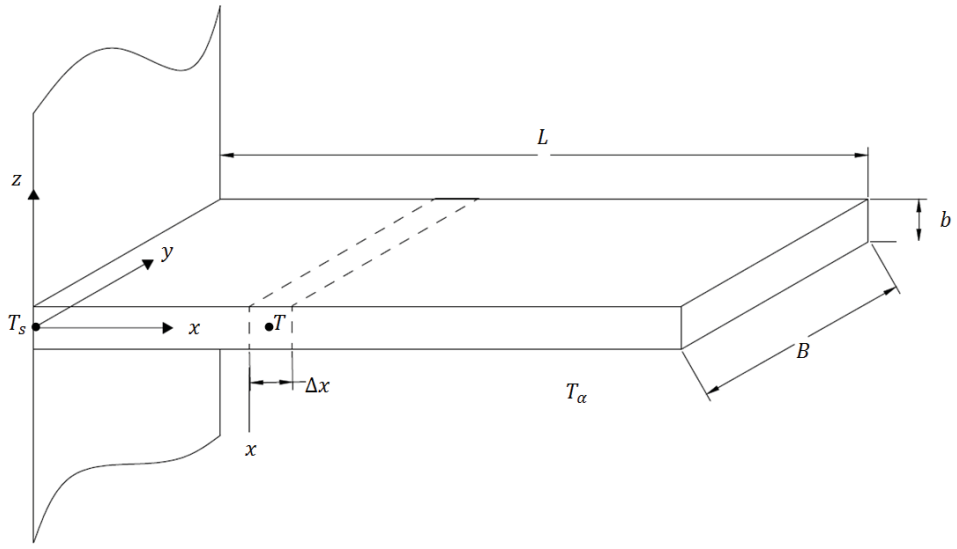

Figure 2.3 Rectangular Fin

$$(Bbq)|_x - (Bbq)|_{x+\Delta x} = 2hB\Delta x(T - T_\alpha) \tag{2-38}$$

$$\frac{q_x - q_{x+\Delta x}}{\Delta x} = 2\frac{h}{b}(T - T_\alpha) \tag{2-39}$$

This equation can then be written in derivative form. Note that q is the heat flux and is defined as $q = -k\frac{dT}{dx}$. Substitution of q results in equation (2-40). If one lets $m^2 = \frac{2h}{kb}$, the equation can be further simplified.

$$k\frac{d^2T}{dx^2} = 2\frac{h}{b}(T - T_\alpha) \tag{2-40}$$

$$\frac{d^2T}{dx^2} = m^2(T - T_\alpha) \tag{2-41}$$

From basic differential equations, it is known that the solution will take the form:

$$T - T_\alpha = C_1 e^{mx} - C_2 e^{-mx} \tag{2-42}$$

The constants C_1 and C_2 are to be obtained through boundary conditions. It is known that at $x = 0$ the fin temperature is the temperature of the wall. It can be assumed that tip of the fin is insulated. Therefore, heat flow is zero at $x = L$. These conditions can be expressed symbolically in equations (2-43) and (2-44). Upon solving these boundary conditions and much rearrangement, a final expression for the heat transferred through the fin can be obtained using equation (2-45).

$$@\ x = 0 \quad T = T_s \quad --\rightarrow \quad T_s - T_\alpha = C_1 + C_2 \tag{2-43}$$

$$@\ x = L \quad \frac{dT}{dx} = 0 \quad --\rightarrow \quad 0 = C_1 e^{mL} + C_2 e^{-ml} \tag{2-44}$$

$$Q_{fin} = (T_s - T_\alpha)\sqrt{2hkbB^2}\tanh(ml) \tag{2-45}$$

As previously stated, these fin equations were not used for determination of the model parameters. Because fin geometry was not known, manufacturer's data was used to solve for overall heat transfer coefficients on the inside and outside of tubes. These equations are however, important for a thorough understanding of how the model parameters may be chosen if the exact fin configuration is known.

CHAPTER III

MODELING METHODOLOGY

3.1 Flow Stream

The physical model consists of a total of 18 nodes, or segments. As previously stated, computations (based on the governing equations established in the previous chapter) take place in the element bock, allowing for outlet properties to be determined. These outlet properties must then be transferred along the flow path so that they may be used as inlet conditions for the next segment. Every output of a given function block represents the outlet conditions for the determined segment size. Therefore each outlet property must be individually connected to the adjacent nodes' input properties. This, in essence, simulates flow across the path. The response can then be viewed at individual nodes or simply the outlet conditions.

As this simulation is meant to be used only as a reasonable approximation of a typical condenser, a most basic model was used. It is quite possible that as the model becomes developed further, allowing for more complexity to be added, flow streams may be compressed with the use of a multi-variable array, as described in Anderson (2008). At this point, such a flow stream compression was deemed to be unnecessary.

3.2 Material Properties

Both fluid side components require that properties, such as enthalpy, density, pressure, and temperature can be determined at any point in time. To obtain the water side properties, a shareware m-file, XSteam was used. This file is made available through MathWorks, and allows for desired water properties to be returned at any point in time, given any other two properties.

No such m-file was readily available for the air side, but was ultimately deemed to be unnecessary. Air side properties were calculated as described earlier, using ideal gas laws and appropriate assumptions. Average enthalpy values were calculated within each metal block using the equations formulated in the previous chapter.

The only metal property that was needed for computations was the specific heat. Since this value remains approximately constant, it need be input only once, and could be used for all metal nodes. The temperature was calculated in each node, for every time step, as stated earlier.

3.3 Physical Model

The physical model excludes the controls and refers to only the condenser portion of the simulation. The physical model consists of the steam/water side, the metal interface, and the air side. An image of the physical model is provided in Figure 3.1. The water side (shown in red) is comprised of six nodes, or segments, and arranged in a two pass configuration. The air nodes (shown in

blue) are arranged in three separate pathways, each path with two nodes. This allows for interaction between each air node and the adjacent metal node, simulating cross flow. There are six metal nodes (shown in gray). These nodes, like the water nodes, are arranged in a two pass configuration, allowing for each node to interact with the water/steam flowing through and the air being pushed across.

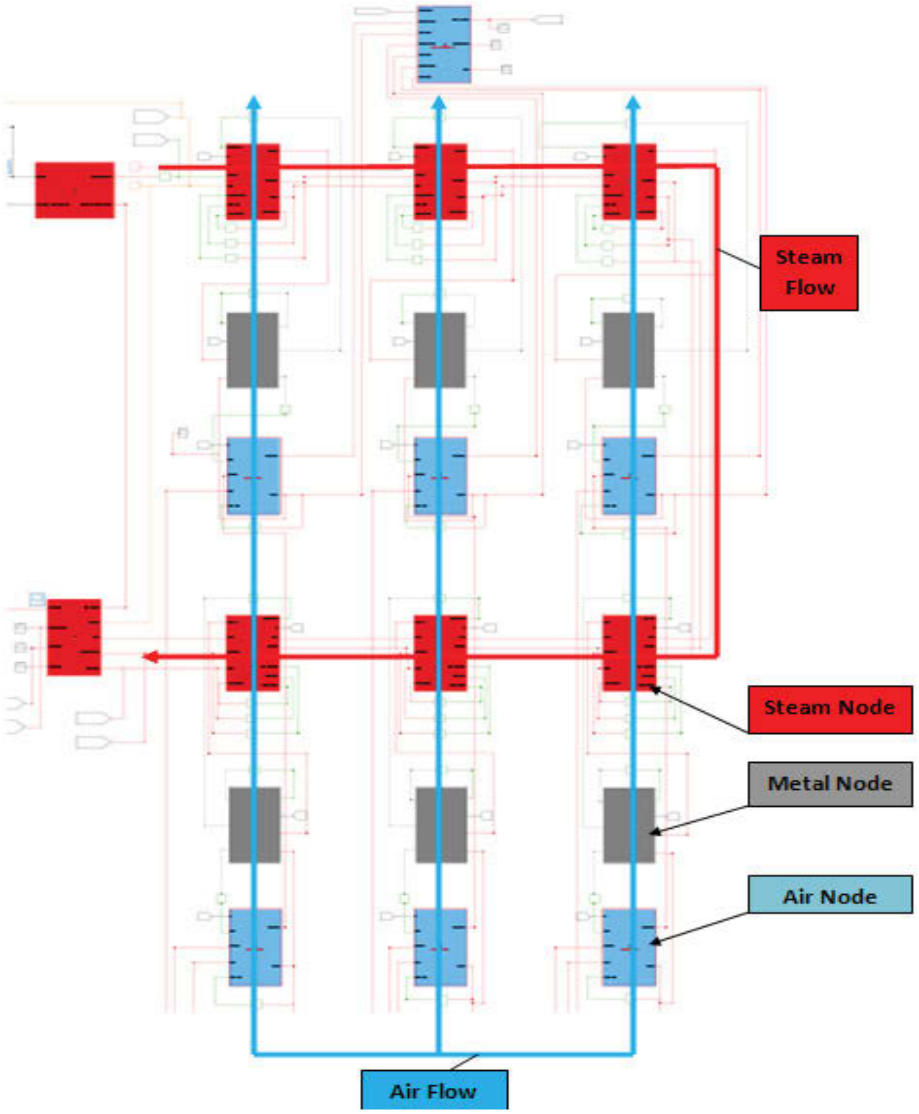

Figure 3.1 Physical Model

The model operates on a fixed time step, defined by the user. This model was run with a 0.1 second time step. It should be noted that determining a time step requires a tradeoff between solution convergence and simulation run time. A smaller time step typically results in better convergence, where as a larger time step will complete the simulation in a shorter time. Upon evaluation of results, it was gathered that a time step of 0.1 was likely an ideal decision for this simulation.

The physical model had to be fully functioning prior to implementing any controls. To do this, the streams were debugged one at a time. First, the water side stream was addressed. Initially, all nodes were disconnected, allowing for codes in the first node to be focused on. This was done by disconnecting the heat transfer between the metal nodes and the fluid. Once the first water node was running as expected, any necessary changes were made for the remainder of the water nodes. With the heat transfer still disconnected, the metal nodes and air pathways were debugged in a similar manner. Finally, the heat transfer between air and water sides was reconnected, completing the physical model.

3.4 Individual Streams

Three different coding blocks exist, one for each stream. All nodes for an individual stream operate on the same code. The most complex of the three codes is for the steam computations. This code implements a while loop to ensure convergence. The while loop computes individual convergence terms for

mass, momentum, and energy equations and then computes a total convergence term based on those three. The bock equations within the loop were then solved until the convergence criterion was met.

The codes used in the air and metal nodes were much simpler, and did not require convergence criteria to be met. Samples of all three codes are provided in Appendix B. It is possible that after a control scheme has been fine tuned, complexity could be added to the model, and therefore the codes. Such complexities will be addressed in the conclusions.

3.5 Control Logic

Initially, the simulation was run without a control loop to be certain of the physical model's integrity. Upon completing the physical model, an initial, simple control block was implemented, using only integral terms. This control system, shown in Figure 3.2, employs three control variables: steam extraction percentage, fans speed, and recirculation percentage. Error values were calculated by subtracting the appropriate target values from the current values. A triple cascade control is created as each error term is a measured by a different control. All three control variables were assigned target values, which are established in the parameters section.

The steam extract percentage (SEP) will produce the quickest response in temperature change, as it will be directly contributing to the condensate stream leaving the condenser. Therefore, SEP error term is calculated using condensate

outlet temperature as a measure. The fan speed (FS) is considered to have the next largest and fastest impact on the condensate temperature. This error term is calculated, using SEP difference from target as a measure. Finally, recirculation percentage (RP) is controlled, using the FS as a measure for the error term. Physically, this would be implemented through louver position. This is important, as ACCs may need to operate in subfreezing temperatures. A conditional control was also added so that the louvers will close, increasing the recirculation percentage in freezing conditions. This control, in essence is a winterization package.

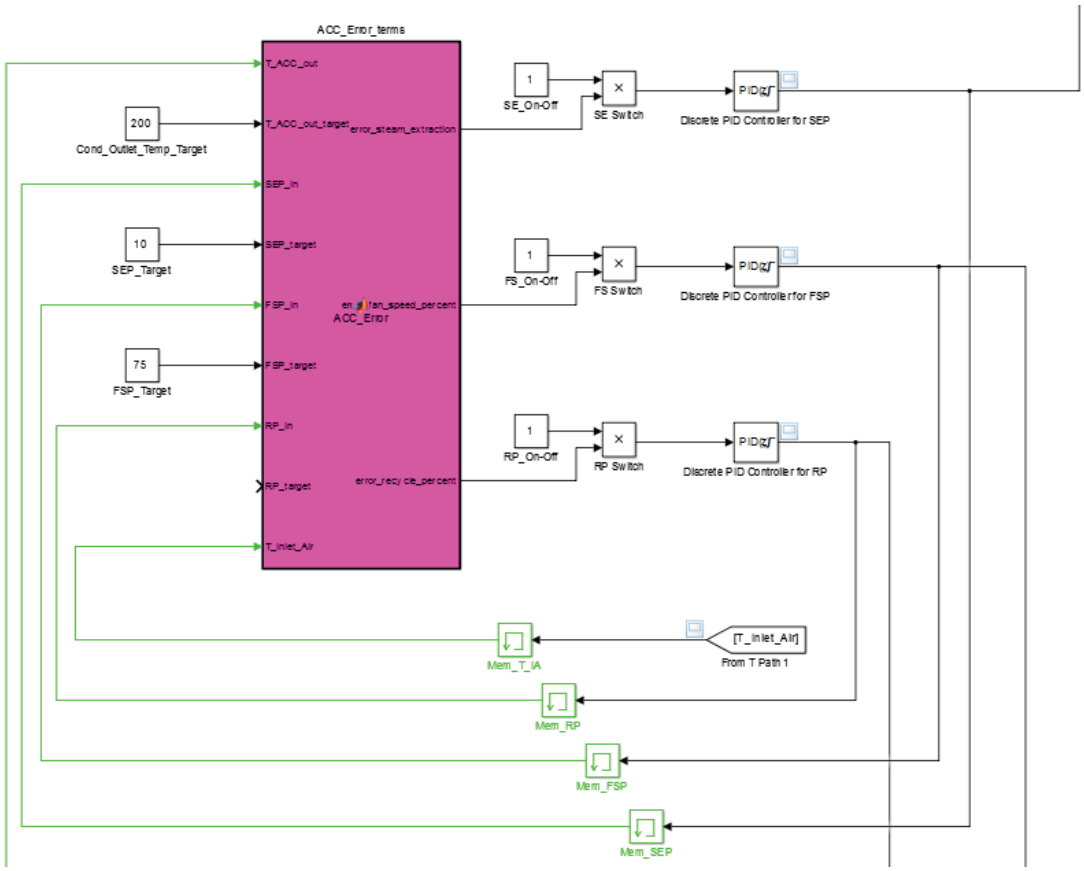

Figure 3.2 Initial Control Block

As different control schemes were being reviewed, another control logic block was developed. This logic, shown in Figure 3.3, is the same as the original, however this logic loop employs some new function blocks, including easy to use on/off switches. The lowest loop of this control is a conditional control, which imposes a physical limitation on the system for freezing conditions. At the time of this thesis, this form of the triple cascade control performed sufficiently, when run with a simple, generic process model. Due to time constraints, the version shown in Figure 3.3 has not been implemented successfully in the full scale ACC simulation.

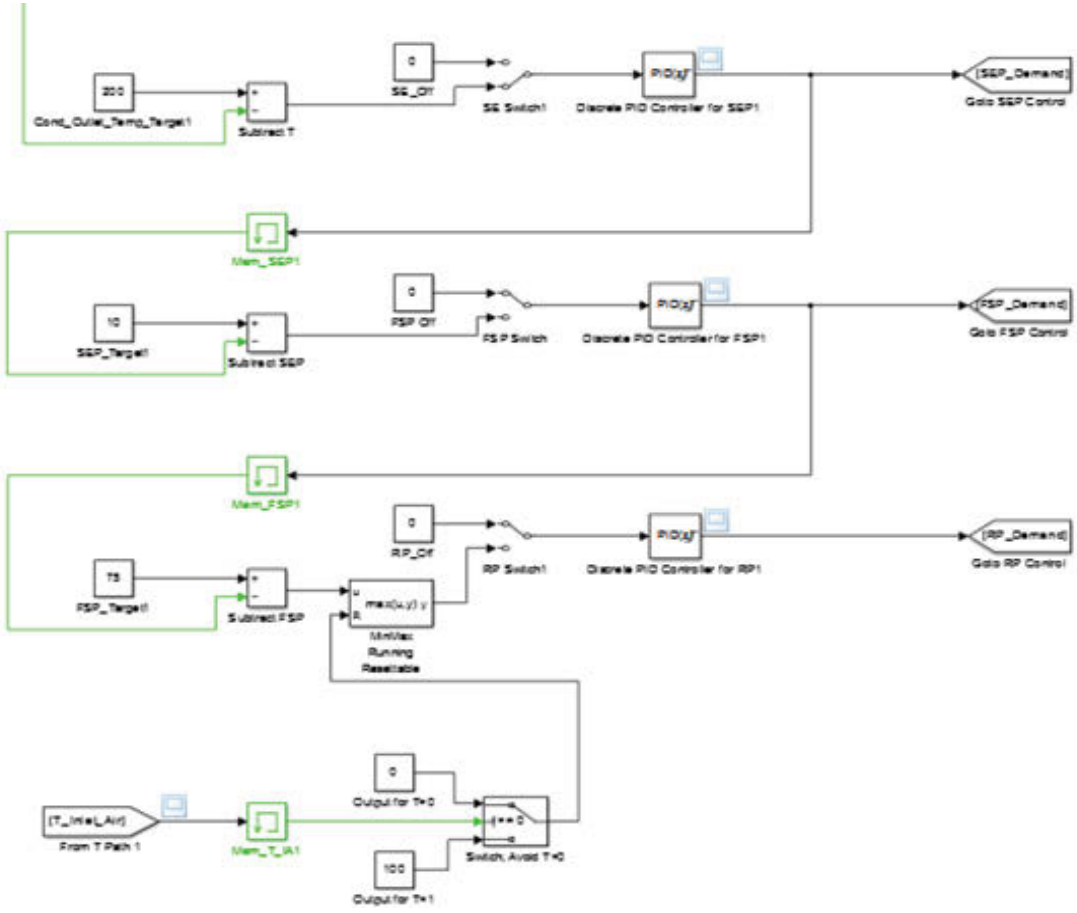

Figure 3.3 New Control Logic Blocks

3.6 Parameters

The model parameters were arrived at using Hudson Coolers manufacturer's data along with some assumptions. First, a reasonable condenser output was chosen. It was decided that a 1MW two pass condenser would be modeled. Two passes were chosen for simplicity of the model. After the model and controls are functional, more passes could easily be added. A 1 MW condenser offers capacity typically expected from a moderately sized power plant. Upon choosing the desired output and overall size for the condenser, values were input to the Hudson Calculator as shown below in Figure 3.4.

Figure 3.4 Hudson Calculator (ACHE, 2013)

The calculator provided material properties of the fins and tube as well as geometric and output values for the condenser and fan. Since the calculator did

not allow for two pass configurations operating at the desired pressure, values were calculated for multiple instances and interpolated to obtain reasonable model parameters. The original calculator output data is available in Appendix C, while results are summarized in Table 3.1.

Table 3.1 Hudson Calculator Results Summary

SCENARIO 1		**SCENARIO 2**		**SCENARIO 3**	
Selections		**Selections**		**Selections**	
Service:	Condensing	Service:	Condensing	Service:	Condensing
Units:	Metric	Units:	Metric	Units:	Metric
Hot Tube Side Fluid:	Steam @ 0 to 20 psig	Hot Tube Side Fluid:	Steam @ 0 to 20 psig	Hot Tube Side Fluid:	Steam @ 0 to 20 psig
Fan Draft:	Forced	Fan Draft:	Forced	Fan Draft:	Forced
Input Parameters		**Input Parameters**		**Input Parameters**	
Heat Duty:	1 MW	Heat Duty:	1 MW	Heat Duty:	1 MW
Inlet Hot Fluid Temp:	300°C	Inlet Hot Fluid Temp:	300°C	Inlet Hot Fluid Temp:	300°C
Outlet Hot Fluid Temp:	200°C	Outlet Hot Fluid Temp:	200°C	Outlet Hot Fluid Temp:	200°C
Inlet Air Temp:	20°C	Inlet Air Temp:	20°C	Inlet Air Temp:	20°C
Tube Length:	3	Tube Length:	3	Tube Length:	3
Tube Rows:	3	Tube Rows:	4	Tube Rows:	5
Tubes and Headers:	Steel	Tubes and Headers:	Steel	Tubes and Headers:	Steel
Heat Exchanger Output Parameters		**Heat Exchanger Output Parameters**		**Heat Exchanger Output Parameters**	
Air Flow Rate:	7.83 kg/s	Air Flow Rate:	7.83 kg/s	Air Flow Rate:	7.83 kg/s
Heat Transfer Rate:	809 W/m²-°C	Heat Transfer Rate:	809 W/m²-°C	Heat Transfer Rate:	809 W/m²-°C
Tube OD:	25.4 mm	Tube OD:	25.4 mm	Tube OD:	25.4 mm
Tube Thickness:	2.79 mm	Tube Thickness:	2.79 mm	Tube Thickness:	2.79 mm
Tubes /Row:	15	Tubes /Row:	10	Tubes /Row:	10
Total Tubes:	45	Total Tubes:	40	Total Tubes:	50
Bare Tube Surface Area:	10.8 m²	Bare Tube Surface Area:	9.58 m²	Bare Tube Surface Area:	12.0 m²
Fin Material:	Aluminum	Fin Material:	Aluminum	Fin Material:	Aluminum
Fin Tube Surface Area:	228 m²	Fin Tube Surface Area:	228 m²	Fin Tube Surface Area:	229 m²
Exchanger Width:	0.91 m	Exchanger Width:	0.61 m	Exchanger Width:	0.61 m
Motor shaft Power:	1.78 KW	Motor shaft Power:	1.31 KW	Motor shaft Power:	1.40 KW

As described in the theory, multiple heat transfer coefficients needed to be included in the simulation. Since the Hudson Products calculator only provides and overall heat transfer coefficient, heat transfer coefficients were determined for the steam side and air side using Shah's equations. The spreadsheet used for these calculations is included in Appendix B. All global and geometric parameters were first calculated in a parameters function block. Parameter blocks were created for ease of use. These codes are available in Appendix B and a comprehensive collection of the parameters is shown in Table 3.2.

Table 3.2 Model Parameters

Global Parameters - Steam Side	
Inlet Pressure	85.77 bar
Inlet Enthalpy	2749.6 kJ/kg
Outlet Pressure	85.28 bar
Outlet Enthalpy	855.3 kJ/kg
Mass Flow Rate	0.528 kg/s
Inlet Density	46.17 kg/m³
Outlet Density	869.9 kg/m³
Condenser Sizing (ACC Parameters)	
Outlet Pressure	85.28 bar
Outlet Enthalpy	644.8 kJ/kg
Outlet Temperature	151.7 °C
Geometric Parameters	
Steel Density	7841.7 kg/m³
Tube Mass	186.4 kg
Total Volume	0.037 m³
# of Tubes	40
Tube ID	0.0198 m
Tube ID Surface Area	7.4682 m²
Tube OD Surface Area	9.5707 m²
Tube Cross Section	0.0123 m²

Note that the condenser pressure (Table 3.2) was much higher than that which was used for the Hudson Calculator (2013) data in Table 3.1. The heat transfer calculations (Figure B.9) allowed for comparison between the extrapolated high pressure model values with the low pressure manufacturer's values.

CHAPTER IV

RESULTS

4.1 Incremental Testing

Due to the nature of this model, it was decided to evaluate results at key stages of the build and tuning process as well as at the most comprehensive simulation level. Since the model can be broken into physical and control components, it was important to analyze each before making any conclusions regarding the simulation as a whole. Furthermore, various control sections have been developed, allowing for comparison of results between the two.

First, it was relevant to perform analysis of the physical model alone. This was done by disconnecting the control section of the model from the physical portion of the model. The model was run at a time step of 0.1 seconds for a span of 7200 seconds. For comparison reasons, all results were generated from models running with the same parameter configurations. The response for the condensate outlet temperature is shown in Figure 4.1. Additional properties for this particular test are included in the appendix. As expected, without the controls, the outlet temperature is not maintained at the ideal 200°C. This graph will be referenced against the full model simulation to illustrate effectiveness of the controller.

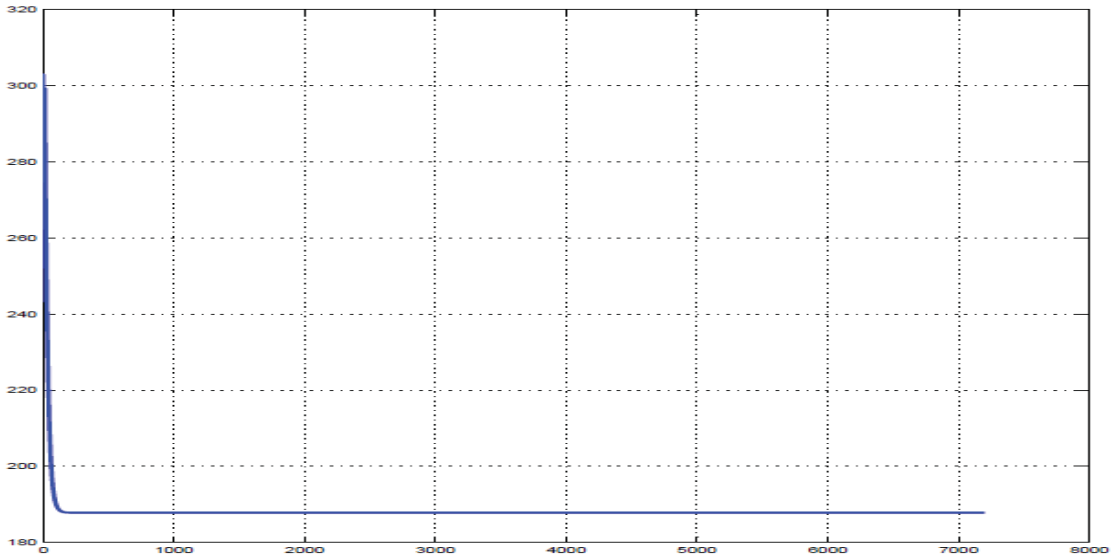

Figure 4.1 Condensate Temperature Response – No Controls

Both control set ups that were discussed in the methodology section were also tested, although only one of them was used in the full model simulation. Ideally, the more recently developed control interface will eventually be used in conjunction with the physical model. Due to time constraints, this newer control system could not yet be incorporated in the full system model. It has, however, been tested with a generic process model to demonstrate its functionality. All controls were tuned using PID coefficients. Results from this testing are presented in Figures 4.2 through 4.5. Additional trials were conducted using Integral control only, in order to investigate whether such a method would be a viable option. It was ultimately decided that all three coefficients would be used for the full model simulation. Results from trials using only Integral control are included in the appendix.

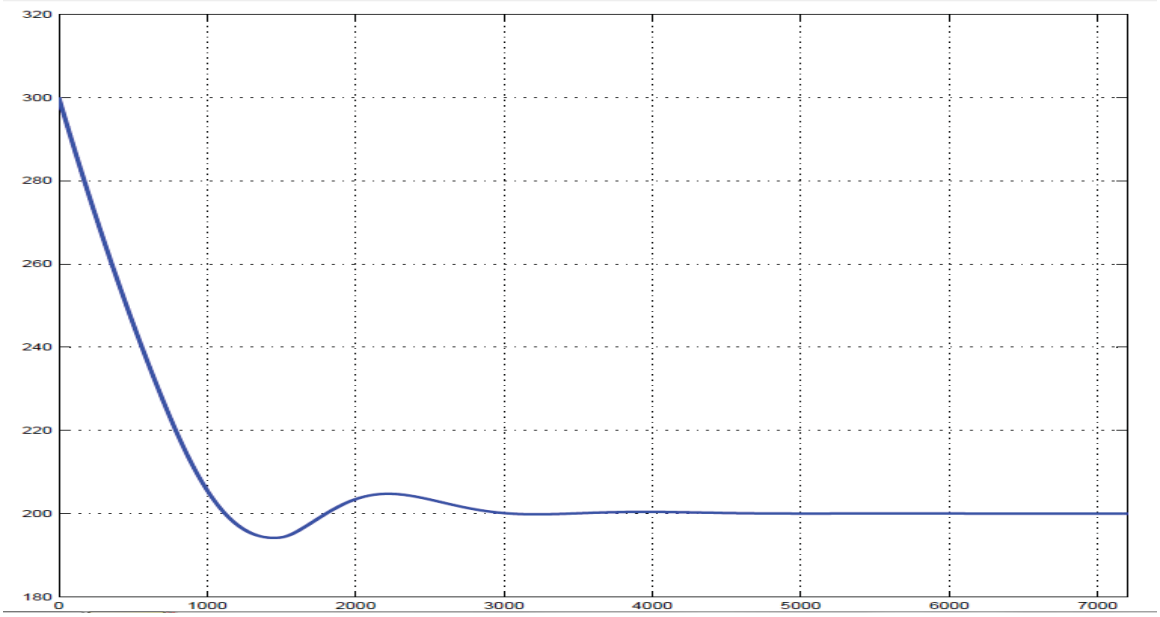

Figure 4.2 Condensate Temperature – New (PID) Controls with Generic Model

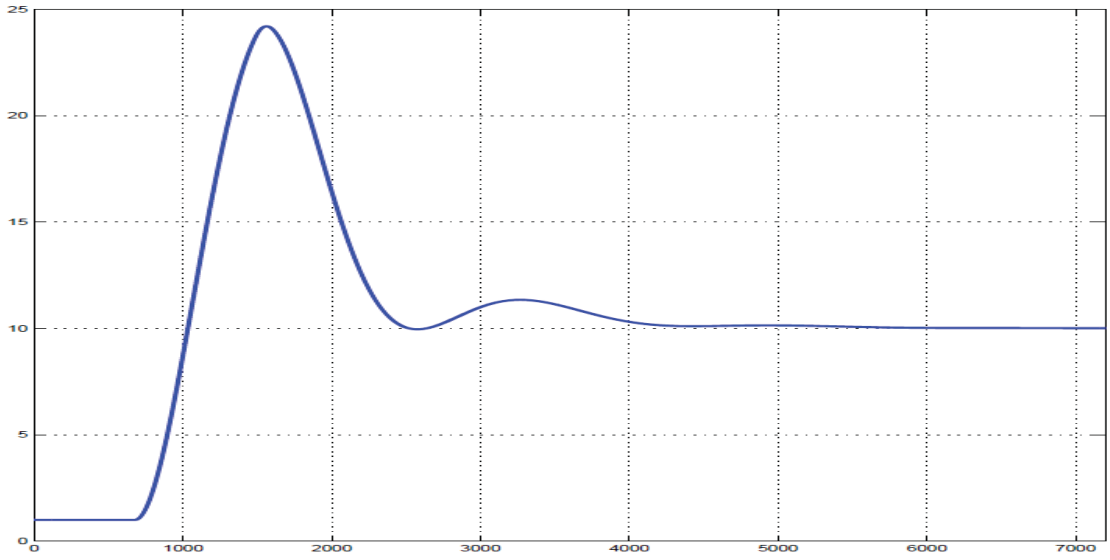

Figure 4.3 Steam Extraction Percent – New (PID) Controls with Generic Model

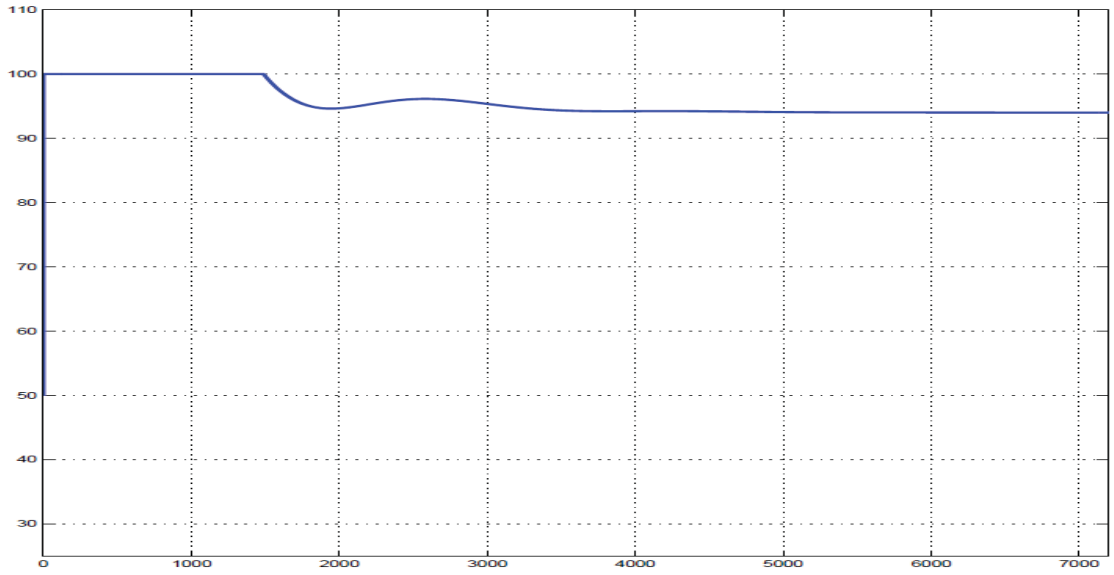

Figure 4.4 Fan Speed Percent – New (PID) Controls with Generic Model

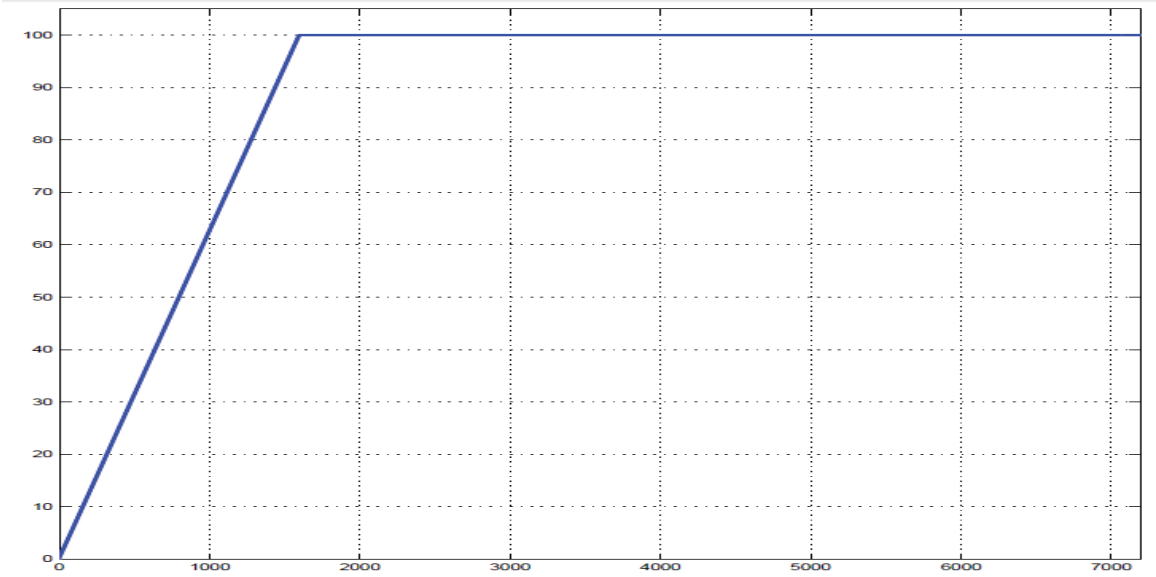

Figure 4.5 Steam Extraction Percent – New (PID) Controls with Generic Model

Note the smoothness of these results. All process variables demonstrate exceptional control, with only minor deviations from their respective target

values. Although these particular Simulink blocks have not been successfully incorporated into the full scale condenser model, results from this model support the triple cascade control theory.

During tuning of the original control parameters, results were examined for progressive levels of system control. The first group of results was taken using only steam extraction as a means of control. The next collection of system responses was taken using both steam extraction and fan speed to control the system. Finally, results were obtained using all three control variables (steam extraction, fan speed, and air recirculation percentage). Relevant results from the final tuning of these parameters are shown below. Additional system responses can be found in the appendix.

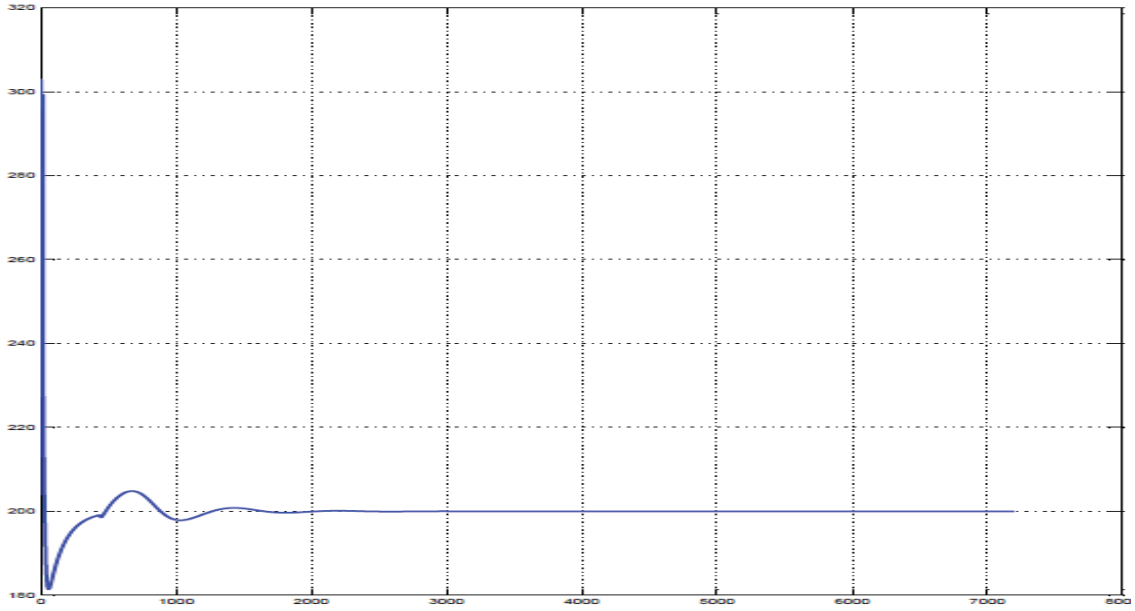

Figure 4.6 Condensate Temperature – (PID) Control – Ambient Air @ 20°C

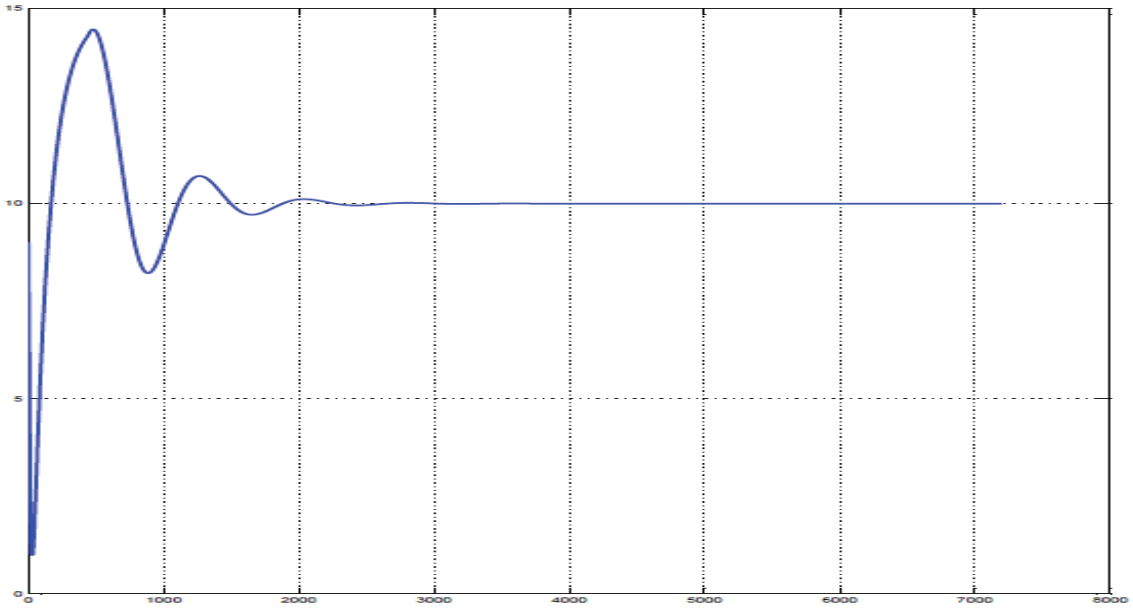

Figure 4.7 Steam Extraction Percent – (PID) Control – Ambient Air @ 20°C

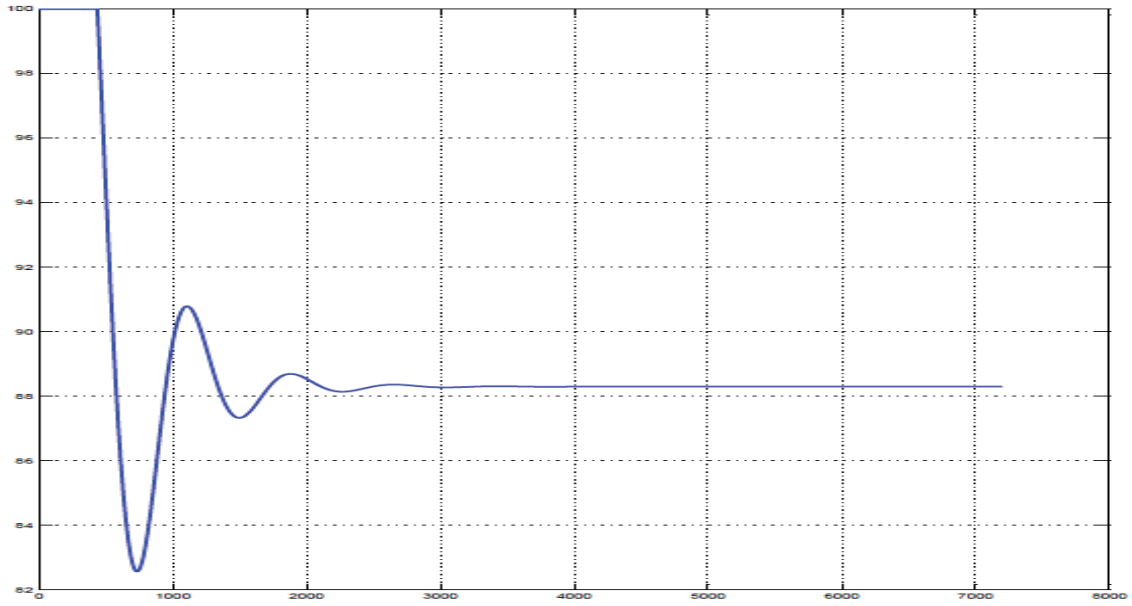

Figure 4.8 Fan Speed Percent – (PID) Control – Ambient Air @ 20°C

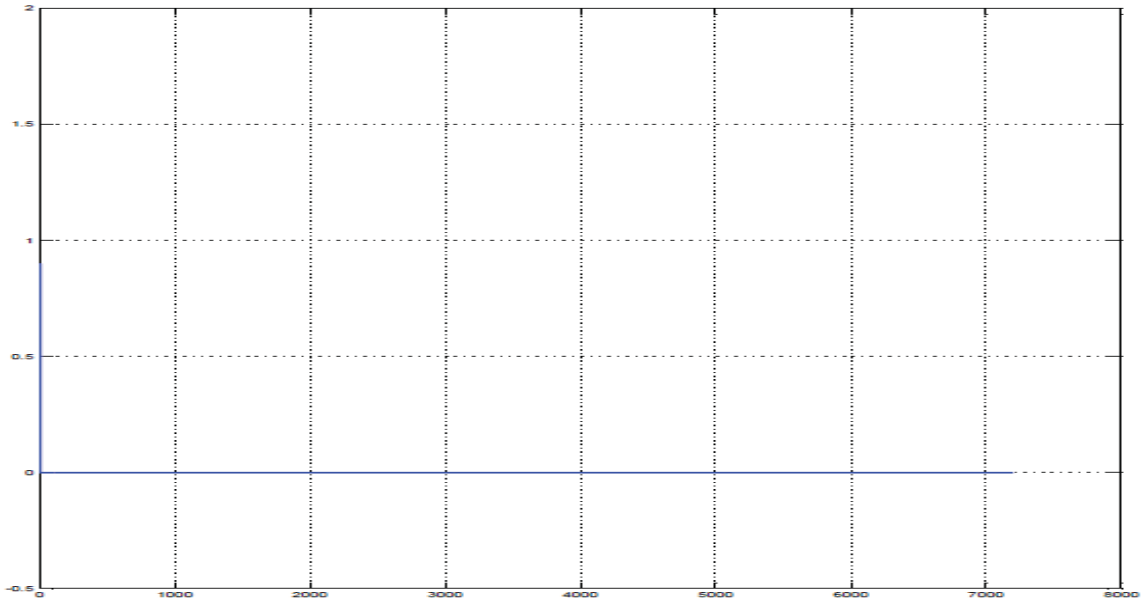

Figure 4.9 Recirculation Percent – (PID) Control – Ambient Air @ 20°C

With the current control settings, the temperature and steam extraction percents are tuned sufficiently to the target values. Note, however, that the fan speed percent (Figure 4.8) reaches steady state at approximately 88 percent. This is a 13 percent difference from the target fan speed. Take note too of the air recirculation percentage response (Figure 4.9) and the recirculation percent error term (Figure A.12). The recirculation percentage is steady at zero percent while the error term is 13, corresponding to the deviation in fan speed percent. This is acceptable, as the fan speed “target” value is actually a floor rather than a true target. If the fan were operating below its target percent, more air would recirculate, causing the demand for fan speed to increase in order to maintain the target ACC temperature and steam extraction percent. However, the fan speed is above “target”, and would require a decrease in air recirculation in order

to reach target. Since the minimum recirculation percentage is zero percent, no further adjustment could be made to correct the fan speed. Therefore, the fan speed is maintained in the target range. The 88 percent fan speed which is reached in the graphs above is the physical limit for the fan speed in this instance.

Recall too that if ambient air temperature drops below freezing, the control should automatically adjust the louvers such that there is 100 percent circulation. To demonstrate effectiveness of this control under the given circumstances, an additional test was run with ambient air at -10°C. These control responses are shown in Figures 4.10 through 4.13, with additional system properties included in the appendix.

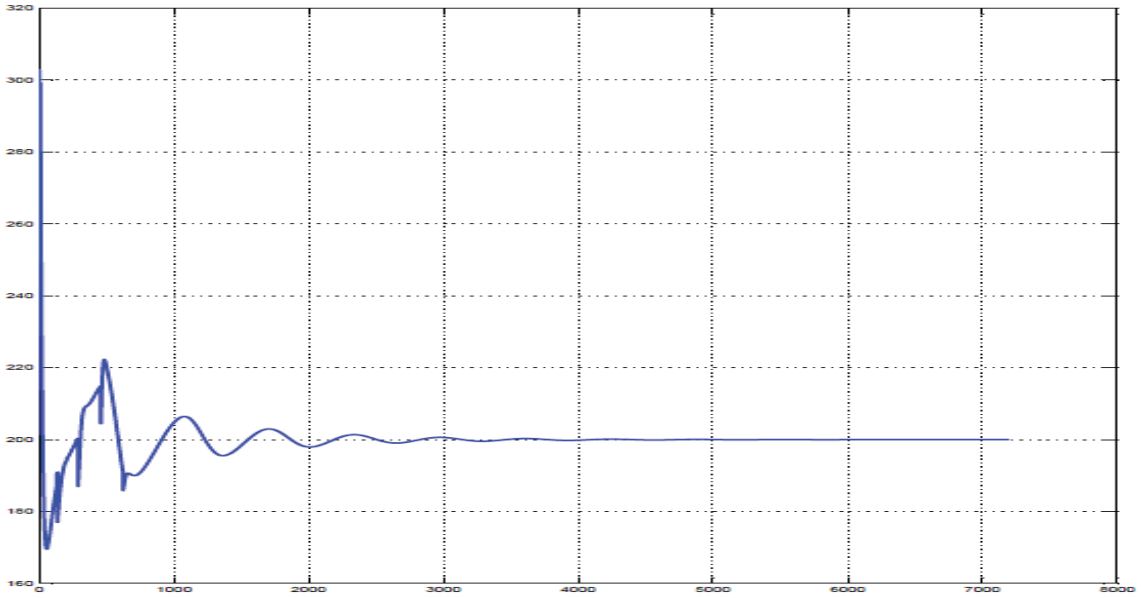

Figure 4.10 Condensate Temperature – (PID) Control – Ambient Air @ -10°C

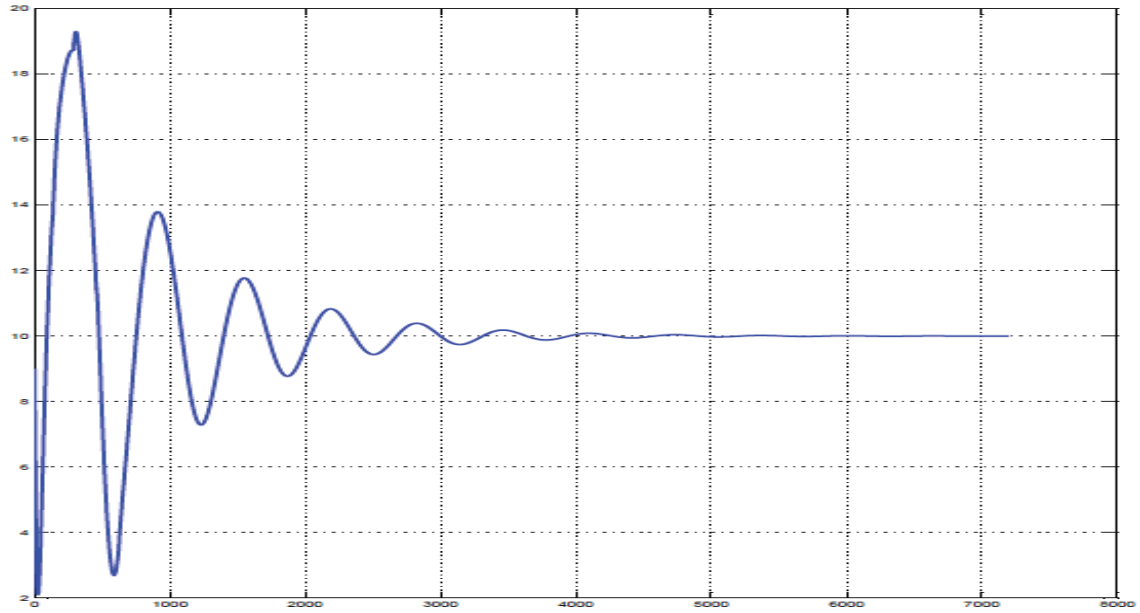

Figure 4.11 Steam Extraction Percent – (PID) Control – Ambient Air @ -10°C

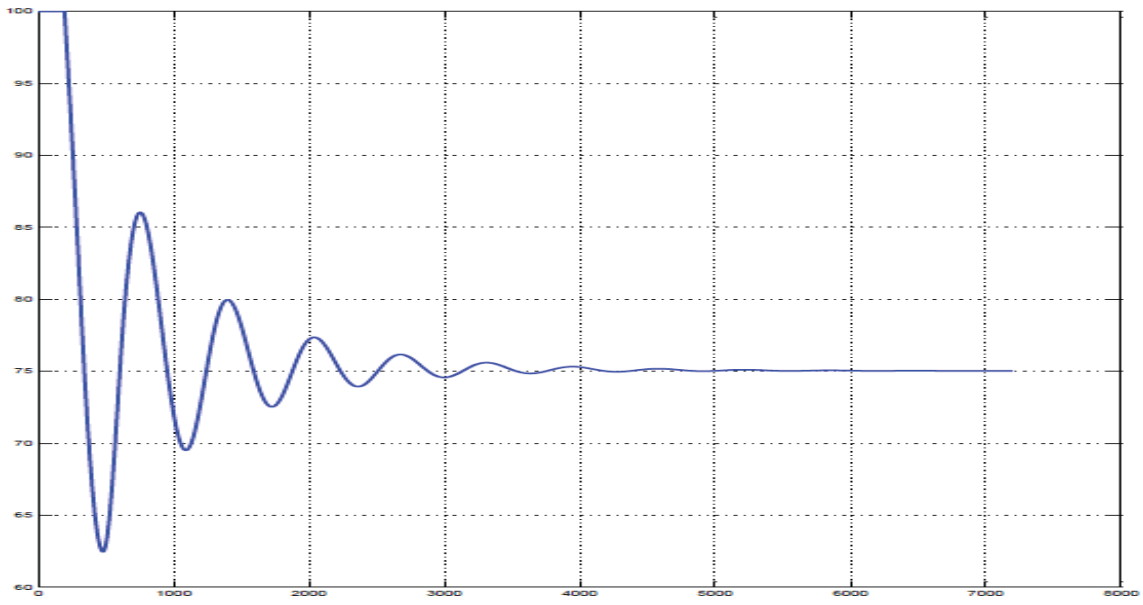

Figure 4.12 Fan Speed Percent – (PID) Control – Ambient Air @ -10°C

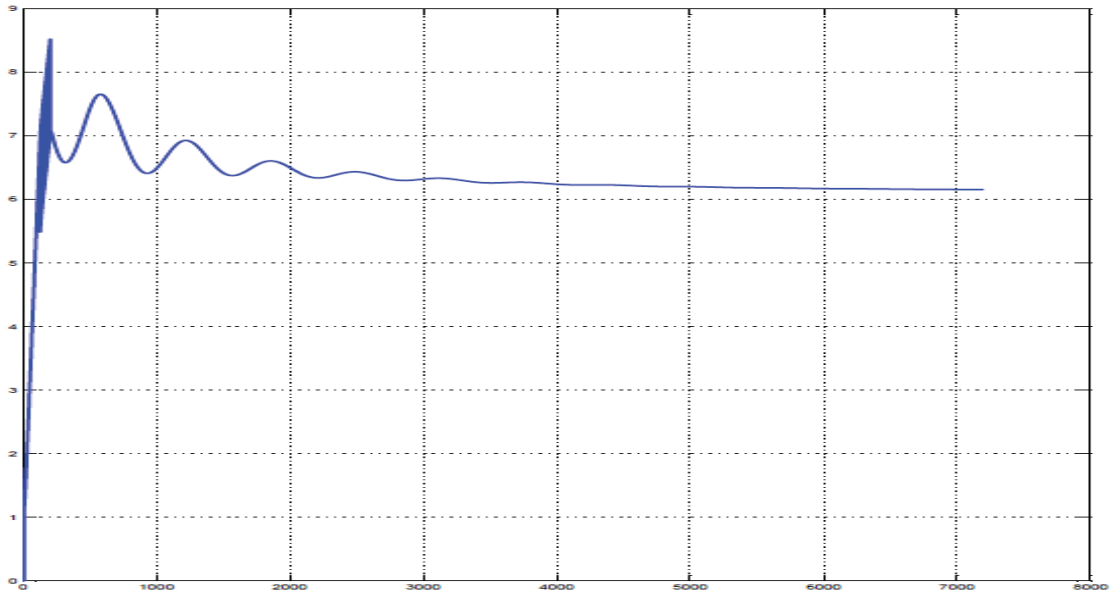

Figure 4.13 Recirculation Percent – (PID) Control – Ambient Air @ 20°C

Responses at ambient air temperature of -10°C are satisfactory, as the recirculation percent is able to maintain the fan speed at target, or “floor” value. In this case, the recirculation percent increases in order to maintain condensate outlet temperature without requiring fan speed to fall below the target 75 percent. It should be noted that while the temperature is controlled fairly well, optimal tuning of this control scheme has yet to be achieved, as will be demonstrated in the next section. It is possible, that better initial conditions may have lessened the amplitude of the initial oscillations. Optimal tuning will require precise tuning of PID coefficients for all three control variables. This trial and error tuning style demands execution of many simulations.

4.2 Disturbances

All incremental results reflect the system responses without the introduction of input disturbances. After acceptable tuning coefficients were identified, the system response to a number of disturbances was tested. Because of the errors experienced with introduction of the PID control, the disturbances were tested using two different models; one with PID control and another with Integral only control. It was hoped that with only three coefficients to adjust, more effective tuning could be achieved. Unfortunately, this method provided no advantage over the full PID control and therefore the Integral only results were excluded from this report.

The first disturbance introduced to the system was a nominal ramped load change. This was simulated by ramping the mass flow into the condenser. The ramp begins at 1800 seconds and ranges from full load (0.528kg/s) to 20 percent load (0.1065 kg/s). Simulations were run at the original ambient air temperature of 20°C. The most pertinent control responses are shown in Figures 4.14 thru 4.17, with additional property scopes in the appendix.

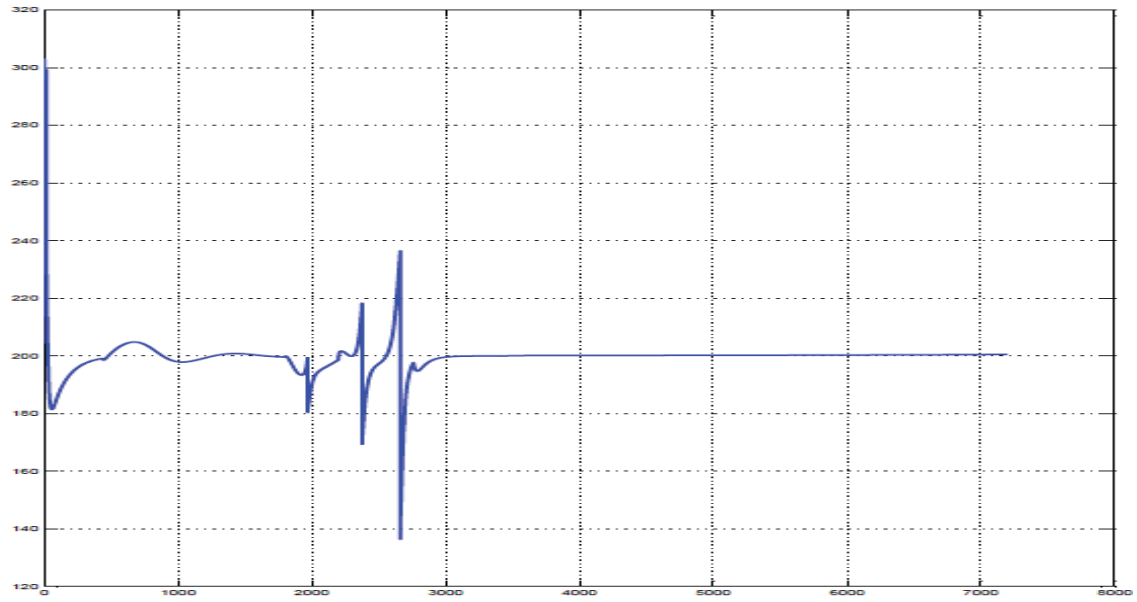

Figure 4.14 Condensate Temperature – (PID) Control with Ramped Load

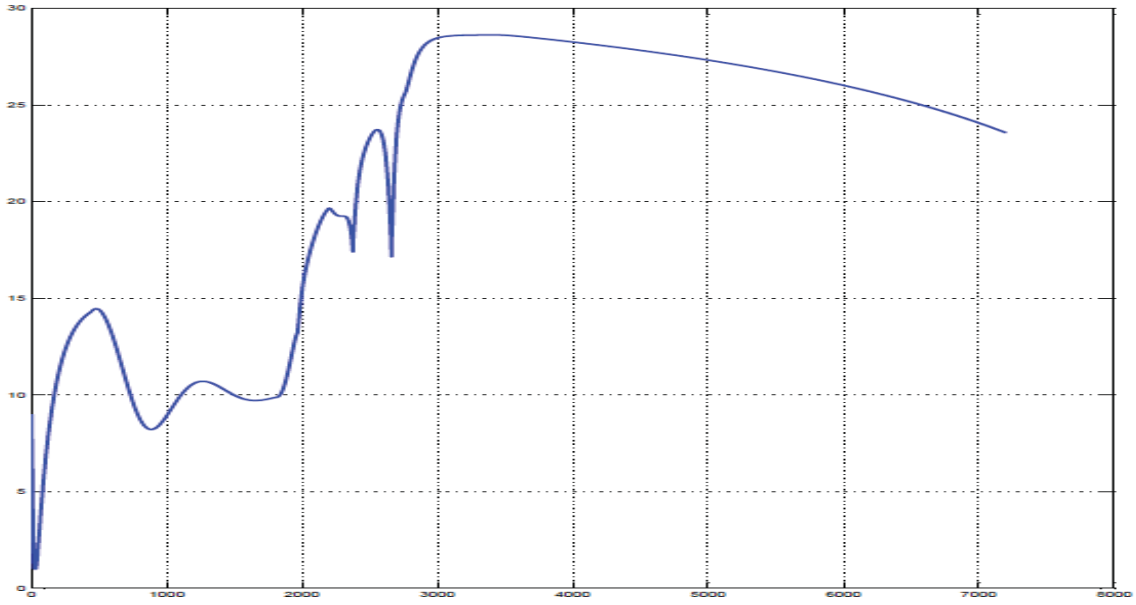

Figure 4.15 Steam Extraction Percentage – (PID) Control with Ramped Load

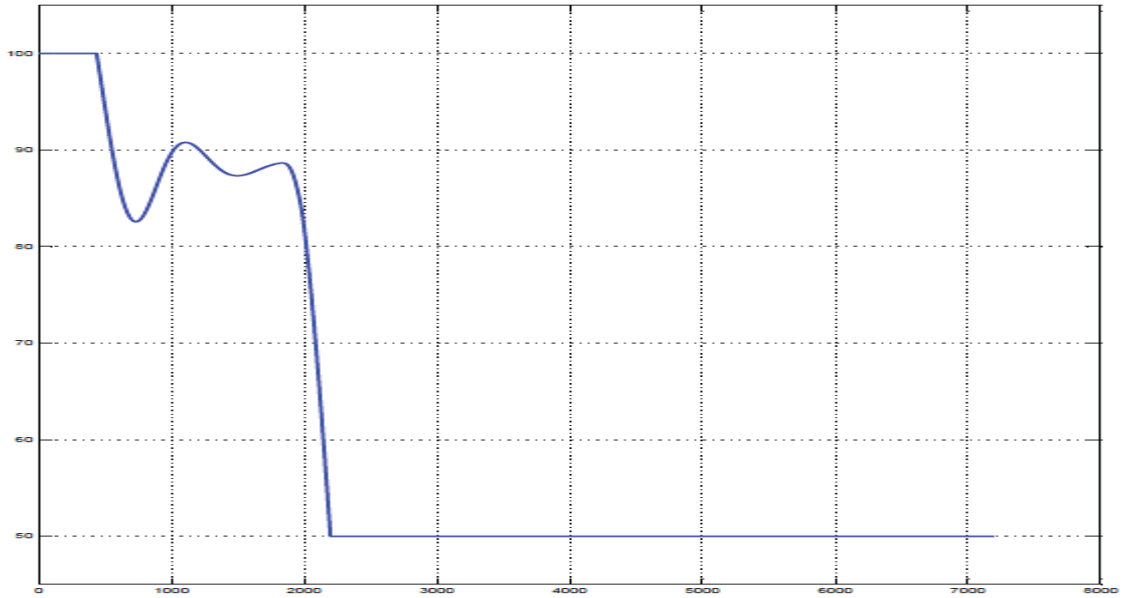

Figure 4.16 Fan Speed Percentage– (PID) Control with Ramped Load

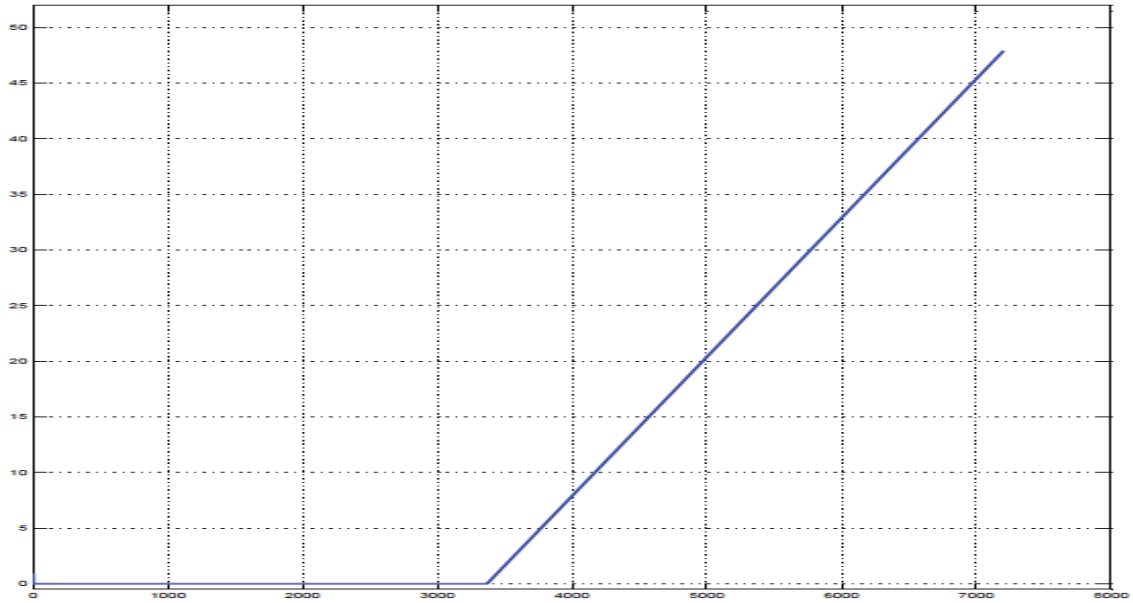

Figure 4.17 Recirculation Percentage– (PID) Control with Ramped Load

These responses will require additional tuning to minimize the effects of the mass load change. After several iterations, it is likely that the process variable could be maintained to their set points.

For the final test, off-nominal spikes in mass flow were introduced to the system, through use of a square input wave. The wave was created through the use of a pulse generator, having five pulses throughout the duration of the simulation. The magnitudes of the pulses were ± 10 percent of the originally sized mass flow rate. The temperature response (Figure 4.18) illustrates the lack of control over the mass flow spikes. Although the largest spikes are quickly corrected, target condensate temperature is manitained for little time. Additional responses of interest are included in the appendix. From this test, it is again gathered that the current control settings do no sufficiently minimize the effect of this transient input disturbance.

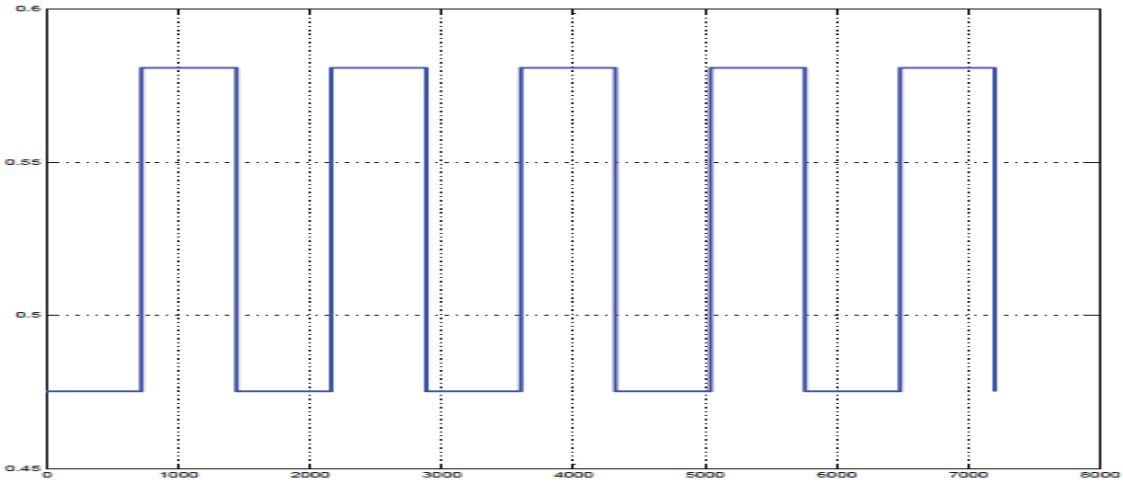

Figure 4.18 Inlet Mass Flow Rate – (PID) Control with Mass Load Spikes

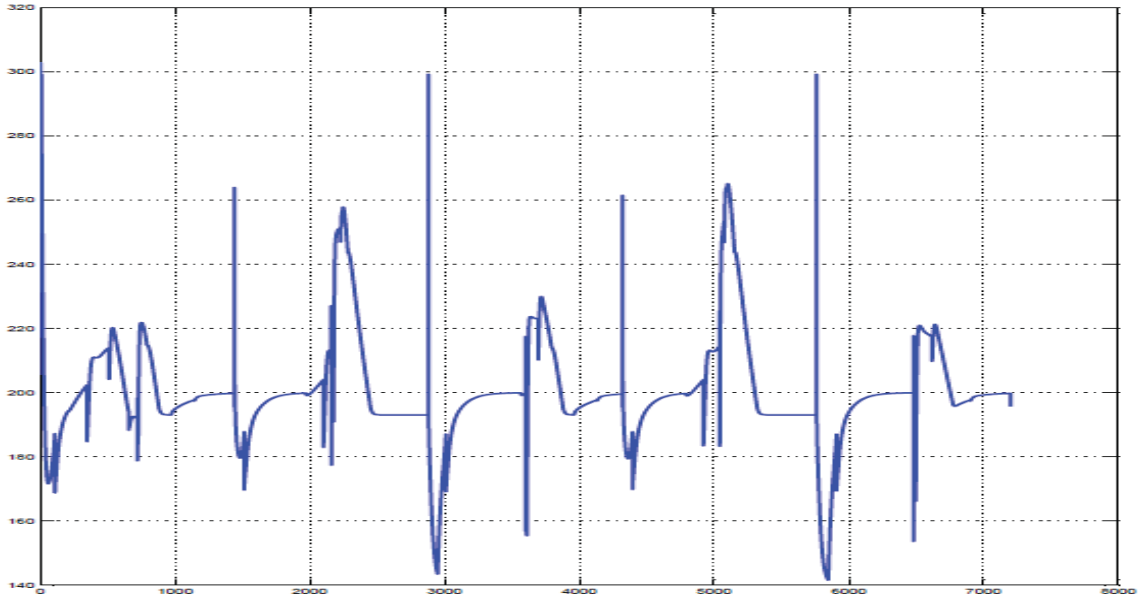

Figure 4.19 Condensate Temperature – (PID) Control with Mass Load Spikes

Although the outlet temperature shows spikes in upwards of 300°C, it should be noted that such mass spikes are not physically feasible, and the pulse was only meant to generate a worst case scenario. Attention should be placed on the instants of infinite slope in the mass flow rate. A smoother, more realistic input would have likely been controlled much better. Despite the temperature spikes, the controller maintains a median temperature value of 200°C, as desired. Further tuning would likely produce better results. As previously mentioned, trial and error tuning generally demands many iterations before an optimal solution is reached.

CHAPTER V

DISCUSSION AND RECOMMENDATIONS

5.1 Discussion

The current model produced successful results for both steady state models that were tested. Although transient models will require further iterations to achieve optimal tuning, much has been accomplished in this study. Both the favorable outcomes and the shortcomings of the model will be addressed.

If the model is again divided into physical and control sections, the physical model may be considered the more successful portion on the surface. Results compare closely to theory, as they should. Since the model makes use of the equations derived in the theory section, it was expected that the physical model would perform exceptionally. However, the physical portion does contain limitations which could be misleading if not recognized. Firstly, the current model does not allow for reversible flow. The integration of a pressure flow solver, such as the one used by Anderson (2008), would eliminate this inadequacy. However, for this study, it was decided that the pressure solver would not be used, as it can create instability in the model.

Most of the remaining limitations arise from assumptions made for simplicity. As previously stated, many assumptions were made regarding heat

transfer across the tube. These assumptions were made because of the limited information provided by the Hudson calculator. If fin geometry information had been provided, it would have been possible to more accurately determine the heat transfer coefficients used for modeling. Based on the results from the physical model, it was concluded that this assumption had little impact on the overall results. If more precise simulation were required, the fin theory could be used to determine heat transfer coefficients given the appropriate parameters. Similarly, it is important to recognize that the parameters taken from the Hudson calculator were not based on a two pass heat exchanger. A two pass heat exchanger was not available for calculation purposes, so three and four pass exchanger parameters were determined and used to extrapolate corresponding data for the two pass model. Furthermore, the pressure used for the Hudson calculations does not agree with the operating pressure of the model. Again, these factors do not appear to have had a significant negative impact on the simulation, but all weaknesses of the model must be disclosed.

Finally, the shortcomings of the controller must be addressed. It was initially hypothesized that the triple cascade control scheme would exhibit exceptional control, while maintaining steam extraction percent, fan speed, and recirculation percentage at optimal levels. Currently, the control scheme is able to maintain the desired optimal levels for these control variables during both of the simulations with steady inlet properties. These results demonstrated the effectiveness of the triple cascade controller, as well as the functionality of the

conditional control for freezing ambient temperatures. It is expected that numerous trials will need to be conducted before optimal PID coefficients can be reached for the transient responses. Since the simulation was configured as a discrete time step model, the PID function blocks could not be auto-tuned. The results from the new control block with the generic process model were very encouraging. With additional time, this control logic could be implemented in the full simulation model and smooth performance curves can be achieved.

5.2 Future Work

For continuation of this work there are a few approaches that can be taken. The first, and probably most important, recommendation would be improvement of the controls. Since PID controls are commonly thought to be simplest, one might start by investigating additional tuning techniques for smoother control. If PID controls are ultimately deemed to be insufficient for optimal control of the transient responses, an advanced control scheme, such as a neural network predictive control, might be implemented. After optimal system control is achieved, one should look to increase the complexity of the process model. This could include improving heat transfer correlations or expanding the model for additional passes. A more involved effort might attempt to incorporate the pressure solver into the pipe segments.

It is imperative to continue to develop this study, as such simulations can be very practical in industry today. Many companies place a very high value on simulation controls which are used for both training personnel and design work.

Typically, double cascade controls are effective and easily modeled. A triple cascade control requires more work, but has been proven to be incredibly useful when tuned properly. In this instance, a triple cascade control could be used to optimize overall performance of the condenser. Successful simulations of such control processes can provide great benefits when designing large scale systems.

REFERENCES

ACHE (Version 2.0) [Software]. (2013) Retrieved from http://www.hudsonproducts.com

Anderson, Scott. "Modeling of a Drum Boiler Using MATLAB/Simulink." Thesis., Youngstown State University, 2008.

Brosilow, Coleman, and Babu Joseph. Techniques of model-based control. Prentice Hall Professional, 2002.

Çengel, Yunus A., and Michael A. Boles. Thermodynamics: an engineering approach. 6th ed. Boston: McGraw-Hill, 2008.

KVA Stainless. “A More Efficient Exchange.” 19 February. 2014. http://www.kvastainless.com/heat-exchangers.html

Lamarsh, John R., and Anthony John Baratta. Introduction to nuclear engineering. Upper Saddle River, NJ: Prentice Hall, 2001.

Larinoff, M. W., W. E. Moles, and R. Reichhelm. "Design and specification of air-cooled steam condensers." *Chem. Engng* 22 (1978).

Shah, M. M. "A general correlation for heat transfer during film condensation inside pipes." International Journal of Heat and Mass Transfer 22, no. 4 (1979): 547-556.

Shah, M. Mohammed. "An improved and extended general correlation for heat transfer during condensation in plain tubes." HVAC&R Research 15, no. 5 (2009): 889-913

Shah, Mirza M. "A new correlation for heat transfer during boiling flow through pipes." Ashrae Trans 82, no. 2 (1976): 66-86.

OMEGA. "Temperature Control Tuning a PID (Three Mode) Controller." OMEGA. 02 April. 2014. http://www.omega.com/temperature/Z/pdf/z115-117.pdf

Toshiba Corporation. "Air Cooled Heat Exchanger." 11 Feb. 2014. http://www.toshiba.com/tane/pdf/27_Air_Cooled_Heat_Exchanger.pdf

U.S. Energy Information Administration (EIA). “Annual Energy Outlook 2014 Early Release Overview.” 16 Dec. 2013. http://www.eia.gov/forecasts/aeo/er/pdf/0383er

APPENDICES

APPENDIX A

RESULTS

Figure A.1 Outlet Air Temperature – No Controls

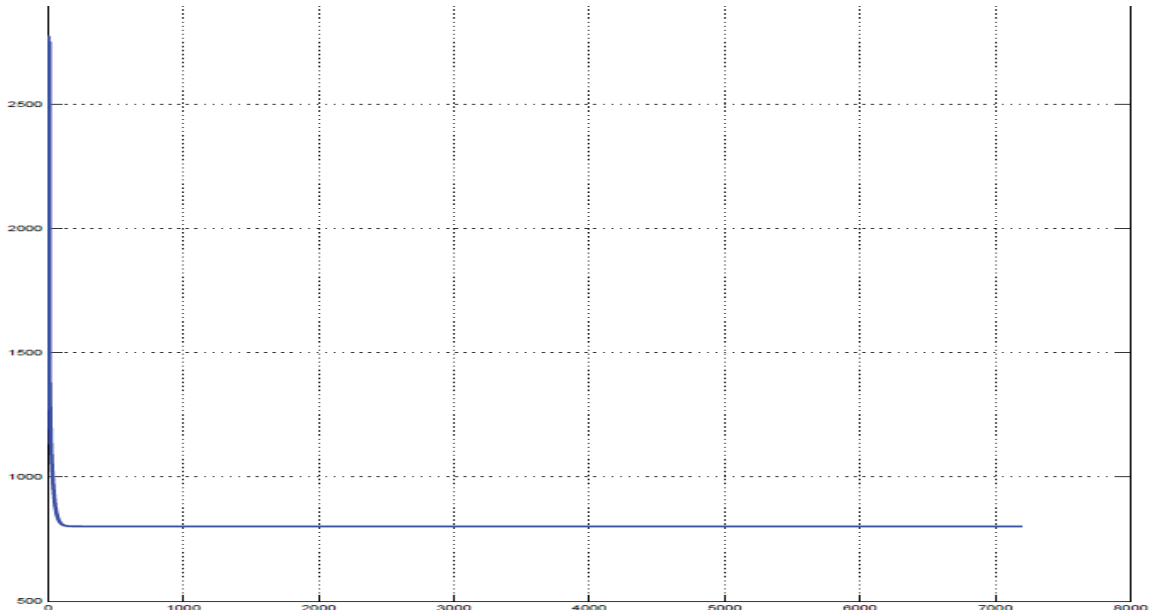

Figure A.2 Outlet Enthalpy – No Controls

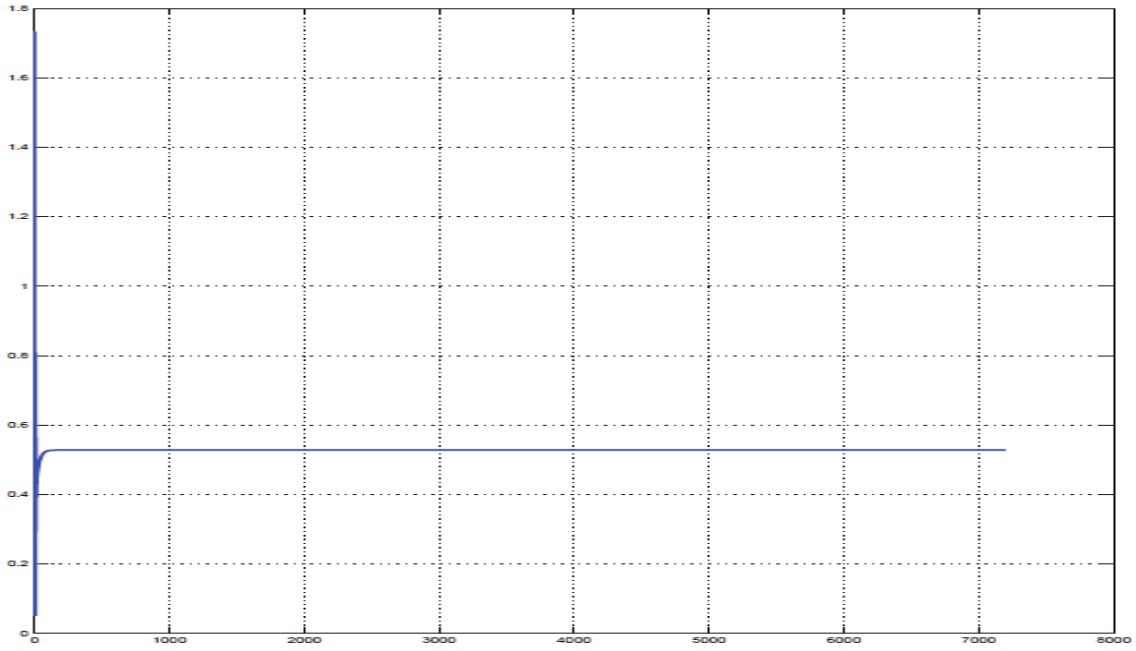

Figure A.3 Outlet Mass Flow Rate – No Controls

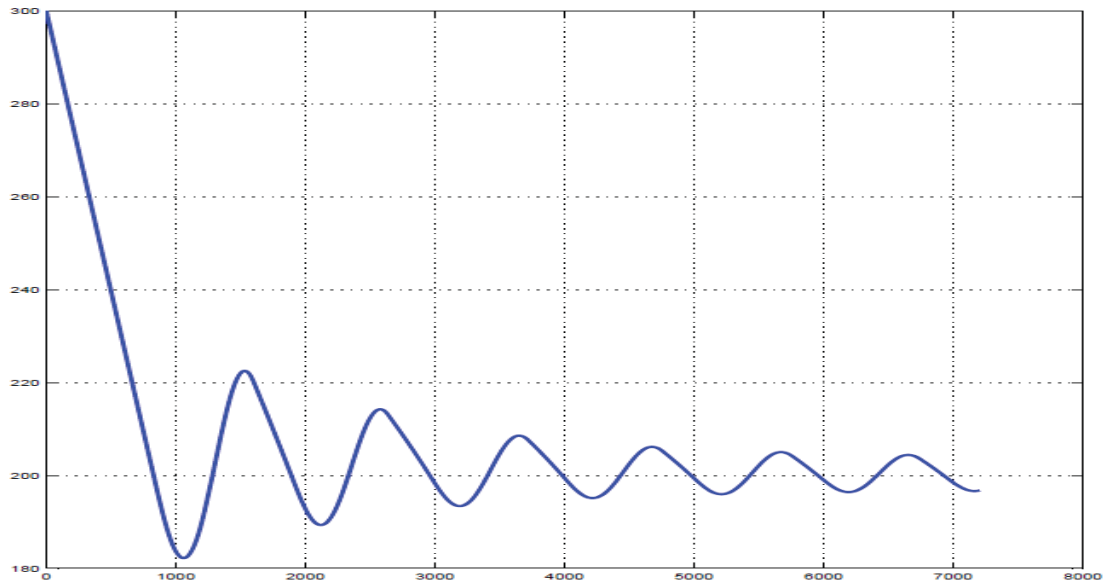

Figure A.4 Condensate Temperature – New (I) Controls with Generic Model

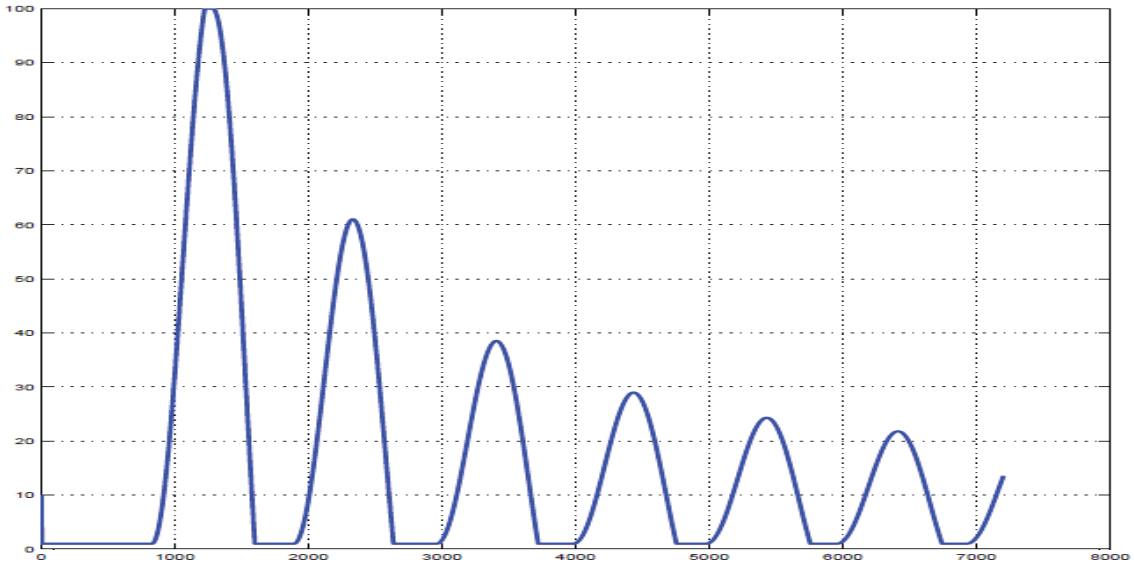

Figure A.5 Steam Extraction Percent – New (I) Controls with Generic Model

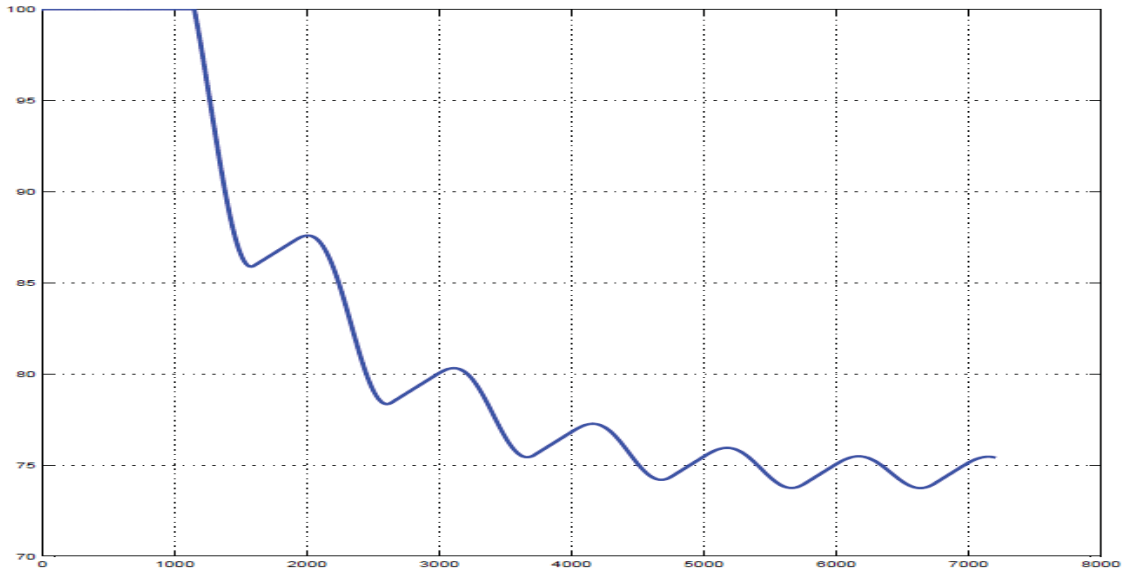

Figure A.6 Fan Speed – New (I) Controls with Generic Model

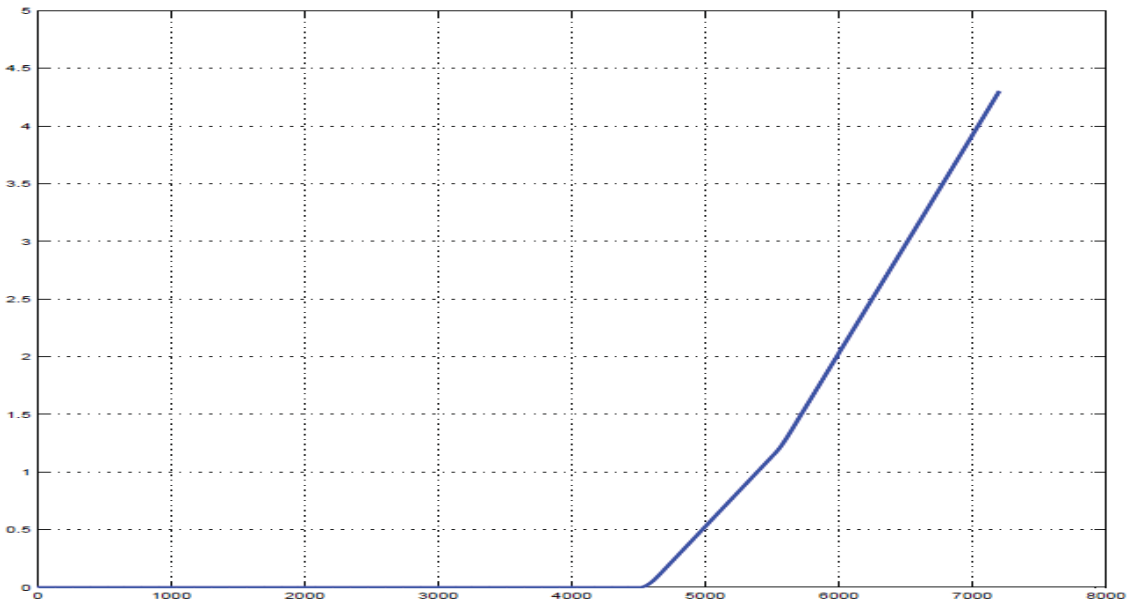

Figure A.7 Recirculation Percent – New (I) Controls with Generic Model

Figure A.8 Inlet Mass Flow – Ramped Mass Models

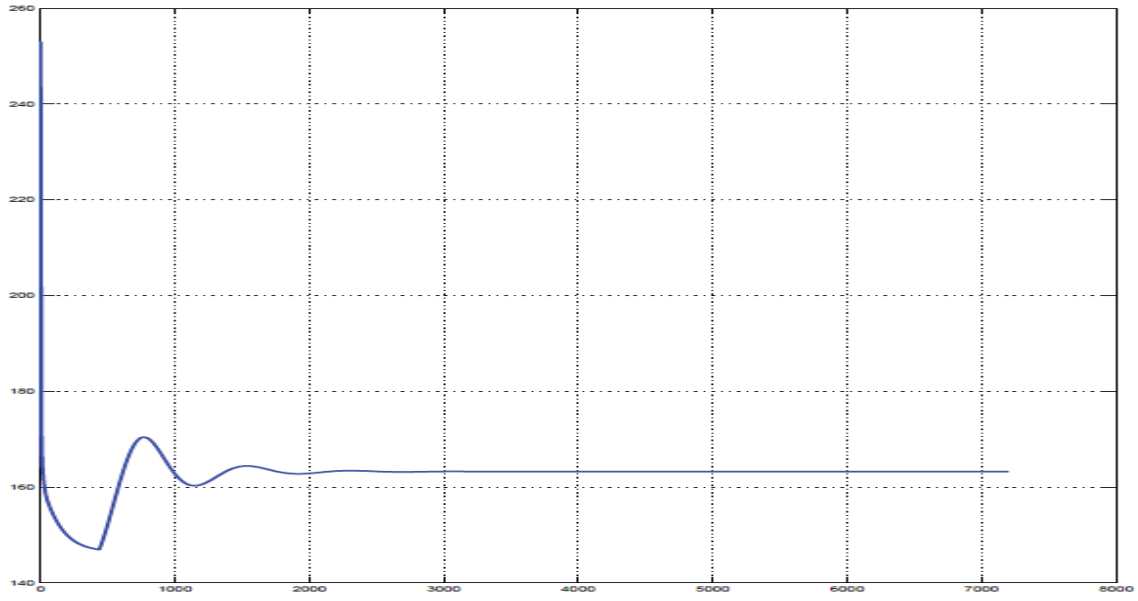

Figure A.9 Recirculation Air Temperature – (PID) Control – Ambient Air @ 20°C

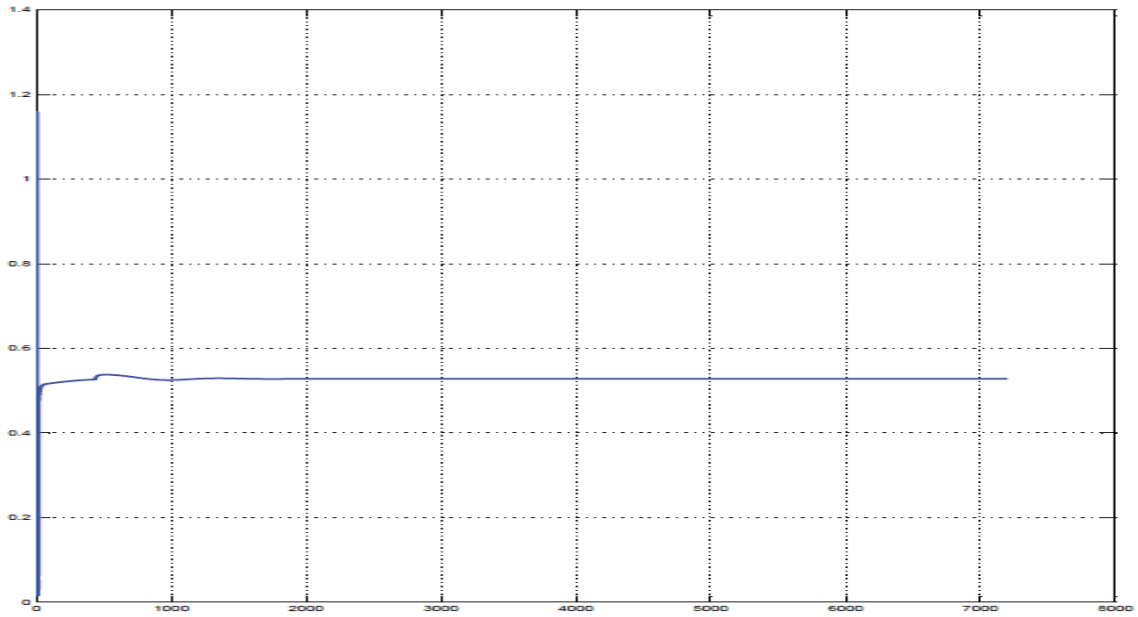

Figure A.10 Outlet Mass Flow Rate – (PID) Control – Ambient Air @ 20°C

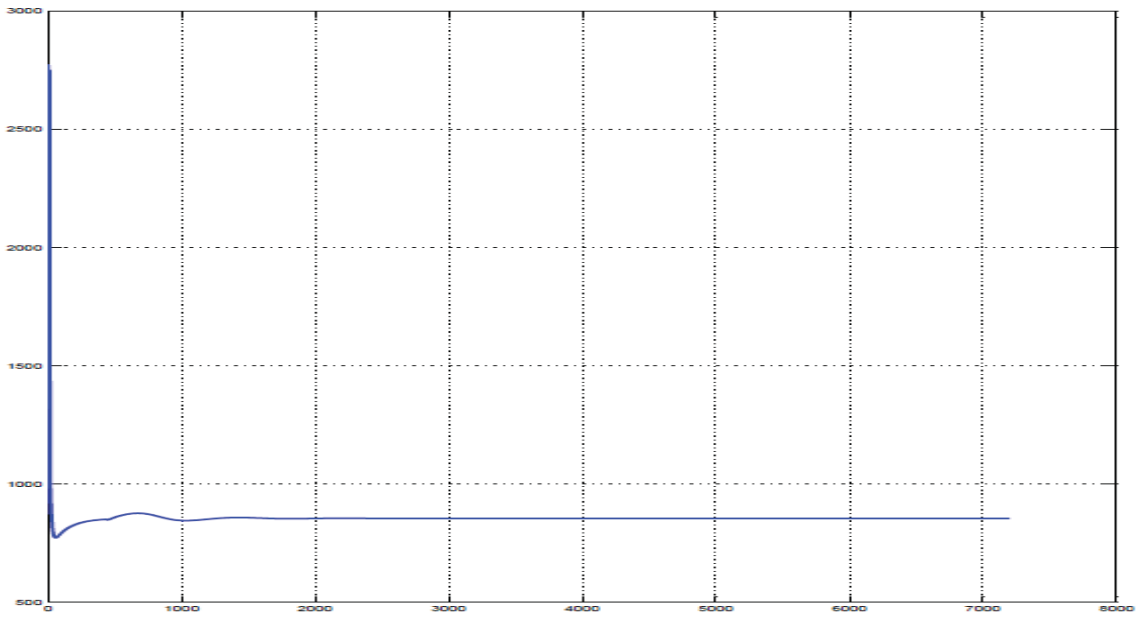

Figure A.11 Outlet Enthalpy – (PID) Control – Ambient Air @ 20°C

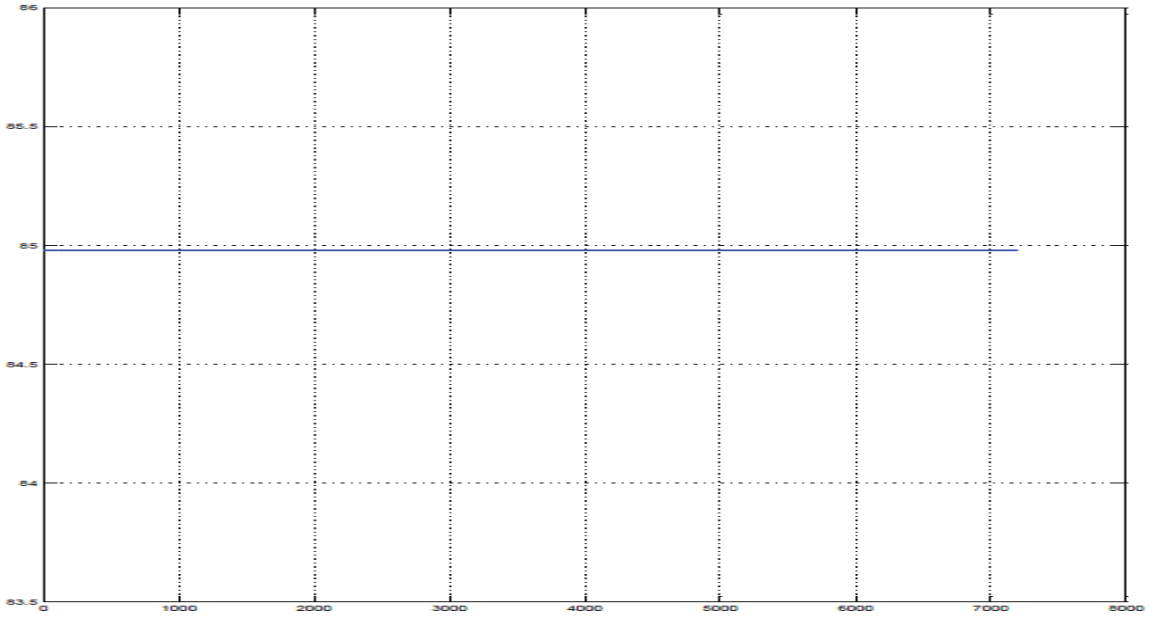

Figure A.12 Outlet Condenser Pressure – (PID) Control – Ambient Air @ 20°C

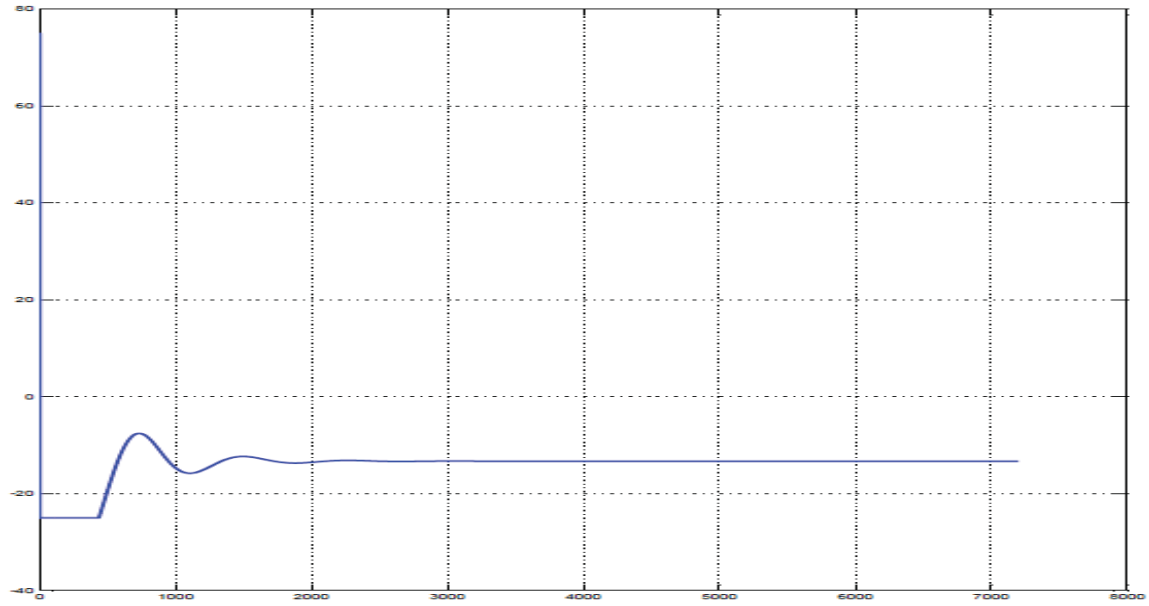

Figure A.13 Recirculation Percent Error – (PID) Control – Ambient Air @ 20°C

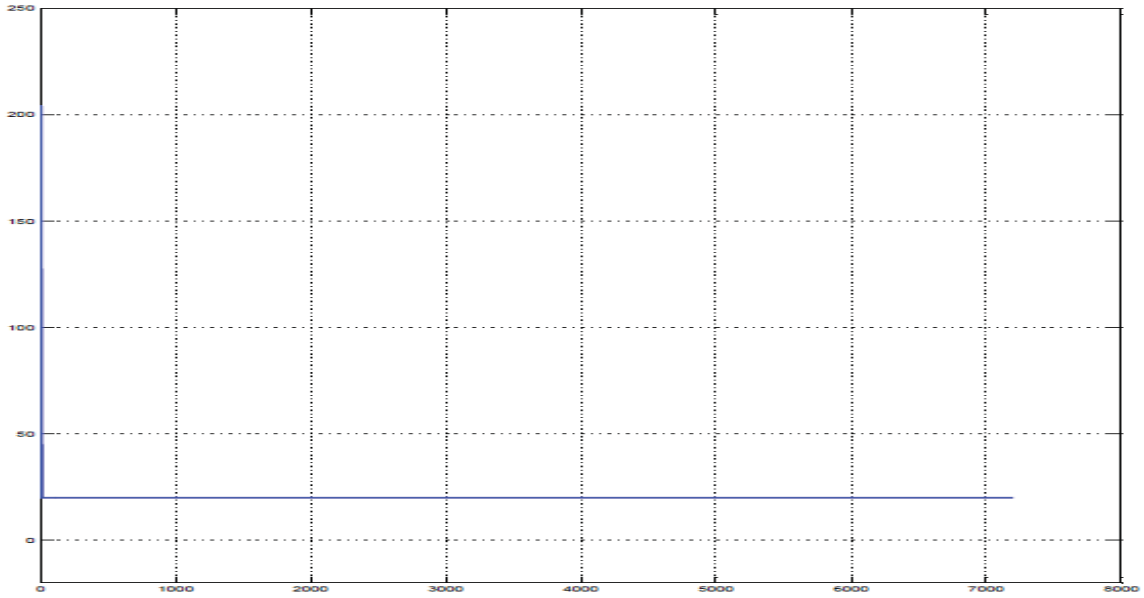

Figure A.14 Inlet Air Temperature – (PID) Control – Ambient Air @ 20°C

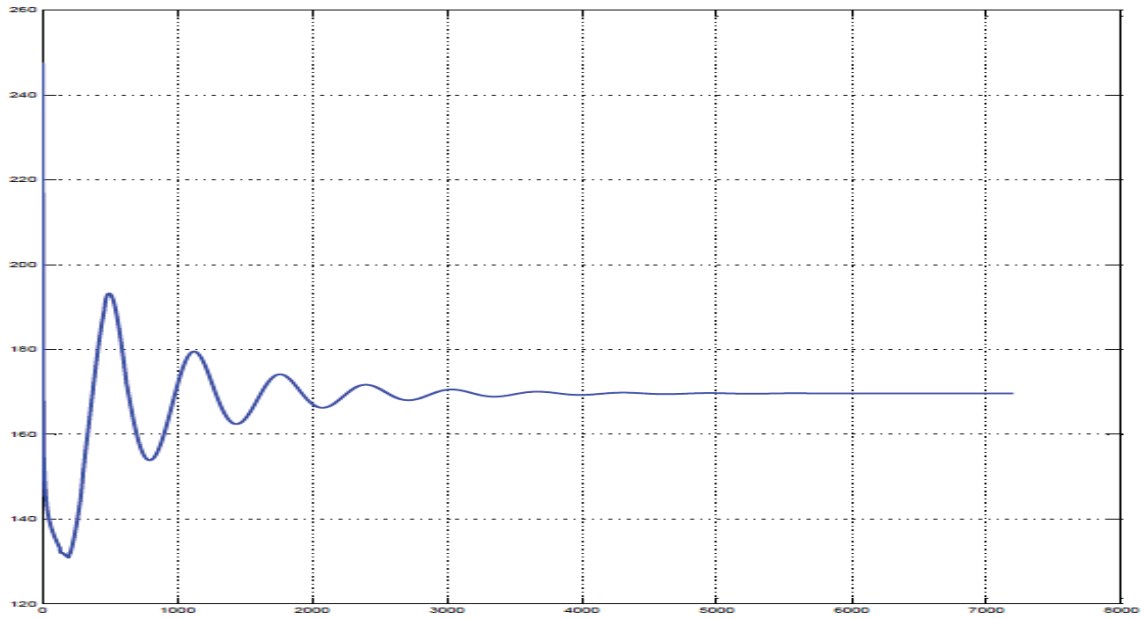

Figure A.15 Recirculation Temperature – (PID) Control – Ambient Air @ -10°C

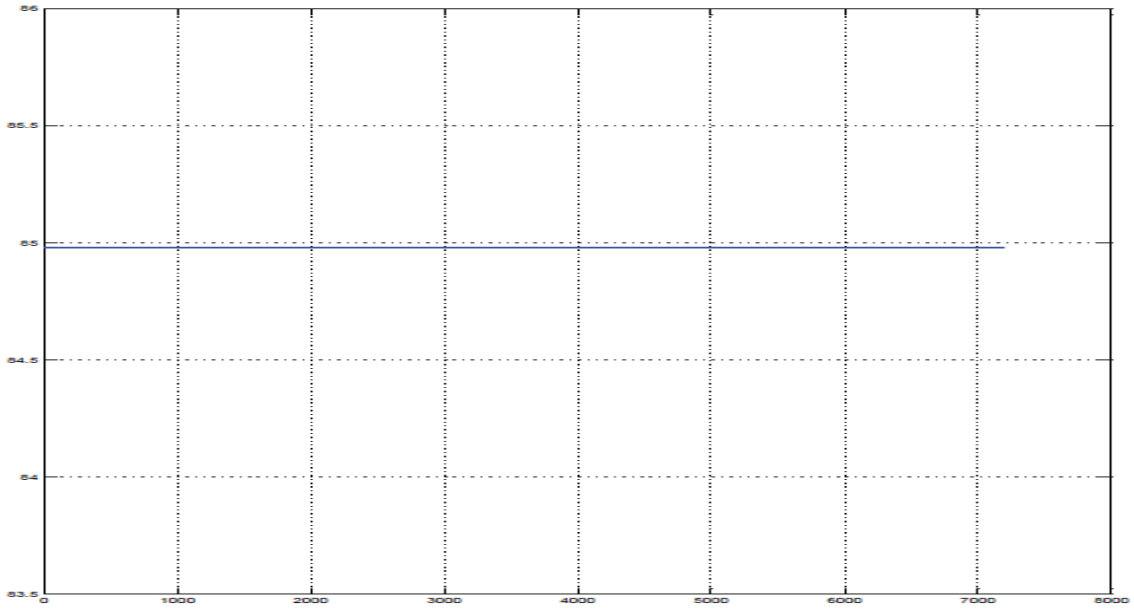

Figure A.16 Condenser Outlet Pressure – (PID) Control – Ambient Air @ -10°C

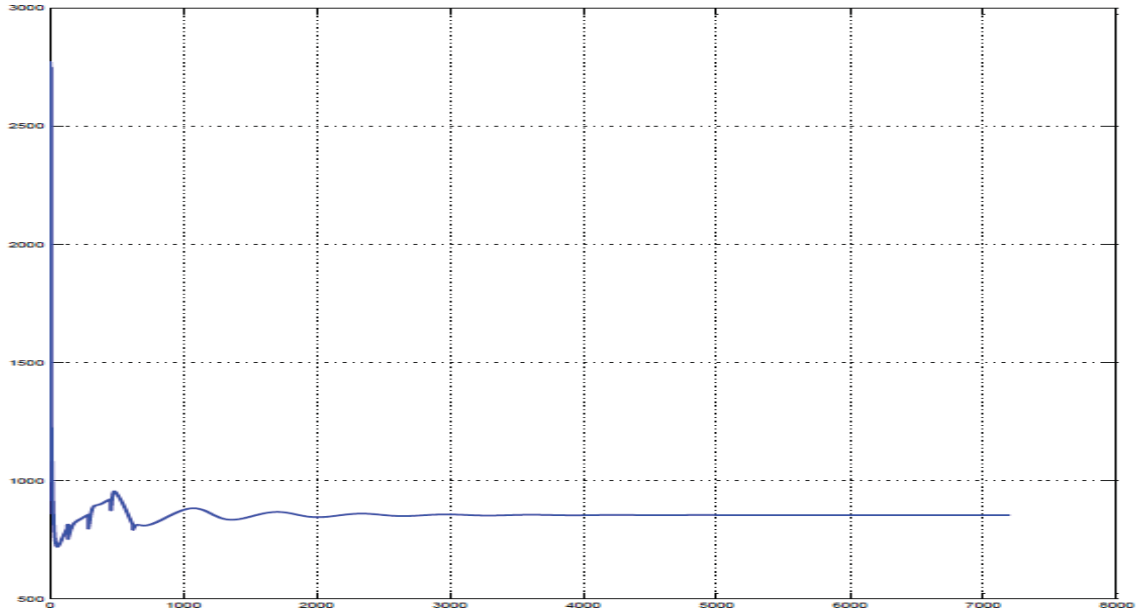

Figure A.17 Outlet Enthalpy – (PID) Control – Ambient Air @ -10°C

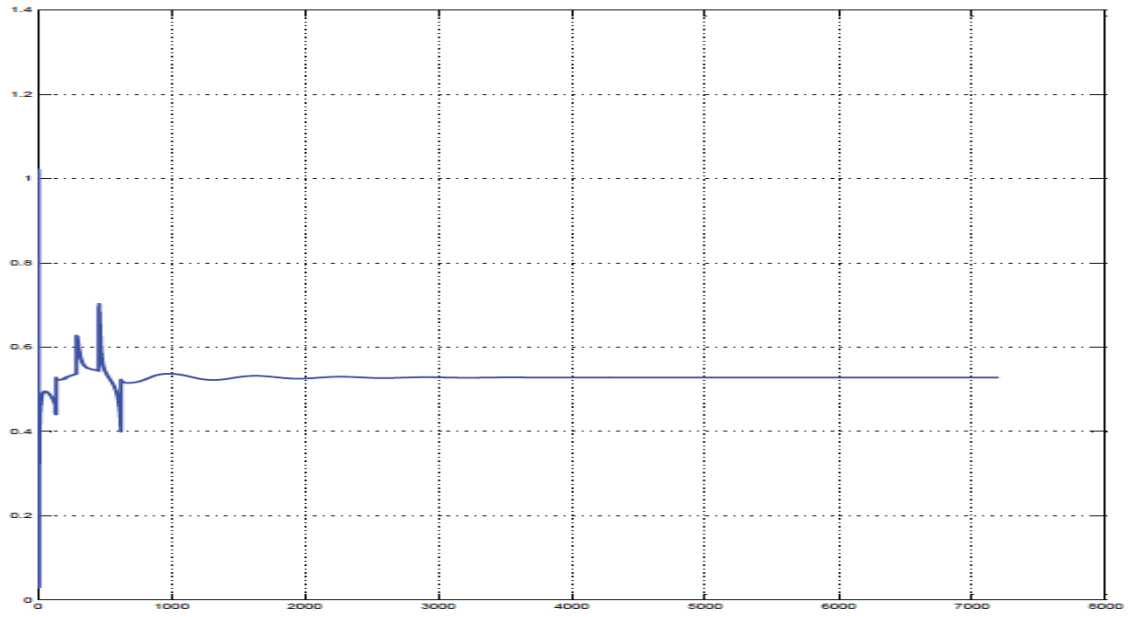

Figure A.18 Outlet Mass Flow Rate – (PID) Control – Ambient Air @ -10°C

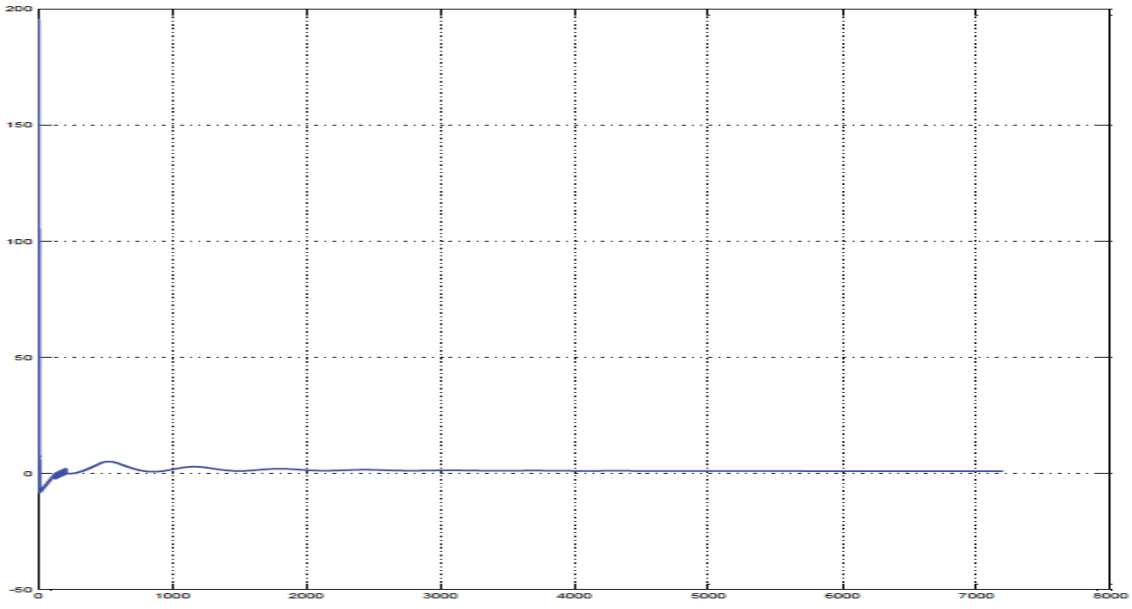

Figure A.19 Inlet Air Temperature – (PID) Control – Ambient Air @ -10°C

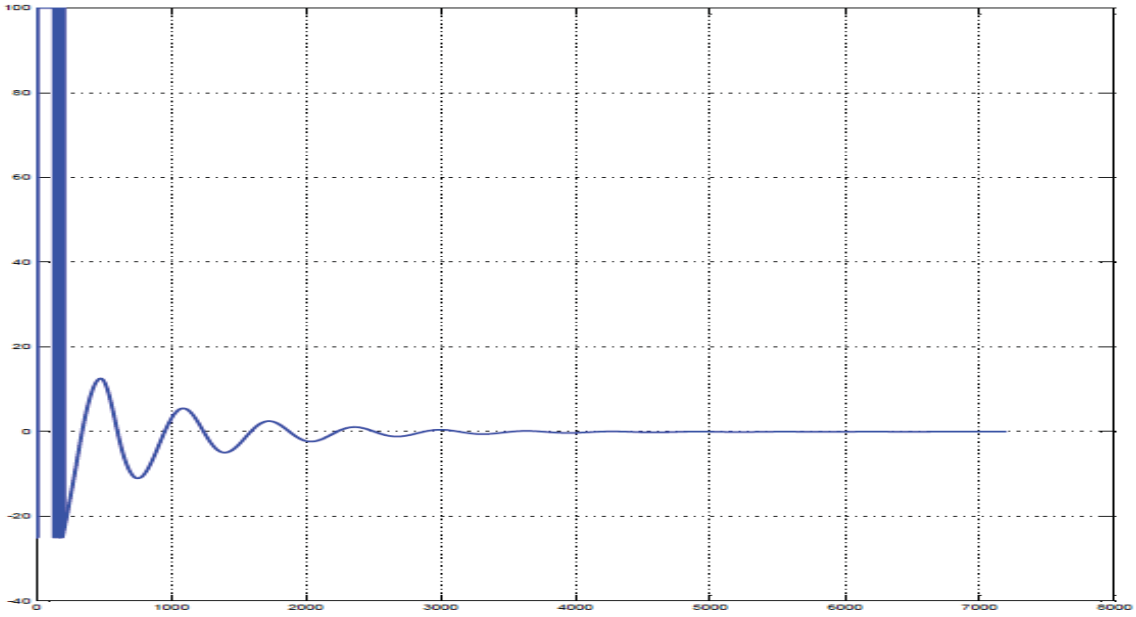

Figure A.20 Recirculation Percent Error– (PID) Control – Ambient Air @ -10°C

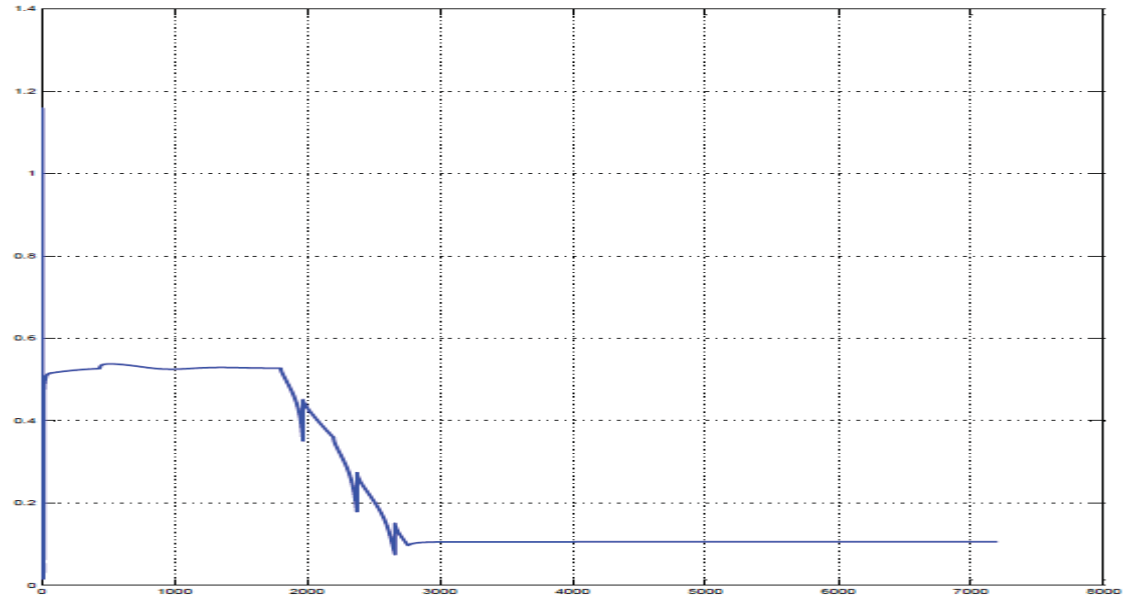

Figure A.21 Outlet Mass Flow Rate – (PID) Control –Ramped Mass Model

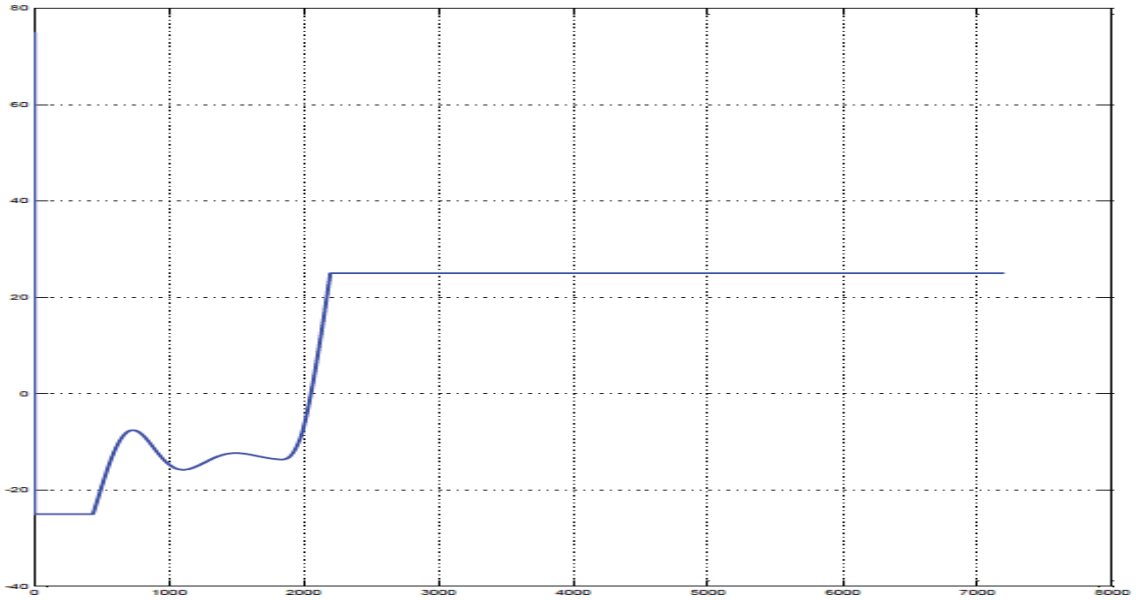

Figure A.22 Recirculation Percentage Error– (PID) Control –Ramped Mass Model

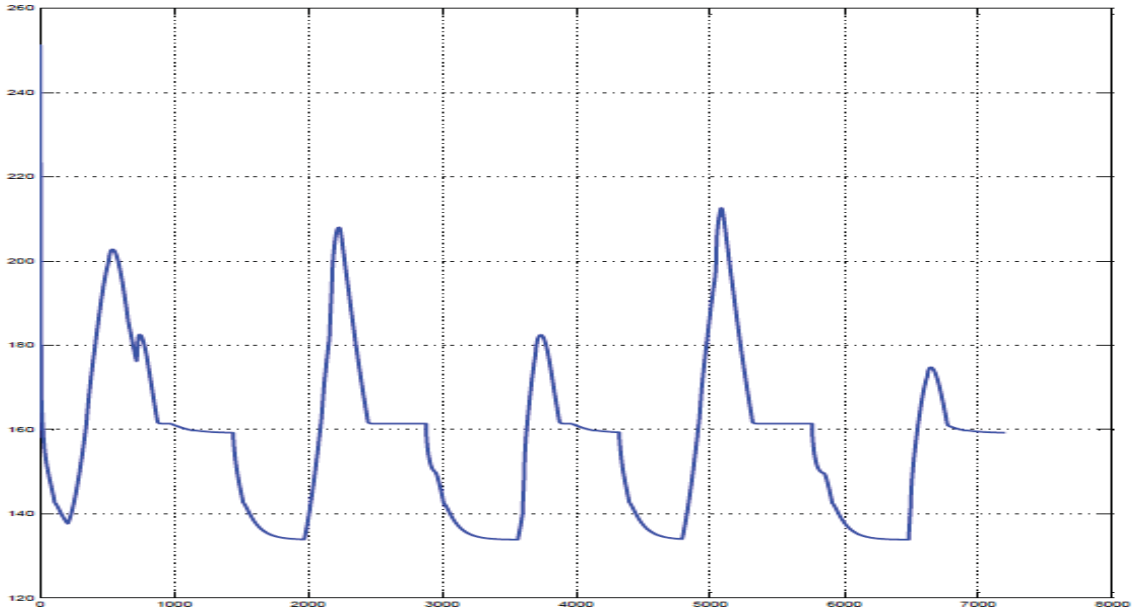

Figure A.23 Recirculation Air Temp – (PID) Control –Spiked Mass Model

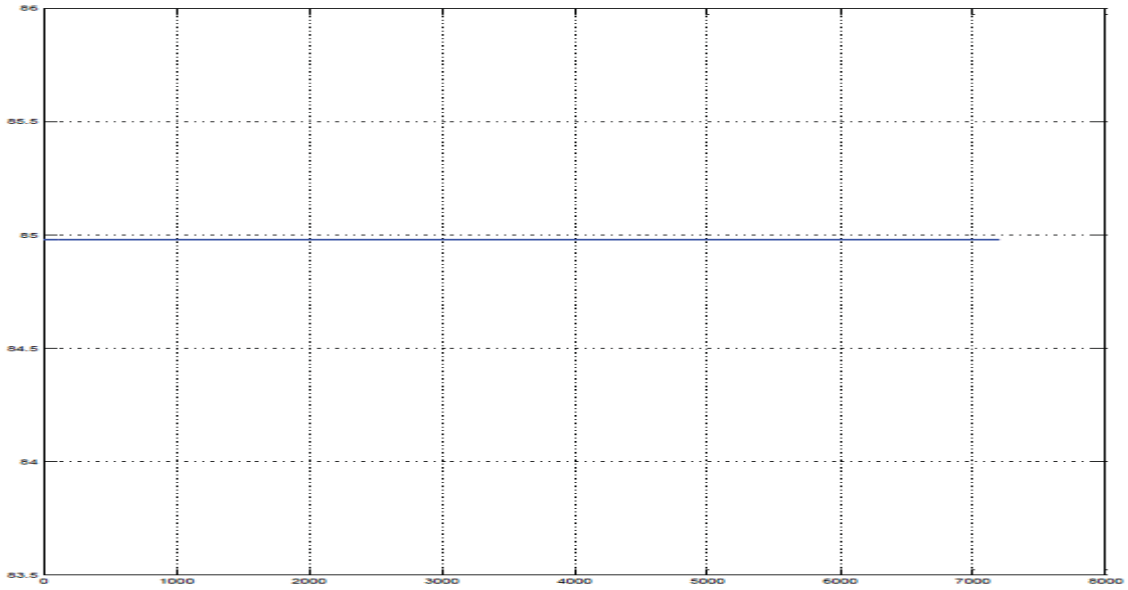

Figure A.24 Outlet Pressure – (PID) Control –Spiked Mass Model

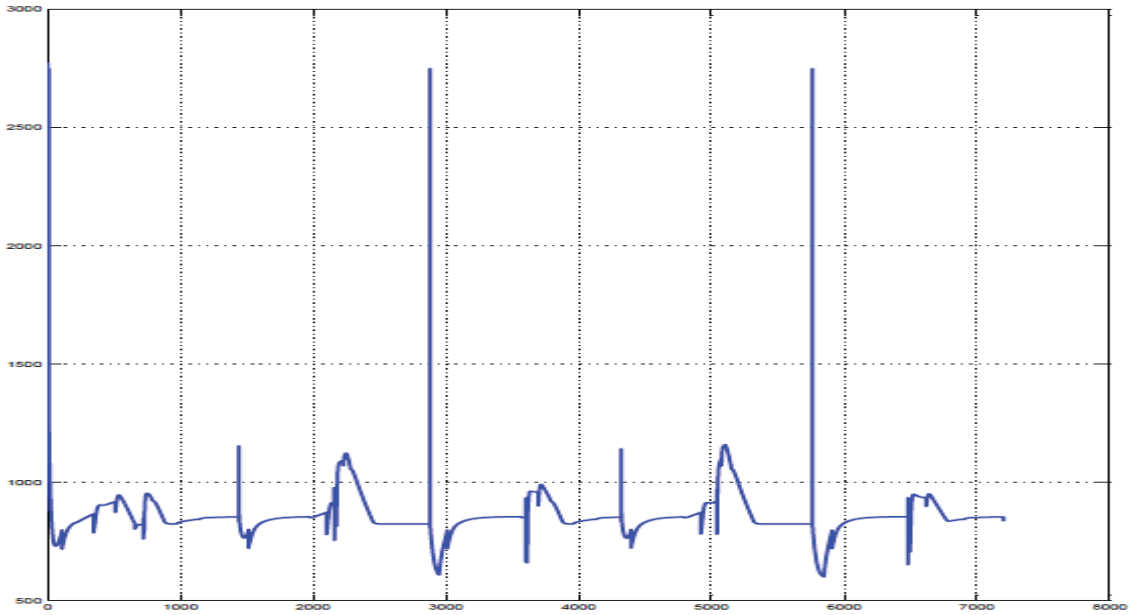

Figure A.25 Outlet Enthalpy – (PID) Control –Spiked Mass Model

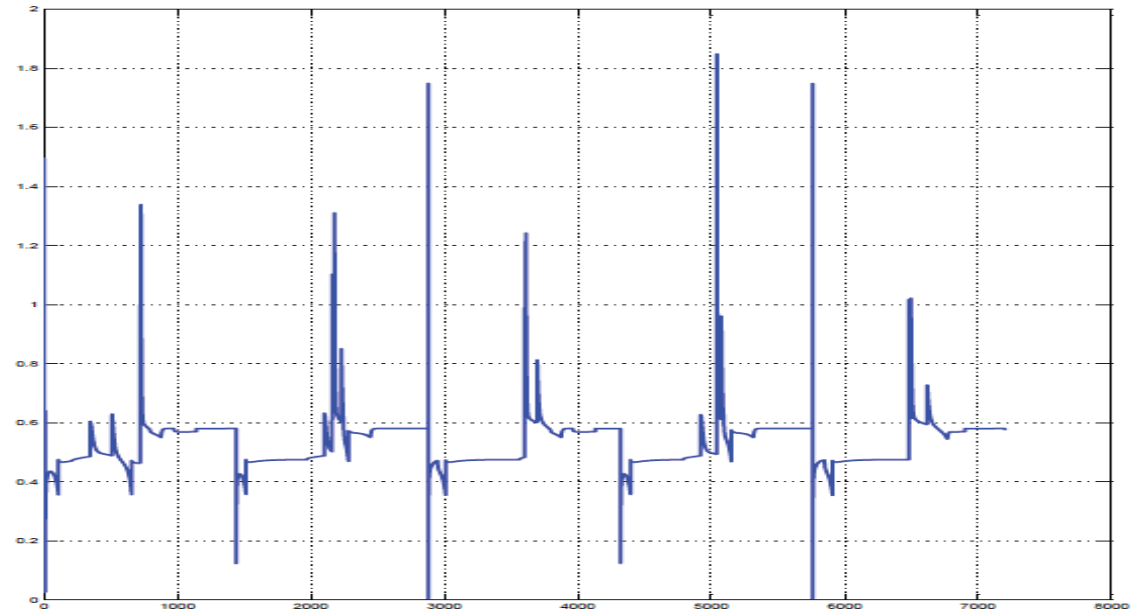

Figure A.26 Outlet Mass Flow Rate – (PID) Control –Spiked Mass Model

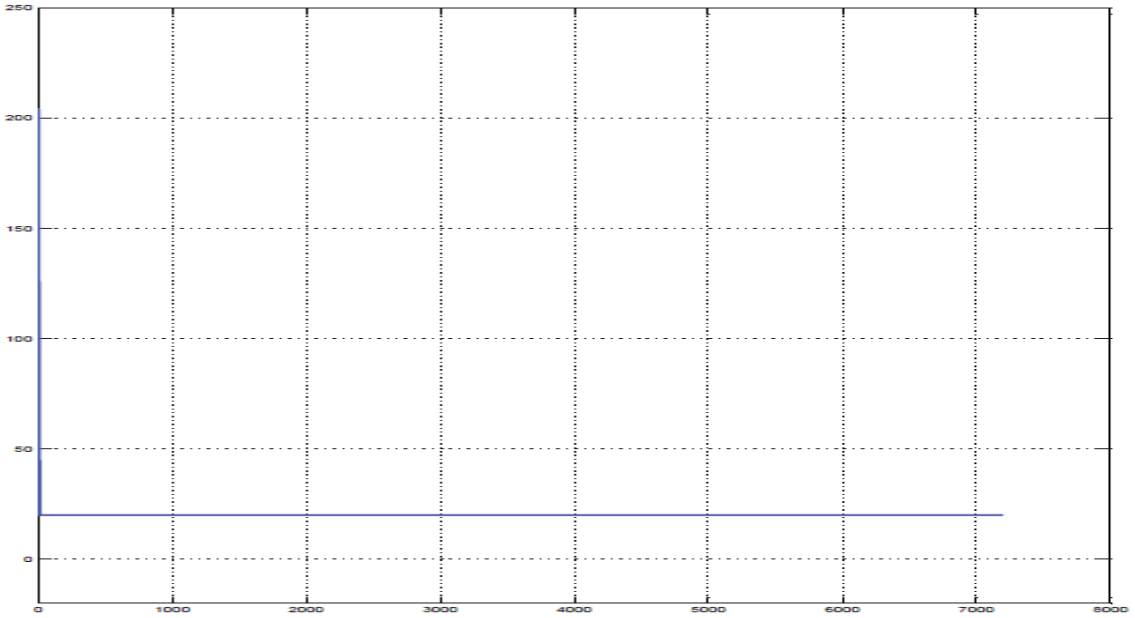

Figure A.27 Inlet Air Temperature – (PID) Control –Spiked Mass Model

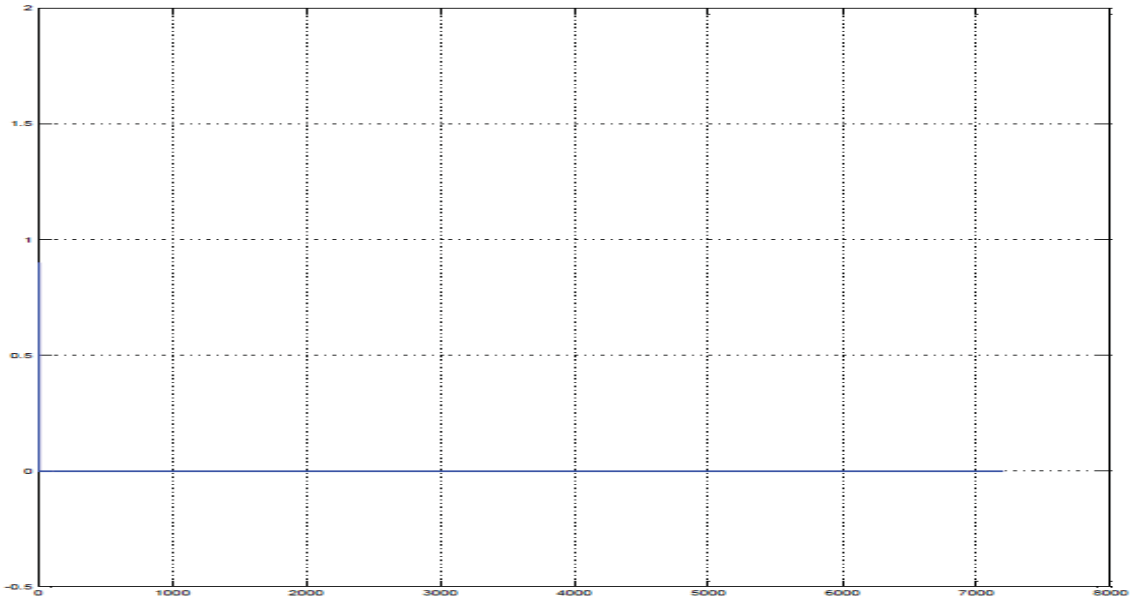

Figure A.28 Recirculation Percent– (PID) Control –Spiked Mass Model

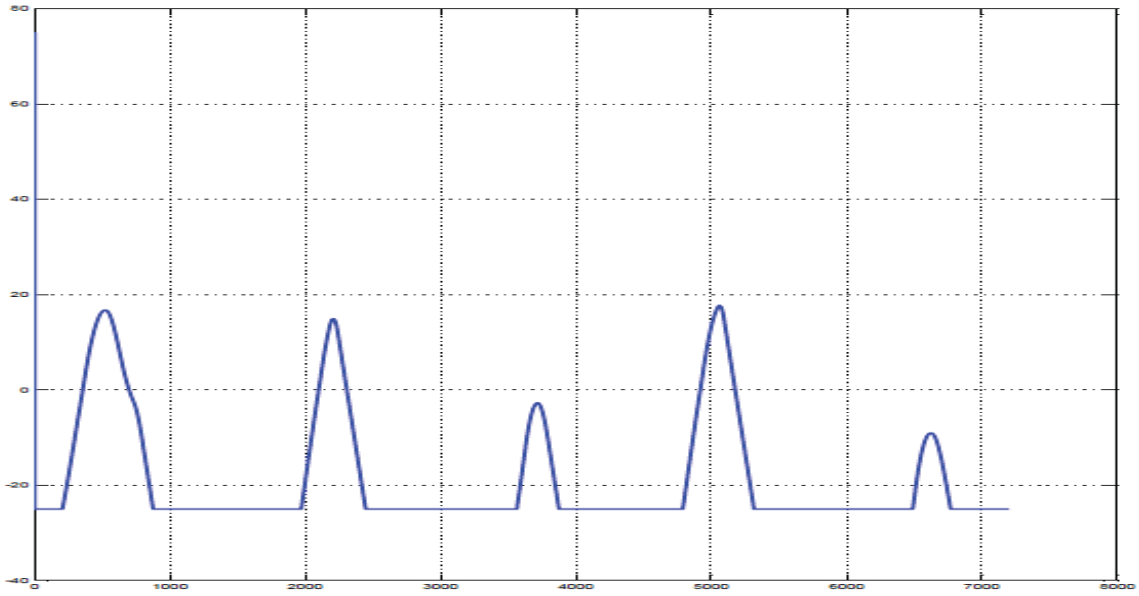

Figure A.29 Recirculation Percent Error – (PID) Control –Spiked Mass Model

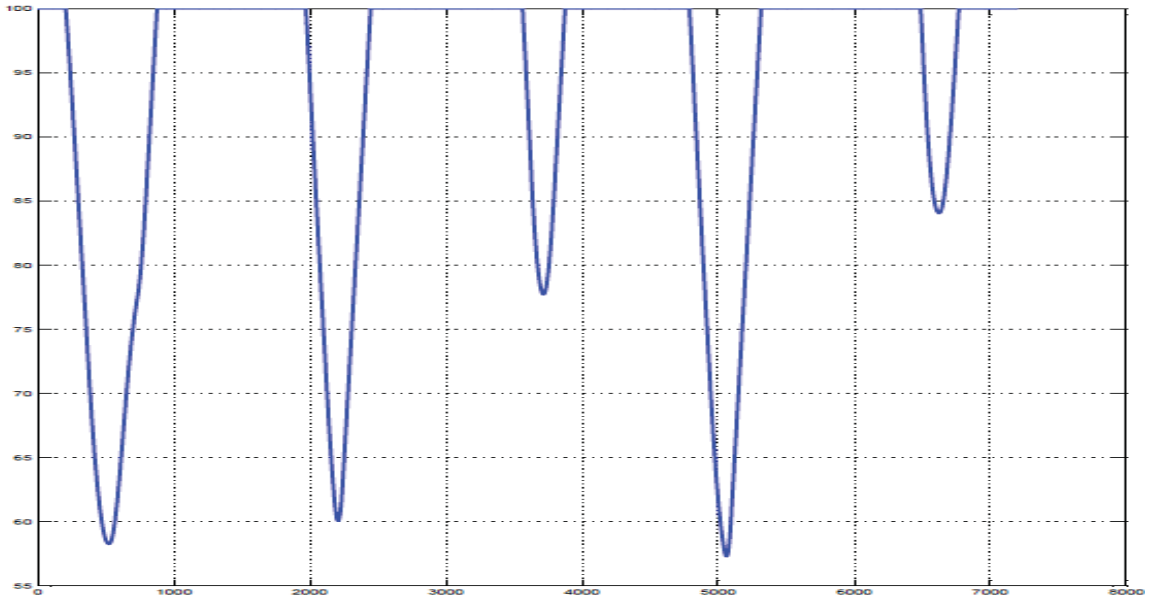

Figure A.30 Fan Speed Percent – (PID) Control –Spiked Mass Model

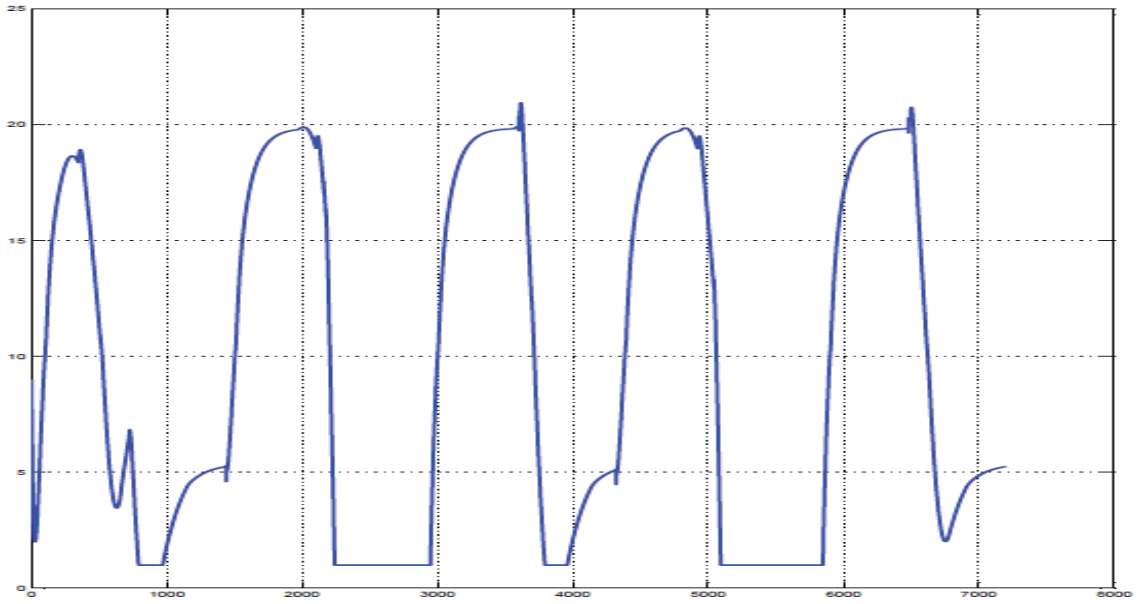

Figure A.31 Steam Extraction Percentage – (PID) Control –Spiked Mass Model

APPENDIX B

CALCULATIONS AND CODES

```
function [tube_mass,total_Volume,n_tubes,tube_ID,tube_ID_area,tube_OD_area,
tube_cross_sec]= Geometry(dummy1,dummy2)
%
%
% Set Parameters - Predetermined/Calculated with Hudson
t_tube          = 0.00279 ;  % [m]
n_tubes         = 40;        % [ ]
tube_Length     = 3 ;        % [m]
tube_OD         = 0.0254 ;   % [m]
rho_steel       = 7841.717;  % [kg/m^3]
%
% Calculate Tube I.D. [m^2]
tube_ID         = tube_OD-(2*t_tube);
%
% Calculate Tube O.D. Area (Surface Area)[m^2]
tube_OD_area    = n_tubes*3.14*tube_Length*tube_OD;
%
%Calculate Tube I.D. Area (Surface Area) [m^2]
tube_ID_area    =n_tubes*3.14*tube_Length*tube_ID;
%
% Calculate Total Tube Cross Section [m^2]
tube_cross_sec  = 3.14*(tube_ID^2)*n_tubes/4;
%
% Calculate Total Voulme [m^3]
total_Volume    = n_tubes*tube_Length*(3.14/4)*tube_ID^2;
%
% Calculate Tube Mass [kg]
tube_mass       = n_tubes*rho_steel*3.14*tube_Length*((tube_OD^2)-
(tube_ID)^2)/4;
```

Figure B.1 Metal Node Function Block Code

```
function [T_ACC,P_out,dMdt_out,h_out,rho_ave_out]=
ACC_TUBE_1(dQdt_ACC,dt,P_in,dMdt_in,h_in,dMdt_out_old,h_out_old,rho_ave_old)
%
% Initialize Xsteam
eml.extrinsic('XSteam')
%
% Initialize variables
h_out           = h_out_old ;
dMdt_out        = dMdt_in ;
f               = 0.0135 ;
P_ave           = P_in ;
rho_ave         = rho_ave_old ;
rho_ave_out     = rho_ave_old ;
P_out           = P_in ;
T_ACC           = 0.0 ;
test            = 0.0 ;
fric            = 0.0135;
n_tubes         = 10000;
Length          = 5;
Diam            = 0.015;
A_squared       = ((3.14).*(3.14)/(16)).*(Diam.*Diam.*Diam.*Diam);
dMdt_tube       = dMdt_out_old./n_tubes ;
%
% Initialize Convergance
Conv_Mass       = 1.0 ;
Conv_Momentum   = 1.0 ;
Conv_Energy     = 1.0 ;
Convergence     = Conv_Mass + Conv_Momentum + Conv_Energy ;
Conv_Criteria   = 1E-10 ;
delta_P_nml     = 0.0 ;
h_ave_nml       = 0.0 ;
dMdt_out_nml    = 0.0 ;
count           = 0 ;
%
% Pipe geometry variables
V_total = 0.0370236 ;
Volume  = V_total/6 ;
Cf      = 0.0 ;
%
% MAIN ITERATION LOOP
while (Convergence > Conv_Criteria)
%
% Compute hydrostatic pressure drop in pipe:   delta_P = rho*g*h ;
% delta_P = (rho_ave_old).*(9.81).*(5)/(100000) ;
% Add friction pressure drop to delta_P ;
% delta_P = delta_P -
((fric).*(Length).*(dMdt_tube).*(dMdt_tube))./(2.*(Diam).*(A_squared).*rho_av
e_old.*100000);
%
delta_P = -0.1 ;
%
% Compute average pressure in pipe
P_ave = P_in + delta_P./2 ;
P_out = P_in + delta_P ;
%
% Compute new h_ave in pipe using conservation of energy
val1    = (dMdt_in.*h_in - dMdt_out.*h_out_old + dQdt_ACC).*(dt./Volume) ;

val2    = rho_ave_old.*h_out_old ;
h_ave   = (val1 + val2)./rho_ave ;
%
% Compute new density in pipe
rho_ave = XSteam('rho_ph',P_ave,h_ave) ;
%
% Compute dMdt_out using conservation of mass
dMdt_out    = dMdt_in - (rho_ave - rho_ave_old).*(Volume./dt) ;
% dMdt_out    = dMdt_in ;
%
% Check valve
if (dMdt_out < 0)
    dMdt_out = 0;
end
%
% Compute new density in pipe
rho_ave = XSteam('rho_ph',P_ave,h_ave) ;
%
% Compute convergence
Conv_Mass       = (1 - (dMdt_out_nml./dMdt_out) )^2 ;
Conv_Momentum   = (1 - (delta_P_nml./delta_P) )^2 ;
Conv_Energy     = (1 - (h_ave_nml./h_ave) )^2 ;
Convergence     = (Conv_Mass + Conv_Momentum + Conv_Energy)^0.5 ;
%
delta_P_nml     = delta_P ;
h_ave_nml       = h_ave ;
dMdt_out_nml    = dMdt_out ;
%
count = count + 1;
if (count < 3)
    Convergence = 1 ;
elseif (count > 40)
    Convergence = 0 ;
end
%
% Compute h_out
h_out       = h_ave ;
%
% Compute rho out
rho_ave_out = rho_ave ;
%
% Compute T_ACC
T_ACC = XSteam('T_ph',P_ave,h_ave) ;
%
end
%
rho_ave_out = rho_ave ;
%
```

Figure B.2 Tube Segment Function Block Code

```
function [mdot_out,T_out]= ACC_Air_1B(dt,Q_in,mdot_in,T_in,T_out_old)
%
% Initialize variables
mdot_out  = 0.0;  % [kg/s]
T_out     = 0.0;  % [C]
Cp        = 1.01; % [kJ/kg]
Volume    = 1.0;  % [m^3]
val1      = 0.0 ;
val2      = 0.0 ;
rho       = 1.0 ; % [kg/m3]

%Calculate Flow Rate Out (assume no mass swell)
mdot_out  =   mdot_in;

%Calculate T_out
% T_out   = T_in+(Q_in/(mdot_out*Cp));

h_in      = Cp*T_in ;
h_out_old = Cp*T_out_old ;
val1      = (mdot_in*(h_in - h_out_old) + Q_in)*(dt/Volume) ;
val2      = rho*h_out_old ;
h_ave     = (val1 + val2)/rho ;
%
T_out     = h_ave/Cp ;
%
```

Figure B.3 Air Node Function Block Code

```
function
[error_steam_extraction,error_fan_speed_percent,error_recycle_percent]=
ACC_Error(T_ACC_out,T_ACC_out_target,SEP_in,SEP_target,FSP_in,FSP_target,RP_i
n,RP_target,T_Inlet_Air)
%
% Initialize variables
error_steam_extraction  = 0.0 ;
error_fan_speed_percent = 0.0 ;
error_recycle_percent   = 0.0 ;
%
% Steam Extraction Error
error_steam_extraction  = (T_ACC_out_target - T_ACC_out) ;
%
% Fan Speed Error
error_fan_speed_percent = (SEP_target - SEP_in) ;

% Recycle Air Error
error_recycle_percent   = (FSP_target - FSP_in) ;
%
% Keep air enterring the condensor above freezing
% If T_Inlet_Air < 0, then increase the recirc percentage asap
if (T_Inlet_Air < 0)
   error_recycle_percent = 100 ;
end
%
```

Figure B.4 Control Function Block Code

```
function [tube_mass,total_Volume,n_tubes,tube_ID,tube_ID_area,tube_OD_area,
tube_cross_sec]= Geometry(dummy1,dummy2)
%
%
% Set Parameters - Predetermined/Calculated with Hudson
t_tube          = 0.00279 ;  % [m]
n_tubes         = 40;        % [ ]
tube_Length     = 3 ;        % [m]
tube_OD         = 0.0254 ;   % [m]
rho_steel       = 7841.717;  % [kg/m^3]
%
% Calculate Tube I.D. [m^2]
tube_ID         = tube_OD-(2*t_tube);
%
% Calculate Tube O.D. Area (Surface Area)[m^2]
tube_OD_area    = n_tubes*3.14*tube_Length*tube_OD;
%
%Calculate Tube I.D. Area (Surface Area) [m^2]
tube_ID_area    =n_tubes*3.14*tube_Length*tube_ID;
%
% Calculate Total Tube Cross Section [m^2]
tube_cross_sec  = 3.14*(tube_ID^2)*n_tubes/4;
%
% Calculate Total Voulme [m^3]
total_Volume    = n_tubes*tube_Length*(3.14/4)*tube_ID^2;
%
% Calculate Tube Mass [kg]
tube_mass       = n_tubes*rho_steel*3.14*tube_Length*((tube_OD^2)-
(tube_ID)^2)/4;
```

Figure B.5 Geometric Parameters Function Block Code

```
function [h_inlet,P_inlet,rho_inlet,mdot,P_outlet,h_outlet, rho_out]=
GlobalParams(dummy1,dummy2)
%
% Initialize Xsteam
eml.extrinsic('XSteam')
%
%Initialize Variables
P_inlet          = 0.0 ;
P_outlet         = 0.0 ;
h_inlet          = 0.0 ;
h_outlet         = 0.0 ;
rho_inlet        = 0.0 ;
rho_out          = 0.0 ;
%
% Set Parameters
Q_remove         = 1000 ; % [Kw]
T_inlet          = 300 ;  % [C]
T_outlet         = 200 ;  % [C]

%
% Calculate Saturation Pressure ; steam at inlet is saturated
P_inlet          = XSteam('psat_T',T_inlet) ;
%
% Calculate Saturation Enthalpy ; steam at inlet is saturated
h_inlet          = XSteam('hV_T', T_inlet) ;
%
%Calculate Outlet Pressure
P_outlet         = P_inlet - 0.6 ;
%
%Calculate Outlet Enthalpy
h_outlet         = XSteam('h_pT',P_outlet,T_outlet) ;
%
%Calculate Mass Flow Rate
mdot             = Q_remove/(h_inlet-h_outlet);
%
%Calculate Rho in
rho_inlet        = XSteam('rho_ph',P_inlet,h_inlet) ;
%
%Calculate Rho out
rho_out          = XSteam ('rho_ph',P_outlet,h_outlet);
```

Figure B.6 Global Parameters Function Block Code

```
function [ACC_P_outlet,ACC_h_outlet,ACC_T_outlet]=
CondenserSizing(mdot_total_in,dummy2)
%
% Initialize Xsteam
eml.extrinsic('XSteam')
%
%Initialize Variables
ACC_P_inlet     = 0.0 ;
ACC_P_outlet    = 0.0 ;
ACC_h_inlet     = 0.0 ;
ACC_h_outlet    = 0.0 ;
ACC_T_outlet    = 0.0 ;       % [C]
ACC_mdot        = 0.0 ;
%
% Set Parameters
ACC_Q_remove    = 1000 ;      % [Kw]
ACC_T_inlet     = 300 ;       % [C]
%
% Calculate steam flow through ACC
ACC_mdot        = 0.9*mdot_total_in ; % [kg/s]
%
% Calculate Saturation Pressure ; steam at inlet is saturated
ACC_P_inlet     = XSteam('psat_T',ACC_T_inlet) ;
%
% Calculate Saturation Enthalpy ; steam at inlet is saturated
ACC_h_inlet     = XSteam('hV_T',ACC_T_inlet) ;
%
% Calculate outlet enthalpy
ACC_h_outlet    = ACC_h_inlet - (ACC_Q_remove/ACC_mdot) ;
%
%Calculate Outlet Pressure
ACC_P_outlet    = ACC_P_inlet - 0.6 ;
%
% Compute outlet temperature
ACC_T_outlet       = XSteam('T_ph',ACC_P_outlet,ACC_h_outlet) ;
%
%
%
```

Figure B.7 Condenser Sizing Function Block Code

```
function [MIX_Thermal_Power,ACC_Thermal_Power] =
Calculations(ACC_mdot_in,ACC_h_in,ACC_mdot_out,ACC_h_out,MIX_mdot_in,MIX_h_in
,MIX_mdot_out,MIX_h_out)
%
% Initialize Variables
ACC_Thermal_Power  = 0.0 ;  % [kW]
MIX_Thermal_Power  = 0.0 ;  % [kW]
%
ACC_Thermal_Power = (ACC_mdot_in*ACC_h_in)-(ACC_mdot_out*ACC_h_out) ;
MIX_Thermal_Power = (MIX_mdot_in*ACC_h_in)-(MIX_mdot_out*MIX_h_out) ;
```

Figure B.8 Power Output Function Block Code

	A	B	C	D	E
1	Mass Flow Rate	Tube ID	Tube C-S Area	α	Mass Flux G
2	[kg/s]	[m]	[m^2]	[ ]	[kg/m^2-s]
3	0.4752	0.01982	0.00030853	1.282	1540
4					
5	Pressure	Pressure	reduced pressure, p_r		
6	[bar]	[MPa]	[ ]		
7	85.88	8.59	0.389		
8					
9	Thermal Conductivity k_f	Viscosity, μ	Specific Heat, C_P	Re_L	Pr
10	[W/m-C]	[Pa-s]	[kJ/kg-C]	[ ]	[ ]
11	0.545	8.64466E-05	5.707	353131	0.905
12					
13	h_L	h_{TPM}	h_T	h_{OD}	β
14	[kW/m^2-C]	[kW/m^2-C]	[kW/m^2-C]	[kW/m^2-C]	[ ]
15	16.674	59.079	0.809	0.823	71.7
16					
17					
18					
19	**CHECK**	h_T (using h_{TPM})	h_T (using h_L)		
20	$(1/h_T)=(\alpha/h_{ID})+(1/h_{OD})$	[kW/m^2-C]	[kW/m^2-C]		
21		0.809	0.774		

Figure B.9 Excel Heat Transfer Calculations Using Shah's Equations

APPENDIX C

HUDSON CALCULATOR DATA

DATE: January 31, 2014 FILE:
PROJECT: The Basics of ACHE Default Problem
ITEM #: Sample case 1
ACHE SERVICE: Condensing FAN DRAFT: Forced
HOT FLUID: Steam @ 0 to 20 psig

HEAT EXCHANGER THERMAL PERFORMANCE

DESCRIPTION	ENGLISH	METRIC
Total Heat Duty, Million Btu/Hr (MW)	3.41	1.00
Hot Fluid Inlet Temperature, °F (°C)	572	300
Outlet Temperature, °F (°C)	392	200
Air Flow Rate, Lbm/Hr (Kg/s)	62,100	7.83
Inlet Temperature, °F (°C)	68.0	20.0
Outlet Temperature, °F (°C)	297	147
Transfer Rate, Btu/(Hr-Sqft-°F)(W/(SqM-°C))	143	809

ACHE DESCRIPTION

Tube	Material (Includes Headers)		Steel
	Length, Feet (Meters)	9.84	3.00
	Outside Diameter*, Inches (mm)	1.00	25.4
	Thickness (12 BWG)*, Inches (mm)	0.110	2.79
Fin	Material*		Aluminum
	Height*, Inches (mm)	5/8	15.9
	Spacing*, Fins/Inch (Fins/mm)	11	0.43
	Type*		Embedded
	Number of Tube Rows		3
	Number of Tubes/Row		15
	Total Number of Tubes		45
	Equilateral Tube Pitch*, Inches (mm)	2.5	63.5
	Bare Tube Surface Area, Sqft (SqM)	116	10.8
	Fin Tube Surface Area, Sqft (SqM)	2,460	228
ACHE	Length, Feet (Meters)	9.84	3.00
	Width, Feet (Meters)	3.00	0.91
	Weight, Lbm (Kg)	1,400	636
	Motor Shaft Power, HP (KW)	2.39	1.78

Figure C.1 Sample Case #1 Calculations

DATE: January 31, 2014 FILE:
PROJECT: The Basics of ACHE Default Problem
ITEM #: Sample case 1
ACHE SERVICE: Condensing FAN DRAFT: Forced
HOT FLUID: Steam @ 0 to 20 psig

HEAT EXCHANGER THERMAL PERFORMANCE

DESCRIPTION	ENGLISH	METRIC
Total Heat Duty, Million Btu/Hr (MW)	3.41	1.00
Hot Fluid Inlet Temperature, °F (°C)	572	300
Outlet Temperature, °F (°C)	392	200
Air Flow Rate, Lbm/Hr (Kg/s)	51,200	6.45
Inlet Temperature, °F (°C)	68.0	20.0
Outlet Temperature, °F (°C)	346	174
Transfer Rate, Btu/(Hr-Sqft-°F)(W/(SqM-°C))	143	809

ACHE DESCRIPTION

Tube Material (Includes Headers)		Steel
Length, Feet (Meters)	9.84	3.00
Outside Diameter*, Inches (mm)	1.00	25.4
Thickness (12 BWG)*, Inches (mm)	0.110	2.79

Fin	Material*		Aluminum
	Height*, Inches (mm)	5/8	15.9
	Spacing*, Fins/Inch (Fins/mm)	11	0.43
	Type*		Embedded
	Number of Tube Rows		4
	Number of Tubes/Row		10
	Total Number of Tubes		40
	Equilateral Tube Pitch*, Inches (mm)	2.5	63.5
	Bare Tube Surface Area, Sqft (SqM)	103	9.58
	Fin Tube Surface Area, Sqft (SqM)	2,190	203
ACHE	Length, Feet (Meters)	9.84	3.00
	Width, Feet (Meters)	2.00	0.61
	Weight, Lbm (Kg)	1,310	595
	Motor Shaft Power, HP (KW)	1.76	1.31

Figure C.2 Sample Case #2 Calculations

DATE: January 31, 2014 FILE:
PROJECT: The Basics of ACHE Default Problem
ITEM #: Sample case 1
ACHE SERVICE: Condensing FAN DRAFT: Forced
HOT FLUID: Steam @ 0 to 20 psig

HEAT EXCHANGER THERMAL PERFORMANCE

DESCRIPTION	ENGLISH	METRIC
Total Heat Duty, Million Btu/Hr (MW)	3.41	1.00
Hot Fluid Inlet Temperature, °F (°C)	572	300
Outlet Temperature, °F (°C)	392	200
Air Flow Rate, Lbm/Hr (Kg/s)	42,800	5.40
Inlet Temperature, °F (°C)	68.0	20.0
Outlet Temperature, °F (°C)	400	204
Transfer Rate, Btu/(Hr-Sqft-°F)(W/(SqM-°C))	143	809

ACHE DESCRIPTION

Tube Material (Includes Headers)		Steel
Length, Feet (Meters)	9.84	3.00
Outside Diameter*, Inches (mm)	1.00	25.4
Thickness (12 BWG)*, Inches (mm)	0.110	2.79

Fin	Material*		Aluminum
	Height*, Inches (mm)	5/8	15.9
	Spacing*, Fins/Inch (Fins/mm)	11	0.43
	Type*		Embedded
	Number of Tube Rows		5
	Number of Tubes/Row		10
	Total Number of Tubes		50
	Equilateral Tube Pitch*, Inches (mm)	2.5	63.5
	Bare Tube Surface Area, Sqft (SqM)	129	12.0
	Fin Tube Surface Area, Sqft (SqM)	2,730	254
ACHE	Length, Feet (Meters)	9.84	3.00
	Width, Feet (Meters)	2.00	0.61
	Weight, Lbm (Kg)	1,270	576
	Motor Shaft Power, HP (KW)	1.88	1.40

Figure C.3 Sample Case #3 Calculations

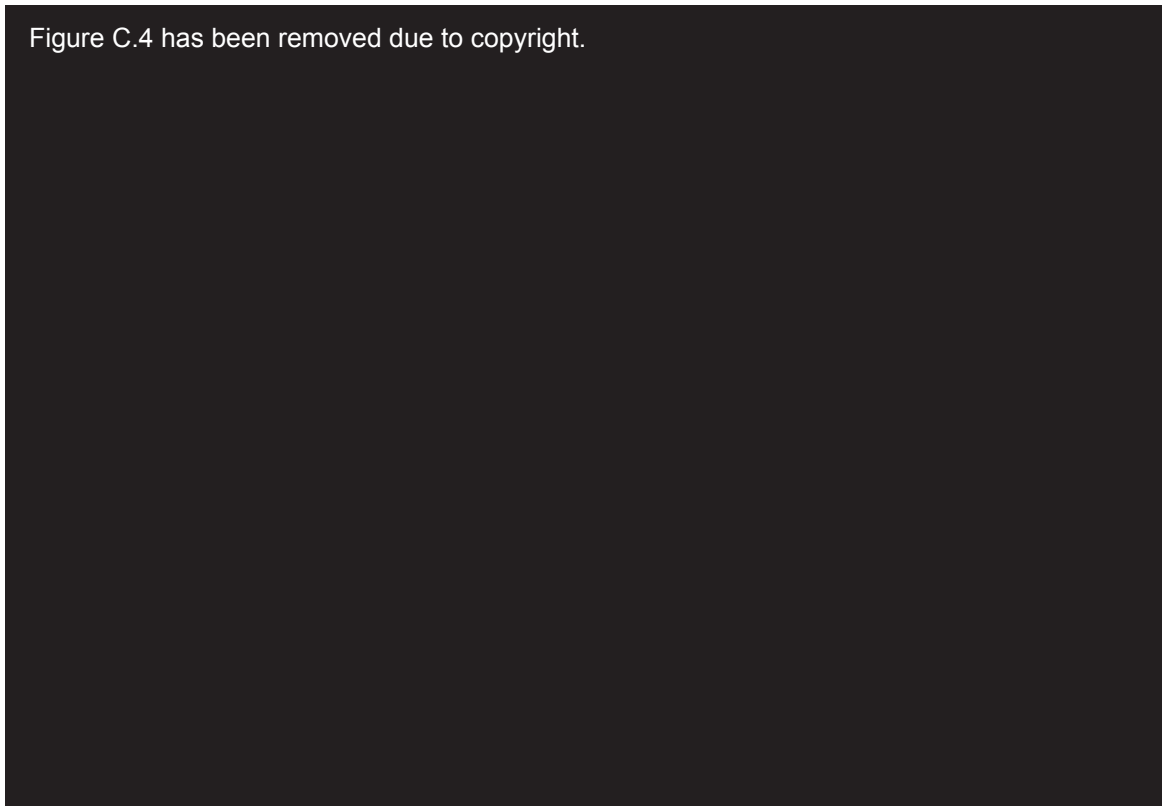

Figure C.4 Calculator Interface (ACHE, 2013)